GROWTH OF Si-Ge NANOSTRUCTURES ON HIGH INDEX SILICON SURFACES USING MOLECULAR BEAM EPITAXY AND THEIR CHARACTERIZATIONS

By

JATIS KUMAR DASH

Institute of Physics
Bhubaneswar, india

A Thesis submitted to the
BOARD OF STUDIES IN PHYSICAL SCIENCES DISCIPLINE

In partial fulfilment of requirements
FOR THE DEGREE OF

DOCTOR OF PHILOSOPHY
OF
HOMI BHABHA NATIONAL INSTITUTE

AUGUST, 2012

Statement By Author

This dissertation has been submitted in partial fulfillment of requirements for an advanced degree at Homi Bhabha National Institute (HBNI) and is deposited in the Library to be made available to borrowers under rules of the HBNI.

Brief quotations from this dissertation are allowable without special permission, provided that accurate acknowledgement of source is made. Requests for permission for extended quotation from or reproduction of this manuscript in whole or in part may be granted by the Competent Authority of HBNI when in his or her judgment the proposed use of the material is in the interests of scholarship. In all other instances, however, permission must be obtained from the author.

Jatis Kumar Dash
Institute of Physics
Bhubaneswar

Declaration

I, Jatis Kumar Dash, hereby declare that the investigations presented in the thesis have been carried out by me. The matter embodied in the thesis is original and has not been submitted earlier as a whole or in part for a degree/diploma at this or any other University/Institution.

Jatis Kumar Dash
Institute of Physics
Bhubaneswar

ACKNOWLEDGEMENTS

It is a great pleasure for me to express my sincere gratitude and indebtedness to my thesis supervisor Prof. P. V. Satyam for his invaluable guidance and constant encouragement to complete this work. I wish to thank him for giving me the total freedom both academically and socially in all spirits during my Ph.D.

I am grateful to The Directors, IOPB for all the help I received from them during my stay here.

I would like to thank Prof. H. W. Yeom, Center for Atomic Wires and Layers(CAWL), Yonsei University, South Korea for allowing me to visit his laboratory, which was a stepping stone for my thesis work.

I take the opportunity to thank Prof. S. M. Shivaprasad and Dr. Mahesh Kumar for providing high index Si(5 5 12) substrates. I would like to acknowledge Dr. Oliver seeck for HRXRD measurement at Petra-III, Germany.

It was a pleasure to work with all my seniors in the lab and I would like to thank Kuntala di, Anupam da for teaching me MBE operation and deposition techniques and Jay da and Umananda bhai for teaching TEM sample preparation during initial days of my Ph.D. It was a pleasure to work with my group members Ashutosh, Raghav, Anjan, Arnab and Rajib. I would like to thank P Santhana Raman for his timely help in RBS simulation. Special thanks to Trilochan for his contribution in theoretical modelling, which is an unavoidable part of this thesis.

I enjoyed the company of all my batchmates: Ashutosh, Sachin, Sourabh, Ambresh and Rajib Batabyal. I would like to thank all my seniors and juniors for their help in making my stay a pleasant experience here at IOPB.

I wish to acknowledge the timely help provided by the technical staff, B. K. Dash, S. R. Mohanty and other technical staff at IBL. The service rendered by the administrative and library staff is highly acknowledged.

Finally, I wish to express my deep sense of gratitude to my parents, my brother Atish and my loving wife Chinmayee. It was their encouragement, support and affection that helped me immensely in completing this thesis work.

TO MY PARENTS

List of Publications

[1] ^{1‡} Universality in shape evolution of $Si_{1-x}Ge_x$ structures on high index Silicon surfaces
J. K. Dash, T. Bagarti, A. Rath, R. R. Juluri, P. V. Satyam
Submitted to Eur. Phys. Lett., arXiv:1204.0578v1 (2012)(Under review).

[2] Growth of Oriented Au Nanostructures: Role of Oxide at the Interface
A. Rath, **J. K. Dash**, R. R. Juluri, A. Rosenauer, Marcos Schoewalter and P. V. Satyam
J. Appl. Phys. **111**, 064322 (2012).

[3] ^{1‡} DC heating induced shape transformation of Ge structures on ultra clean Si (5 5 12) surfaces
J. K. Dash, A. Rath, R. R. Juluri, P. Santhana Raman, K. Muller, A. Rosenauer and P. V. Satyam
J. Phys.: Condens. Matter **23**, 135002 (2011).

[4] ^{1‡} Shape transformation of $Si_{1-x}Ge_x$ structures on ultra clean Si (5 5 7) and Si (5 5 12) surfaces
J. K. Dash, A. Rath, R. R. Juluri, K. Mueller, A. Rosenauer, P. V. Satyam
J. Phys: Conf. Series **326**, 012021 (2011).

[5] Nano scale phase segregation and alloy formation in Au-Ge system on ultra clean surfaces
A. Rath, **J. K. Dash**, R. R. Juluri, A. Rosenauer and P. V. Satyam
J. Appl. Phys. **111**, 104319 (2012).

[6] ^{1‡} Shape evolution of MBE grown $Si_{1-x}Ge_x$ structures on high index Si(5 5 12) surfaces: A temperature dependent study
J. K. Dash, A. Rath, R. R. Juluri, P. V. Satyam
Submitted to J. Physics D: Appl. Phys.(Under review)(2012).

[7] ^{1‡} Compositional analysis of Aligned trapezoid Si-Ge structures on Si(5 5 12) surfaces
J. K. Dash, A. Rath, R. R. Juluri, P. V. Satyam
To be published (2012).

[8] Temperature dependent electron microscopy study of Au thin films on Si(100) with and without native oxide layer as barrier at the interface
A. Rath, **J. K. Dash**, R. R. Juluri, A. Rosenauer and P. V. Satyam
J. Physics D: Appl. Phys., **44**, 115301 (2011).

[9] Epitaxy-like orientation of nanoscale Ag islands grown on air-oxidized Si(110)-(5 × 1) surfaces
Anupam Roy, **J. K. Dash**, A. Rath and B. N. Dev
Surface and Interface Anlysis (wileyonlinelibrary.com) DOI 10.1002/sia.3837.

[10] Growth of oriented Ag nanocrystals on air-oxidized Si surfaces: An insitu high nergy electron diffraction study
Anupam Roy, K. Bhattacharjee, **J. K. Dash** and B. N. Dev
Thin Solid Films **520**, 853-860 (2011).

[11] Migration and extrusion of metal nanowire inside the filled multi-walled carbon nanotube
Pawan K. Tyagi, Umananda M. Bhatta, Ashutosh Rath, J. Raghavendra Rao, **Jatis K. Dash**, Sanjeev Kumar, and P. V. Satyam
Submitted to Carbon (2012).

[12] Observation of grain growth in swift heavy ion irradiated NiO thin films
P. Mallick, Chandana Rath, **J. K. Dash**, R. Biswal, D. C. Agarwal, D. Behera, D. K. Avasthi, D. Kanjilal, P. V. Satyam and N. C. Mishra
Ind. J. Phys. **84 (10)**, 1399-1404 (2010).

[13] Formation of aligned nano-silicide structures in MBE grown Au/Si(110) system: A real time temperature dependent TEM study

Umananda M. Bhatta, **J. K. Dash**, Anupam Roy, A. Rath and P. V. Satyam J. Phys.: Condens. Matter **21** ,205403 (2009).

[14] Real time study of oxide mediated liquid - solid growth of high aspect ratio - aligned gold silicide microrods on Si (110) substrates
Umananda M. Bhatta, Ashutosh Rath, **Jatis K. Dash**, Jay Ghatak, Lai Yi-Feng, Chuan-Pu Liu, P. V. Satyam
Nanotechnology **20**, 465601 (2009).

[15] Structural phase transitions in Au thin films on Si (110): An in-situ temperature dependent transmission electron microscopy study
Umananda M. Bhatta, **J. K. Dash**, A. Rath, P. V. Satyam Appl. Surf. Sci., **256**, 567 (2009).

[16] Growth of oriented crystalline Ag nanoislands on air-exposed Si(001) surfaces
A. Roy, K. Bhattacharjee, **J. K. Dash** and B. N. Dev
Appl. Surf. Sci., **256**, 361(2009).

Conference Presentations

1. Shape transformation of $Si_{1-x}Ge_x$ structures on ultra clean Si (5 5 7) and Si (5 5 12) surface
J. K. Dash, A. Rath, R. R. Juluri, K. Mueller, A. Rosenauer, P. V. Satyam
Microscopy of Semiconducting Materials, MSM-2011, Churchill College, Cambridge, UK.

2. Shape Evolution of MBE Grown $Si_{1-x}Ge_x$ Structures on High Index Silicon Surfaces: A Temperature Dependent Study
J. K. Dash, A. Rath, R. R. Juluri, P. V. Satyam
ICANN-2011, Indian Institute of Technology Guwahati (IITG).

3. Poster pressentation at Workshop on Elecron Microscopy (WEM-2011) held at Institute of Physics, Bhubaneswar, India.

4. presented a poster in International conference on Ion beam induced nanopatterning of materials (IINM-2011), Institute of Physics, Bhubaneswar, India.

5. Oral presentation at Seminar on Physics and Technology of Novel Materials (PTNM-2010) at Sambalpur University,Sambalpur, Odisha, India.
6. Poster presentation at International Conference on Physics at Surfaces and Interfaces, PSI-2009, Toshali Sands, Puri, India.

Synopsis

The thesis reports the shape evolution of Si-Ge nanostrucrures on various high index silicon surfaces, grown by molecular beam epitaxial (MBE) under ultra-high vacuum (UHV) conditions. The morphological dynamics have been analyzed in different thermodynamic growth conditions and substrate orientations. A comparative study of the Si-Ge structures on the reconstructed high index surfaces, such as, Si(5 5 12), Si(5 5 7) and Si(5 5 3), has been presented in terms of shape transformations with varying substrate temperature, growth coverage and mode of annealing conditions.

The anisotropic surface reconstruction inherent to high-index silicon surfaces makes them potentially significant substrates for electronic device fabrication. These surfaces, consisting of periodic steps and terraces, have attracted renewed attention as templates for the controlled growth of aligned one dimensional (1D) nanostructures [1-4]. The implementation of Ge nanostructures into Si based devices is of great potential for future high-speed devices, due to advantages like enhanced carrier mobilities and smaller bandgap, and hence is attracting an increasing interest in fundamental and applied research [5,6]. A large number of experimental works were devoted to investigate the formation of Si-Ge islands on clean silicon substrates of various orientations due to its use as a model system to understand complex issues related to hetero-epitaxy and technological applications [7-9]. Application of Ge/Si may be found in silicon-based optoelectronics. Due to the indirect band gap, Si devices are not well suited for optoelectronic applications. New devices employing Ge/Si epitaxial layers are expected to overcome this restriction [10]. $Si_{1-x}Ge_x$ alloys show smaller fundamental bandgaps compared to Si, because of larger lattice constant and altered lattice constituents and, due to the acquired tetragonal symmetry in pseudomorphic layers. Strained Si-Ge technology has been recognized as a promising solution for high-performance devices, because of its cost-effectiveness and high carrier mobility. To maximize the transport properties, it is required to tailor the defect morphology as well as the surface morphology properly. Composition grading is one of the well-established techniques to prevent dislocations from reaching the surface [11,12].

The surface symmetry of the substrate influences the strain relaxation and hence the morphology of self-assembled Ge nanostructures. Therefore, in the Ge/Si system following the Stranski-Krastanov (SK) growth mode, stress relaxation and diffusion are crucial for the controlled fabrication of Ge nanostructures on Si substrates [7-10]. Strain relief in hetero-epitaxial system like Ge, or $Si_{1-x}Ge_x$ on a single crystalline silicon surface is a major factor determining the various shapes formed during the growth process. It is known that strained epitaxial layers tend initially to grow as dislocation-free islands and as they increase in size, may undergo a shape transition [13,14]. Below a critical size, islands can have a compact symmetric shape. But at larger sizes, they adopt a long shape, which allows better elastic relaxation of the island's stress [13,14]. Tersoff et al. showed the shape transition of Ge islands from square to rectangular structures [13]. Sekar et al. reported the shape transition as one of the strain relief mechanism in the formation of aligned gold silicide structures (triangular to trapezoidal shape transformation) [14].

In the past, the growth of Ge nanostructures on low index silicon substrates (such as Si(100), Si(111)) has been studied extensively. However, less attention has been paid to Ge growth on high-index Si substrates. Hence, the study of self-assembly of Ge on high-index silicon surfaces would be an important field of research in obtaining various types of aligned nanostructures that may be useful in optoelectronic devices. Among the high index silicon surfaces, Si(5 5 12) is oriented 30.5° away from (001) towards (111) with one-dimensional periodicity over a large unit cell width [15]. Si(5 5 7) with vicinal angle of 9.45° from (111) towards $(11\bar{2}\ )$ [16] and Si(5 5 3) , tilted at -12.27° from the (111) plane towards the (001) plane [17], are important high index Si surfaces. In all the above vicinal surfaces, the step edges are along $\langle 1\bar{1}0\rangle$ direction.

In the chapter one of the thesis, an introduction to high index surfaces and the motivation for the Ge growth to form aligned nanostructures are included. The past and present status of Si-Ge alloy structures on various low index and high index planes are described. The use Compositional grading and importance of graded Si-Ge aligned structures on high index silicon surfaces are emphasized.

Chapter two includes the experimental techniques, which have been used for the growth and characterizations in the thesis work. Different epitaxial growth techniques including molecular beam epitaxy (MBE) are described. The mechanism of the characterization techniques, such as, scanning electron microscopy (SEM), transmission electron microscopy (TEM), high resolution TEM (HRTEM), scanning TEM (STEM), electron dispersive x-ray analysis (EDX), scanning tunneling microscopy(STM), reflection high energy electron diffraction(RHEED), rutherford backscattering spectrometry (RBS), high resolution x-ray diffraction (HRXRD) are briefly presented. The rest of the chapters are based on the analysis of the growth and shape evolution of Si-Ge structures under different thermodynamic growth conditions.

In the first part of the thesis work, growth of Ge nanostructures and microstructures on ultra-clean, reconstructed high index Si(5 5 12) surfaces show that self-assembled growth at optimum thickness of the overlayer leads to interesting shape transformations, namely, from nanoparticle to trapezoidal structures, at higher thickness values. The reconstruction has been confirmed with in-situ reflection high energy electron diffraction (RHEED). Thin films of Ge of varying thickness from 3 to 12 monolayer (ML) were grown under ultrahigh vacuum conditions on a Si(5 5 12) substrate while keeping the substrate at a temperature of 600°C. The substrate heating was achieved by two methods: (i) by heating a filament under the substrate (radiative heating, RH) and (ii) by passing direct current (DC) through the samples in three directions (perpendicular, parallel and at 45° to the step direction $\langle 1\bar{1}0 \rangle$). The temperature was monitored with an infra-red pyrometer, calibrated with a thermocouple attached to the sample holder. We found irregular, more spherical-like island structures under RH conditions. The shape transformations have been found under DC heating conditions and for Ge deposition more than 8 ML thick [18]. The longer sides of the trapezoid structures are found to be along $\langle 1\bar{1}0 \rangle$) irrespective of the DC current direction. Also the absence of such a shape transformation in the case of Ge deposition on Si(111) substrates has been shown. Scanning transmission electron microscopy (STEM) measurements suggested the mixing of Ge and Si [18,19] . This has been confirmed with a quantitative estimation of the intermixing using Rutherford backscattering spectrometry (RBS) measurements [18].

A comparative study has been done for the growth of Ge nano/micro structures on ultra clean, high vicinal silicon surfaces under two substrate heating conditions: direct current (DC) and radiative heating (RH). These were grown under ultra high vacuum conditions while keeping the substrate at a temperature of 600°C.

The results for 10 monolayer (ML) and 12 ML thick Ge deposited on the above surfaces show spherical island structures for RH conditions while aligned trapezoidal structures were observed under DC conditions of heating. In the case of 10 ML Ge deposited on Si (5 5 7), elongated $\mathrm{Si}_{1-x}\mathrm{Ge}_x$ nanostructures with an average length of $\sim$ 300 nm and a length/width ratio of $\sim$ 3.1 have been formed along the step edges. Under similar conditions for 10 ML Ge growth on Si(5 5 12), we found aligned $\mathrm{Si}_{1-x}\mathrm{Ge}_x$ trapezoidal microstructures of length $\sim$ 6.25 μm and an aspect ratio of $\sim$ 3.0. The longer side of the trapezoidal structures is about $\sim$ 21 times larger in case of Si(5 5 12) compared to Si(5 5 7). STEM measurements showed the mixing of Ge and Si at the interface and throughout the over-layer . Detailed electron microscopy studies SEM and STEM reveal the structural aspects of these microstructures [19].

To have more understanding of Ge-Si structures on high index surfaces, similar analysis were done on 3 to 10 ML Ge/Si(5 5 3) systems. As an outcome, it has been experimentally observed that $\mathrm{Si}_{1-x}\mathrm{Ge}_x$ grown on reconstructed high index surfaces, such as, Si(5 5 12), Si(5 5 7) and Si(5 5 3) show a universality in the shape evaluation, irrespective of the substrate orientations and size of the island structures. In the case of Ge/Si (5 5 12) system, the size of the aligned structures are of micrometer size. But for the Si(5 5 7) and Si(5 5 3) systems, the size of the aligned structures are of nanometer size, though the shape evolution and also the aspect ratios are similar to that of Si(5 5 12) . The aspect ratios of the Si-Ge elongated structures on Si(5 5 12), Si(5 5 7) and Si(5 5 3) increase in a similar fashion as a function of increasing Ge growth coverages [20] .

A part of the thesis work is devoted to the theoretical modeling which complements the shape evolution mechanism. The theoretical model includes 2D kinematic Monte Carlo (kMC) simulation, which is a phenomenological model that was intended to explain the phenomena of shape transition observed in the experiments. In our model, we introduce anisotropy through binding energies of different types of bonds and the dependence of surface barrier on the direction of hopping. A deviation parameter (ϵ) was introduced in the surface barrier term (E_D) to take the effect anisotropic diffusion , as one of the plausible mechanisms [21]. In this work, the kinetic Monte Carlo simulations were performed on a $L \times L$ square lattice with $L = 100, 200, 300, 400$. The coordinate system has been chosen in view of the reconstructed high index silicon surfaces, such that the x-axis is directed perpendicular to the step edges and Si-Ge structures are formed along the y-axis, along the step direction. We have experimentally observed a universality in the growth of the islands for all three high index surfaces by evaluating the aspect ratios and size of the Si-Ge structures. The kMC simulations show that such variations can be understood by introducing a deviation parameter ϵ in surface barrier term E_D. The experimentally observed shape variations and the growth exponent values are in good agreement with kMC simulations. This suggests the role of stochastic process involved in the shape transitions of nanoscale structures.

To see the effect of substrate temperature during growth, a temperature dependent shape evolution study was carried out. The morphological evolution depending on the various substrate temperatures during growth and the mode of heating the substrate has been analyzed. Ge-Si structures were obtained by depositing 10 ML of Ge on reconstructed Si(5512) using Molecular Beam Epitaxy (MBE) under ultra high vacuum(UHV) at different substrate temperatures ranging from room temperature (RT) to 800°C with two modes of substrate heating i.e. by RH and DH. The post-growth characterization of the samples was carried out ex-situ by FEGSEM , cross-sectional transmission electron microscopy(X-TEM) and Rutherford Backscattering Spectrometry . In the radiative heating (RH) case, we found spherical island structures of average size ∼15.5 nm at 600°C with a bimodal distribution, which upon increasing temperature got faceted at 700°C. At 800°C thick (∼ 100nm) dome like structures are formed. In the case of DC heating case, from RT to 400°C no regular aligned structures found; but after the critical temperature 600°C, well aligned trapezoidal $Si_{1-x}Ge_x$ structures starts forming along the step edges [21].

In the last part of the thesis work, a compositional analysis of the Ge-Si structures were carried out .The composition of these nanostructures has been characterized by using STEM - EDS. Rutherford backscattering spectrometry and the synchrotron-based high resolution x-ray diffraction (HRXRD). The HRXRD showed presence of graded $Si_{1-x}Ge_x$ system for the Si(5 5 12)and is also confirmed by RBS measurements [22]. While RBS measurements show no prominent graded $Si_{1-x}Ge_x$ structures for the case of Si(5 5 3)and Si(5 5 7) substrate orientations.

In conclusion, the thesis work has dealt with growth, shape evolution and compositional analysis of $Si_{1-x}Ge_x$ structures on three high index silicon surfaces Si(5 5 12), Si(5 5 7) and Si(5 5 3). A comparative analysis of these structures has been done under different growth conditions varying growth coverages, substrate temperature and mode of heating. A phenomenological theoretical modeling with 2D kinetic Monte Carlo Simulation compliments the experimental findings.

References

[1] J. R. Ahn, Y. J. Kim, H. S. Lee, C. C. Hwang, B. S.Kim, and H.W. Yeom , Phys. Rev. B **66**, 153403 (2002).

[2] Mahesh Kumar, and S. M. Shivaprasad, J.Nanosci. Nanotechnol. **9**, 5420 (2009).

[3] Huiting Li, Y.-N. Xu, Y.-Z. Zhu, Hidong Kim, and Jae M. Seo, Phys. Rev. B **75**, 235442 (2007).

[4] H. Kim, G. Duvjir, O. Dugerjav, Huiting Li and Jae M. Seo, Phys. Rev. B **81**, 245422 (2010).

[5] Y. Wu, R. Fan, and P. Yang, Nano Lett. **2**, 83 (2002).

[6] Minjoo L. Lee, Eugene A. Fitzgerald, Mayank T. Bulsara, Matthew T. Currie, and Anthony Lochtefeld J. Appl. Phys. **97**, 011101 (2005).

[7] Y -W Mo, D. E. Savage, B. S. Swartzentruber, and M. G. Lagally, Phys.Rev. Lett. **65** , 1020 (1990).

[8] L. Persichetti, A. Sgarlata, M. Fanfoni, and A. Balzarotti, Phys.Rev. Lett. **104**, 036104 (2010).

[9] Bert Voigtlander, Surf.Sci.Rep. **43**, 127 (2001).

[10] A. I. Yakimov, A. V. Dvurechenskii, Yu Yu Proskuryakov , A. I. Nikiforov , O. P. Pchelyakov , S. A. Teys , and A. K. Gutakovskii,Appl. Phys. Lett. **75**, 1413 (1999).

[11] J. M. Baribeau, T.E.Jackman, D.C.Houghton,P. Maigne, M. W. Denhoff, J. Appl. Phys. **63**, 5738 (1988).

[12] E. A. Fitzgerald, Y. H. Xie, M. L. Green, D. Brasen, A. R. Kortan, J. Michel, Y. J. Mii, B. E. Weir,Appl. Phys. Lett. **59**, 811 (1991).

[13] J. Tersoff, and R. M. Tromp, Phys.Rev. Lett. **70**, 2782 (1993).

[14] K. Sekar, G. Kuri, P. V. Satyam, B. Sundaravel, D. P. Mahapatra, B. N. Dev, Phys. Rev. B **51**, 14330 (1995).

[15] A. A. Baski, S. C. Erwin, and E. J. Whiteman, Science **269**, 1556 (1995).

[16] A. Kirakosian, R. Bennewitz, J. N. Crain, Th. Fauster, J.-L Lin , D. Y. Petrovykh, and F. J. Himpsel Appl. Phys. Lett. **79**, 1608 (2001).

[17] S. Hara, M. Yoshimura, and K. Ueda, J. J. Appl. Phys. **47**, 7 (2008).

[18] J. K. Dash, A. Rath, R. R. Juluri, P. Santhana Raman, K. Müller, A. Rosenauer and P. V. Satyam,J.Phys. Condens. Matter **23**, 135002 (2011).

[19] J. K. Dash, A. Rath, R. R. Juluri, P. Santhana Raman, K. Müller, M. Schowalter, R. Imlau, A. Rosenauer, P. V. Satyam, J.Phys. Conf. Series **326**, 012021 (2011).

[20] Universality in shape evolution of $Si_{1-x}Ge_x$ structures on high index silicon surfaces, J. K. Dash, T Bagarti, A. Rath, R. R. Juluri and P. V. Satyam, Submitted to Eur. Phys. Lett.(2012) (Under review); arXiv:1204.0578v1.

[21] Shape evolution of MBE grown $Si_{1-x}Ge_x$ structures on high index Si(5 5 12) surfaces : A temperature dependent study, J. K. Dash , A. Rath, R. R. Juluri and P. V. Satyam,Submitted to J. Physics D: Appl.Phys. (2012)(Under review) ; arXiv:1205.6039v1.

[22] Compositional analysis of Aligned trapezoid Si-Ge structures on Si(5 5 12) surfaces, J. K. Dash, A. Rath, R. R. Juluri and P. V. Satyam, To be published (2012).

Contents

List of Figures

Chapter 1

Introduction

In recent years, the field of nanoscience and nanotechnology has experienced a veritable explosion of ideas, which resulted in many potential applications for nanostructured materials. The key feature that nanostructures offer for such a diverse range of potential applications is the ability to tailor the electronic , optical, and magnetic structures and properties of materials [1–6]. The ability to easily synthesize nanometer scale structures is an essential ingredient for further advances in nanoscience and nanotechnology. It is desirable to have a very clean environment (ultrahigh vacuum condition, UHV) where the concentration of impurity atoms present is extremely low so that they can hardly change the properties of nanostructures significantly. Recently, self-assembled techniques have attracted considerable interest for nanoscale device applications because these techniques offer the potential to fabricate nanoscale elements such as quantum dots, quantum wires and electronic device configuration without direct use of conventional lithography techniques. A number of self-assembly techniques have been reported for fabricating nanoscale structures. Molecular beam epitaxy (MBE) is one of the most important techniques working under UHV ($\approx 10^{-10}$ mbar) condition for growing self-assembled nano-structures with precise control on growth [7]. The most important feature of MBE grown structures is their crystalline quality and very low impurity level which is an important requirement for modern microelectronics. In this thesis work, growth of Ge and $\mathrm{Si}_{1-x}\mathrm{Ge}_x$ structures by MBE method and their characterization by ion, x-ray and electron scattering methods would be presented.

Heteroepitaxy is one of the main routes to the growth of self-assembled nanostructures on silicon surfaces. The parameters that determine the thermodynamically favored growth modes are *surface and interface energies* and *strain.* Epitaxial growth can occur in diferent modes depending on the surface free energies of the overlayer , the substrate and their lattice misfit. Three established growth modes are (a) Frank-van der Merwe (FM) or layer-by-layer [8], (b) Volmer-Weber (VW) or island [9] and (c) Stranski-Krastanov (SK) or layer-plus-island growth [10]. If the materials of the film and the substrate are same, it is called *homoepitaxial* growth whereas in *heteroepitaxial* growth, the materials of the film and the substrate are different. The heteroepitaxial growth can, in general, be categorized as crystal growth under stress and usually produces a strained epitaxial layer due to lattice mismatch between the overlayer and the substrate. The strained layers grow pseudomorphically upto a critical thickness beyond which there is a strain relaxation by introducing dislocations [11].

The growth of Ge nanostructures on atomically clean Si surfaces is a classic example of heteroepitaxial Stranski-Krastanov (SK) growth. Ge/Si is a prototype for elemental semiconductor heteroepitaxy that exhibits self-organization. The system is currently seen as one of the most promising for a variety of device applications [5, 12–14]. Due to 4.2% lattice mismatch between Ge and Si, a pseudomorphic Ge layer grows with a strain. As the strain energy builds up, the competition between the surface energy and the strain energy eventually causes the film to undergo a 3-D island growth at higher coverages. Incorporation of germanium into a silicon lattice can be achieved over the entire compositional range of $\mathrm{Si}_{1-x}\mathrm{Ge}_x$ for $0 < \mathrm{x} < 1$ to form a random alloy with the lattice parameter varying almost linearly with composition. Technological advancements using strictly Si devices are beginning to push fundamental limits of physics. Si-Ge based heterostructures offer possible alternatives with strain based engineering, and self-assembled nanostructures [15–18]. Due to the indirect band gap, Si devices are not well suited for optoelectronic applications. New devices employing Ge/Si epitaxial layers are expected to overcome this restriction. $\mathrm{Si}_{1-x}\mathrm{Ge}_x$ nanostructures can be used in Si-based future high-speed devices, due to advantages like enhanced carrier mobility and smaller bandgap [19–21].

Due to its process- and damage-free features, structural self-organization has received wide interest in modern research. Of particular importance is the formation of coherent low dimensional nanostrucures during epitaxial growth in lattice-mismatched materials, including Ge/Si and In(Ga)As/GaAs, by molecular-beam epitaxy [22,23]. These islands have usually been grown on low-index substrate surfaces and their growth has been extensively studied from experimental and theoretical viewpoints. More recently, the study of self-organization has been extended to the use of high-index surfaces and there has been some success in obtaining various types of nanostructures that have unique electrical and optical properties [24,25]. However, regarding Ge/Si systems, most previous work has focused on the growth of Ge on Si(100)and Si(111) substrates and little attention has been paid to Ge growth on high-index Si substrates.

A high index (vicinal) surface is misoriented from the low index plane by a small angle θ(vicinal angle or miscut angle), relative to low index surfaces e.g., [001] or [111]. The reconstructed surface shows periodic steps and terraces. The anisotropic surface reconstruction on high-index silicon surfaces makes them potentially significant substrates for the growth ordered nanostructures. Such matrices can be used as templates for self-assembling arrays of low dimensional with controlled size and periodicity.The width of the terraces and step height can easily be modulated with temperature and coverage. Several previous works have been reported on the formation of aligned low dimensional metal and semiconductor nanostructures on high index surfaces [26–32]. In this thesis work, stable high index surfaces, like Si(5 5 12), Si(5 5 7) and Si(5 5 3) substrates have been used for the study of Ge growth , varying different growth parameters, such as, substrate temperature, growth coverage and modes of annealing.A detailed study of growth dynamics,shape evolution of Ge-Si nanostructures , theoretical kinetic MonteCarlo modeling and the compositional analysis is presented in the thesis. The Ge-Si structures undergo a variety of shapes like spherical quantum dots, elongated rectangular structures, aligned trapezoidal islands and faceted dome structures, according to the substrate orientations and growth conditions.

We have used the kinetic Monte Carlo (kMC) method to study the shape transition of Ge island on Si surfaces. The kMC method takes into account only the microscopic interaction between the neighboring particles and the system evolve according to the master equation [33]. The transition between different states of the system is given by a transition probability which depends in general on the initial and the final states. Kinetic Monte Carlo method has been used extensively to study the formation of nanoisland in a number of works [34, 35], however Monte Carlo studies of island formation with shape transition has hardly been studied. Anisotropic island growth has been studied previously by a number of authors [36–38]. Theoretical modeling using kMC studies of anisotropic growth has been carried out to show elongated island formation in Ref. [39]. Our model closely follow the above model in which both isotropic and anisotropic growth of islands are seen. We will also see the shape transition from rod shaped islands at lower coverage to trapezoidal islands at higher coverage. This has been obtained by introducing only a single parameter ϵ that accounts for the assymetry that arises due to the applied DC current through the sample. The details are described in the thesis chapters.

Strained Ge-Si technology has been recognized as a promising solution for high-performance devices, because high carrier mobility is realized with the cost-effectiveness being kept at the current level by utilizing this material system. In particular, electron mobility is enhanced significantly. To maximize the transport properties, it is required that the defect morphology as well as the surface morphology are well-tailored. Deterioration of the morphology is brought about during the growth of as train-relaxed Si-Ge which is involved to impose stress on the Si layers.Composition grading is one of the well-established techniques to prevent dislocations from reaching the surface [40–42]. We have observed an interesting phenomena where in graded $Si_{1-x}Ge_x$ structures are grown in a single step procedure. The experimental analysis using STEM-EDS, HRXRD and RBS has been carried out in the thesis work.

The classic Ostwald ripening model and its extensions to 3D islands on surfaces [43,44] predict that the chemical potential of an island decreases continuously with size because of the decreasing radius of curvature and surface/volume ratio. The atoms then have a higher probability to detach from smaller islands and to attach to larger ones, thus the larger islands grow at the expense of the smaller ones, which means that the average island size increases with time and the surface number density of islands decreases. The island size distribution on Ge/Si samples with co-existing pyramids and domes remains bimodal during growth and annealing [45]. So, it clearly does not correspond to a simple Ostwald ripening. It has been suggested that a discontinuous change in the chemical potential of an island during its shape transformation could modify Ostwald ripening kinetics to produce a bimodal distribution [46,47]. The evolution of spherical Ge island to strained Ge-Si faceted dome structures is investigated as a function of growth temperature .

The thesis is organized as follows. Following an introduction in chapter 1, chapter 2 presents the different techniques for growing self-assembled nanostructures, different growth modes and description and principles of operation of characterization techniques used in this work. In chapter 3, the DC heating induced shape transformations of Ge-Si structures on Si(5 5 12) surfaces are presented. We show that self-assembled growth at optimum growth coverage leads to interesting shape transitions, namely from nanoparticle to trapezoidal structures along the step edge, at higher thickness values. The DC heating, in this case, is a necessary condition for the formation of aligned Trapezoidal structures along the step $\langle 1\bar{1}0\rangle$. A comparative study of Ge-Si structures on the Si(5 5 12), Si(5 5 7) and Si(5 5 3) surfaces under two substrate heating conditions: direct current (DC) and radiative heating (RH), is presented in chapter 4. We have observed a universality in the growth dynamics in the three systems irrespective of the size of the nanostructures and orientation of the substrates. We present a quantitative measurement of critical area of the Ge-Si island for the shape transition. A phenomenological kinetic Monte Carlo simulation supplements the shape evolution mechanism in the high index Si surfaces. The details of the growth dynamics in terms of aspect ratio, size exponent and the theoretical modeling are presented. Chapter 5 describes the temperature dependent study of the Ge-Si islands in the three high index systems. The shape evolution has been investigated as function of substrate temperature and mode of heating the substrate(RH and DH). In the RH condition, we show the formation of spherical islands with a bimodal distribution. At elevated temperatures, we have observed strained Ge-Si faceted dome structures at the expense of smaller islands. In DH case,we show that at an optimum critical temperature, there is shape variation occurred to form well aligned trapezoidal structures parallel to the step direction. We have performed the detailed compositional analysis of the $\mathrm{Si}_{1-x}\mathrm{Ge}_x$ structures , which has been described in the chapter 6. Chapter 7 presents the summary and conclusions of this thesis work.

Chapter 2

Growth of Self-assembled nanostructures and characterization techniques

2.1 Introduction

A brief overview of thin film growth techniques and characterization methods is presented in this chapter. This is a prelude to the details in subsequent chapters on fundamentals of growth phenomena, details of growth processes, and characterization tools employed in the thesis work.

Thin film growth is an essential part in modern device fabrication. It requires a very precise control over the thickness and uniformity of films as thin as a few nanometers. In addition, excellent material homogeneity and purity, sharp interfaces between the layers, and controlled doping profiles are required. To achieve these high quality films, epitaxial growth techniques such as molecular beam epitaxy (MBE) is the most suitable among the various growth techniques.

2.2 Self-assembled growth

”Self-assembly” refers to the spontaneous formation of structures with a well-defined size and shape distribution typically determined by thermodynamic stability of the structures and/or growth kinetics by virtue of which a disordered system of preexisting components forms an organized structure or pattern as a consequence of specific, local interactions among the components themselves, without external direction. When the constitutive components are molecules, the process is termed molecular self-assembly.

Self-assembled growth is a bottom-up process, where nanostructures are formed from their basic building blocks, such as atoms or molecules. Self-assembled growth is associated with the growth of atoms or molecules that undergo exquisitely selective binding and obey highly specific rules for self-assembly. The general importance and desirability for advancement of technology requires a high degree of control of composition, size and structure. This is so critical to the area of nanostructure synthesis that self-assembly has been an increasing hallmark of this field.

2.3 Growth Modes

A thin film grown on a substrate by various methods may be amorphous, polycrystalline or single crystalline depending upon the substrate, the substrate temperature, the material of the film and the method of deposition. In case of single crystallinity, the film may be epitaxial. *Epitaxy* is ordered growth of a crystalline film on a preexisting single crystalline substrate. The term epitaxy comes from a Greek root ("*epi*" means above and "*taxis*" means in ordered manner) which could be translated to "*arrange upon*". The deposited film is called the epitaxial film or epitaxial layer or simply an epilayer. If an epitaxial film is grown on a substrate of the same composition, the process is called homoepitaxy; otherwise, it is called heteroepitaxy. What differentiates epitaxial growth from crystal growth are the nature and the strength of the chemical bonds of both the substrate and deposit crystal on one hand, and the crystal lattice parameters on the other. In other words, both crystals differ energetically and geometrically. If both crystals do not differ simultaneously energetically and geometrically, which means that they are identical, we have the usual crystal growth [48]. Three principal growth modes [49] of epitaxial growth are generally distinguished in Fig.2.1. These modes are named after their original investigators and are as follows:

(1) *Layer-by-layer* or *Frank-van der Merwe* (FM) growth mode (Fig. 2.1(a)), refers to the case when the film atoms are more strongly bound to the substrate than to each other. As a result, each layer is fully completed before the next layer starts to grow, i.e., strictly two-dimensional growth takes place [8].
(2)*Island or Volmer-Weber (VW)* growth mode (Fig. 2.1(c)) corresponds to the situation when film atoms are more strongly bound to each other than to the substrate. In this case, three-dimensional islands nucleate and grow directly on the substrate surface [9].
(3) *layer-plus island* or *Stranski-Krastanov* (SK) (Fig. 2.1(b)) represents the intermediate case between FM and VW growth. After the formation of a complete two-dimensional layer, the growth of three-dimensional islands takes place. The nature and thickness of the intermediate layer (often called the Stranski-Krastanov layer) depend on the particular case (for example, the layer might be a submonolayer surface phase or a strained film several monolayers thick) [10].

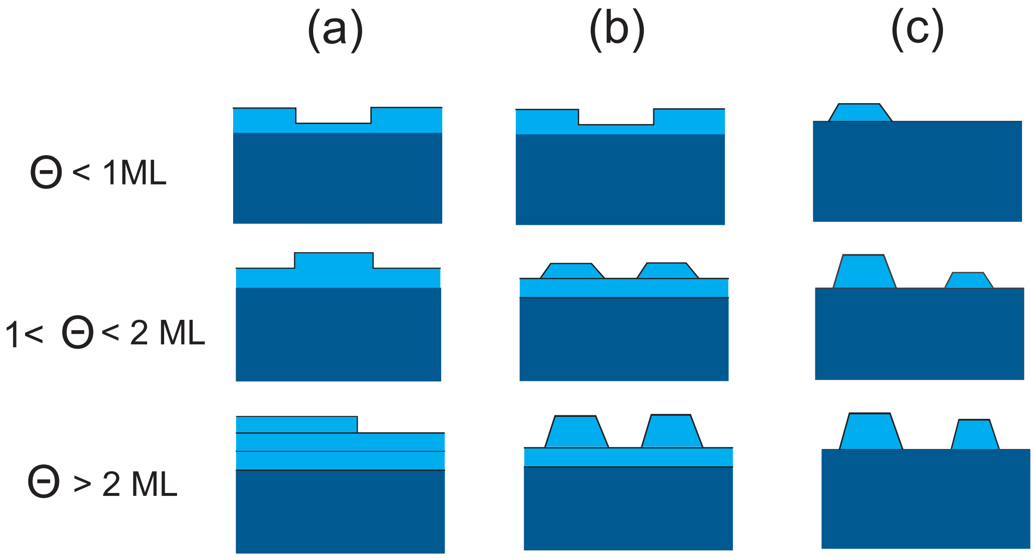

Figure 2.1: Schematic representation of the three main growth modes: (a) layer-by-layer (Frank-van der Merwe, FM) growth mode (b) layer-plus-island (Stranski-Krastanov, SK) growth mode (c) Island (Volmer-Weber, VW) growth mode [50].

The occurance of different growth modes can be understood qualitatively in terms of the surface or interface tension or surface free energy σ. This is defined as the work that must be performed to build a surface (or interface) of unit area. σ can also be interpreted as a force per unit length of boundary, considering the contact point of the island and the substrate (Fig. 2.2). If the island contact angle is ϕ, the force equilibrium can be written as

$$\sigma_s = \sigma_i + \sigma_f cos\phi \tag{2.1}$$

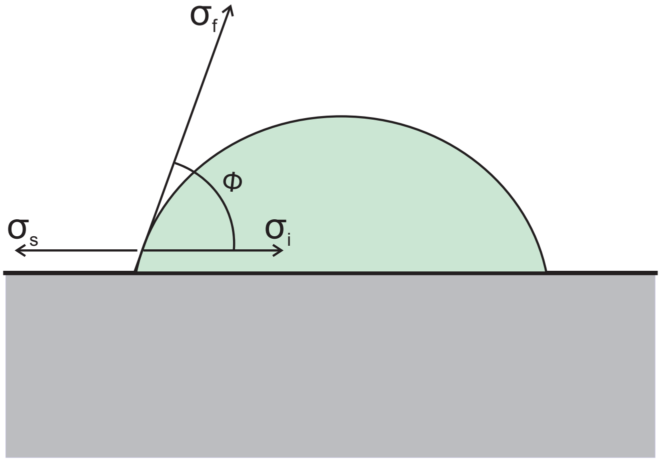

Figure 2.2: Schematic of an island film on a substrate. σ_s is the surface free energy of substrate, σ_f is the surface free energy of film surface and σ_i is that for film/substrate interface. The balance of forces acting along the substrate surface yields equation 2.1 [50].

where, σ_s is the surface free energy for the substrate surface, σ_f is that for the film surface and σ_i is the surface free energy of the film/substrate interface called interfacial energy [50]. Layer-by-layer growth (FM growth) is obtained when

$$\Delta\sigma(n) = \sigma_f(n) + \sigma_i(n) - \sigma_s \leq 0 \tag{2.2}$$

for all n (i.e., independent of the thickness). "n" corresponds to the number of monolayers in the film [49]. Here the n-dependent strain energy in the film has been absorbed in $\sigma_i(n)$. σ_f and σ_s are the values for the semi-infinite crystals, and σ_f(n) deviates somewhat from σ_f due to n-dependent surface strain. The condition for the FM growth is rigorously fulfilled only for the homoepitaxial growth in which case $\sigma_f \equiv \sigma_s$ and $\sigma_i(n) \equiv 0$, or more generally for zero misfit, i.e., when the strain contribution σ_i^ϵ(n) to σ_i(n) is zero and

$$\sigma_f + \sigma_i^0(n) - \sigma_s \leq 0 \tag{2.3}$$

Here $\sigma_i^0(n)$ is the zero strain contribution to $\sigma_i(n)$ which depends on the specific chemical interaction between film and substrate atoms and rapidly approaches zero within the first few monolayers, depending upon the range of the interatomic forces. In all other cases, the increase of the strain energy with n leads to an increase of σ_i(n) until at a given n = n* the FM condition is not fulfilled any longer and three dimensional crystals form (SK mode). If the FM condition is not fulfilled from the very beginning (n = 1) then three dimensional crystals form immediately on the substrate (VW mode). These three growth modes have also been subsequently [51] called class I, II, and III behaviour for the FM, SK, and VW modes, respectively, and have recently been studied in great details in the theory of wetting and layering transitions as complete wetting, incomplete wetting, and nonwetting cases [52–54].

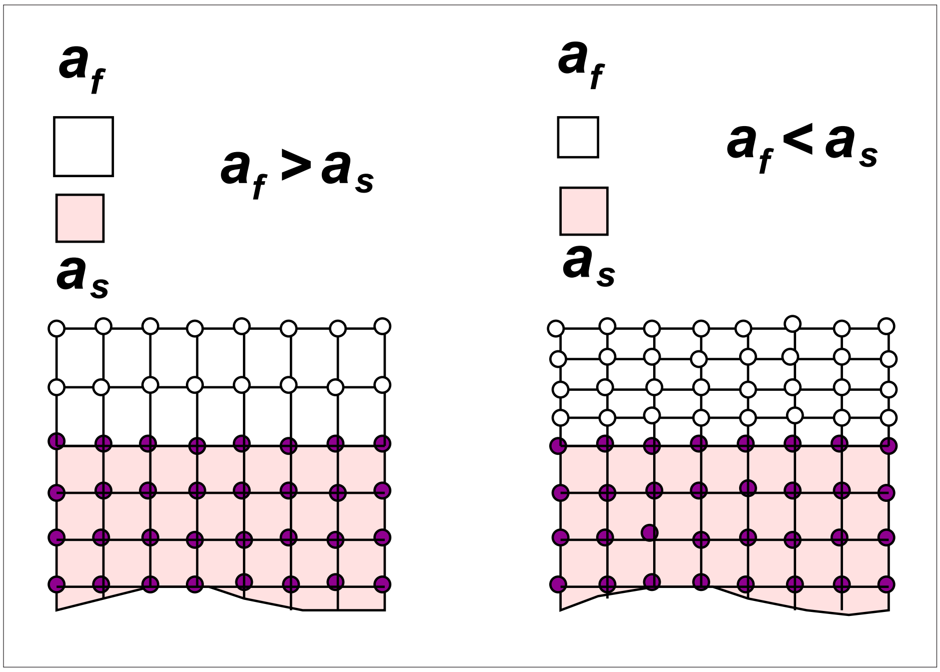

Figure 2.3: Illustration of strain of the overlayer due to the lattice mismatch of substrate and film material [55].

The role of lattice misfit between the film and the substrate which leads to a strain energy that serves as the driving force for island formation in almost every case. Strain in the epitaxial layer due to lattice mismatch is schematically shown in Fig. 2.3. A surprising result is the fact that systems with strong film-substrate interactions do not, in most cases, produce uniform films of arbitrary thickness. The more common observation in this case is the Stranski-Krastanov configuration shown in Fig. 2.1.The relative strength of the film-substrate potential (W) is defined as the ratio of the interfacial energy of the film-substrate interaction (σ_i) and the energy of the film-film interaction (σ_f), i.e.,

$$W = \frac{\sigma_i}{\sigma_f} \tag{2.4}$$

Large film-substrate interactions are represented by W $\gg$ 1. The degree of misfit, η is defined as the difference between the film lattice constant (a_f) and the substrate lattice constant (a_s), normalized by the substrate lattice constant (a_s), i.e.,

$$\eta = \frac{a_f - a_s}{a_s} \tag{2.5}$$

Equilibrium growth modes [56], as a function of misfit (η) and strength of film-substrate interaction (W), are shown by the so-called phase diagram in Fig.2.4. From Fig. 2.4, it is seen that the only driving force for uniform films (FM) is a strong interaction between the film and substrate which requires that W > 1 and zero misfit. For zero misfit ($\eta = 0$), VW growth occurs for W < 1. For non-zero misfit, VW growth occurs when W $\geq$1. For smaller misfit while W > 1 corresponds to SK growth. For higher misfit, VW to SK transition may occur when W $\gg$ 1.

2.4 Epitaxial growth techniques

There is a great variety of techniques used for the growth of thin films. In the last few decades, some more modern epitaxial techniques - like molecular beam epitaxy (MBE), metal organic vapour phase epitaxy (MOVPE), hydride vapour phase epitaxy (HVPE) etc. have been developed.In this section we present a brief description of some of the techniques which are used for epitaxial growth.In this thesis work, we have used only MBE method for the growth (discussed in details at subsection 2.4.5). For the sake of completeness, a brief summary of the other commonly used experimental methods have also been described.

2.4.1 Chemical Beam Epitaxy

Thin film growth performed by means of surface chemical reactions is defined by the general term *chemical vapour deposition* (CVD). In this technique, the source material

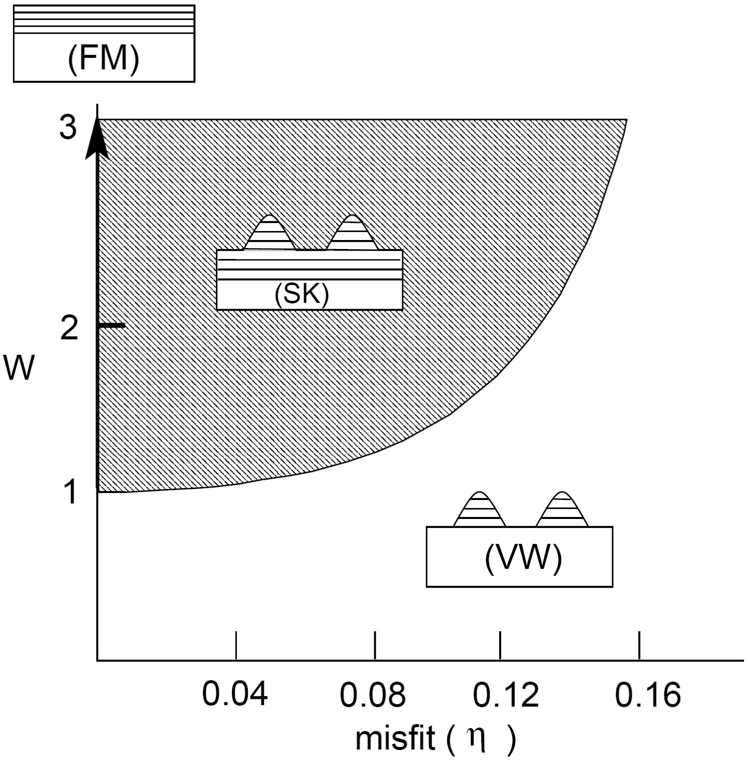

Figure 2.4: Equilibrium growth modes, as a function of misfit (η) and strength of film-substrate interaction (W). The solid line separates the regions of VW mode and SK mode. FM mode is confined to the region η= 0.0 with W > 1.

is supplied to the sample surface in the form of its gaseous compounds. Precursor gas molecules decompose at the hot surface, leaving there the desired species, while the waste fragments of the molecules are desorbed from the surface. The group IV and the group V compounds are supplied usually as hydrides, such as SiH_4, GeH_4, AsH_3, PH_3 etc., while the group III components are supplied as metal-organic compounds, such as trimethyl gallium [$Ga(CH_3)_3$ (TMGa)], trimethyl indium [$In(C_2H_5)_3$ (TMIn)], etc. Conventionally the term metal-organic CVD (MOCVD) refers to growth conducted at relatively high pressures ($\sim$ 1 - 760 Torr). If the growth is performed under ultrahigh vacuum (UHV) conditions, the technique is called *metal organic* MBE (MOMBE) or *chemical beam epitaxy* (CBE). Due to a large mean free path of the gas molecules at low pressure, CBE growth is not affected by reactions in the gas phase and only surface chemistry here determines the growth process. In comparison to MBE, CBE is far more complex and conventionally requires higher temperatures. However, it provides higher growth rates with conservation of high film crystallinity.

2.4.2 Solid Phase Epitaxy

Solid phase epitaxy (SPE) is a specific regime of MBE growth, in which an amorphous film is first deposited at a lower temperature and is then crystallized upon heating to a higher temperature. Generally, the crystallinity of films grown by SPE is slightly lower than that of MBE-grown films. However, SPE might be advantageous over MBE in achieving abrupt doping profiles in epitaxial semiconductors films.

2.4.3 Liquid Phase Epitaxy

Liquid Phase Epitaxy (LPE) was the first epitaxial process used for the growth of compound semiconductors [57]. By placing a seed crystal wafer in contact with a liquid solution saturated with the constituents can be used to grow an epitaxial layer by LPE as the solution is cooled very slowly. LPE allows for epitaxy at lower temperatures and produces relatively pure films, but it does not produce films of uniform thickness.

2.4.4 Vapor Phase Epitaxy

Many semiconductor materials can be grown epitaxially by allowing a suitable mixture of gaseous vapours containing the constituent elements to react with a heated seed or substrate, a process known as *vapor phase epitaxy* (VPE). It involves the physical transport of gas phase precursors, or atomic/molecular constituents, to a heated crystalline solid substrate surface, where epitaxial growth occurs and gaseous byproducts are released. The reactant species is transported to the substrate by a carrier gas (generally highly purified hydrogen or nitrogen gas). Depending on the transport gas species, the deposition process is termed as - chloride VPE (ClVPE), hydride VPE (HVPE) and metal-organic VPE (MOVPE). VPE using metal-organic compounds as the precursor is known as MOVPE, also termed as metal-organic chemical vapour deposition (MOCVD). This technique is extensively used to grow III-V compound semiconductors where the standard precursors are organometallic compounds of group III elements and hydrides of group V elements. The technique is ideally suited for large area growth and produces material with excellent control of morphology, thickness, composition and doping. VPE is a relatively rapid method of film growth which is readily scaled to manufacturing volume, but VPE takes place at relatively high temperatures which can enhance the bulk diffusion.

2.4.5 Molecular Beam Epitaxy

In *molecular beam epitaxy* (MBE), growth occurs under UHV conditions and the material for the growing film is delivered to the sample surface by beams of atoms or molecules, i.e., via deposition. During growth, the substrate is conventionally kept at a moderately elevated temperature, which is sufficient to ensure that the arriving atoms migrate over the surface to the lattice sites, but at the same time is not too high to induce diffusion intermixing between the substrate and the already grown film. Fig. 2.5. schematically shows the process of MBE growth.

Ge growth presented in the thesis work has been carried out using MBE. First we describe the equipments used for the growth and characterizations of self-assembled epitaxial nanoislands. A custom-made compact MBE system along with the capability to transfer the MBE-grown samples to a UHV transfer chamber/suitcase as well as to a commercial UHV STM, designed by us in collaboration with and assembled by Omicron Vacuumphysik GmbH, has been installed in our laboratory. A UHV variable temperature scanning tunneling microscope (VTSTM from Omicron) has been coupled with the MBE system at a later date. With the system shown in Fig. 2.6, it

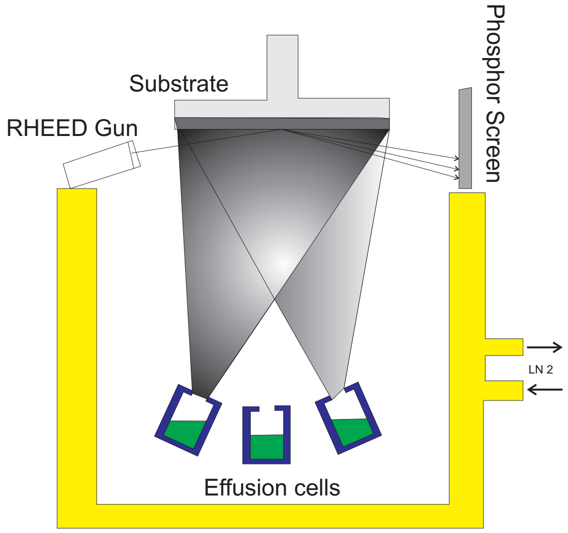

Figure 2.5: Schematic sketch of the main facilities used in MBE growth, including deposition sources (Knudsen cells), shutters, substrate at the heating block, RHEED system for monitoring sample surface structure prior to and in the course of deposition, all installed in a UHV chamber.

is possible to grow and characterize thin epitaxial layers of metals and semiconductors on atomically clean surfaces of single crystal substrates. The MBE system has three Knudsen cells, a low power electron beam evaporator, a quartz microbalance (QM) and a residual gas analyzer (RGA). There is also a *reflection high energy electron diffraction* (RHEED) equipment fitted to the MBE unit for monitoring surface reconstruction and growth. For sample cleaning, it has direct heating as well as Ar ion sputtering facilities. The sample manipulator has a Z-translation (vertical) and the azimuthal angle can be varied over 360°. It also has a resistive heating facility so that the substrate temperature can be raised up to 900°C by resistive heating. Epitaxial growth of different materials are controlled by the substrate temperature and the rate of deposition. Out of the three Knudsen cells, one is capable of reaching 1400°C, the other two cells can reach 1700°C. The electron beam evaporator is used for deposition of silicon. With the option of three Knudsen cells and the electron beam evaporator, epitaxial multilayers can be grown. A load-lock chamber is attached with the main MBE chamber for initial sample mounting. A mounted sample in the load-lock chamber is transferred to the MBE chamber using a sample transfer mechanism on a magnetically coupled transfer rod. Using another transfer rod the sample can be transferred to the VT STM stage for STM studies without disturbing the UHV condition. The temperature range achievable in the VTSTM is 25 K - 1400 K. The best base pressure achieved in the MBE chamber is 3×10^{-11} mbar and that in the VTSTM chamber is 6×10^{-11} mbar. This combined MBE-VTSTM system and its initial performance have been described in ref [58].

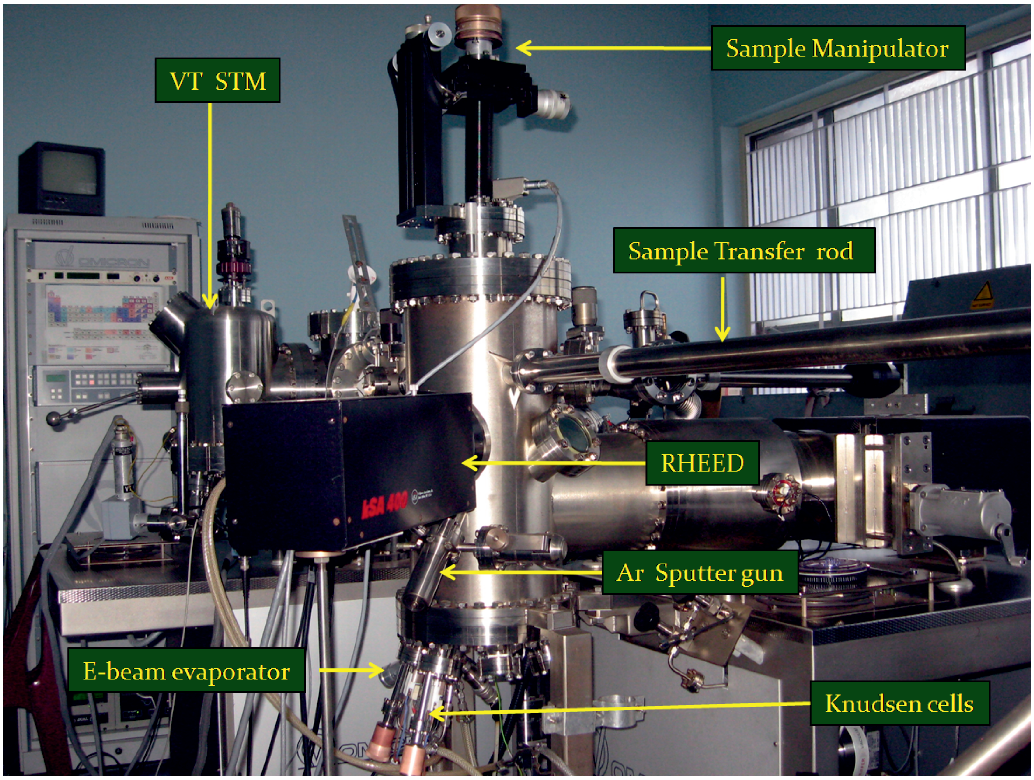

Figure 2.6: A custom-designed compact MBE system (MBE chamber diameter: 250 mm) and a UHV variable temperature scanning tunneling microscope (VTSTM) attached to it [58].

2.5 Characterization techniques

To have a comprehensive study of the materials properties of the grown films, an understanding of the structural aspects is important. Various characterization tools used to study the Ge-Si structures in the thesis work will be discussed briefly in the following sections.

2.5.1 Scanning Tunneling Microscopy

The *scanning tunneling microscopy* (STM) was developed in the early 1980s by Gerhard Binnig and Heinrich Rohrer, who were awarded the Noble Prize in Physics in

1986 for this invention. The atomic resolution capability of STM directly in real space for surfaces of conducting materials has become the most important feature. The extremely high lateral as well as vertical resolution makes STM an outstanding microscopy. In addition, the atomic resolution capability in real space has several important consequences.

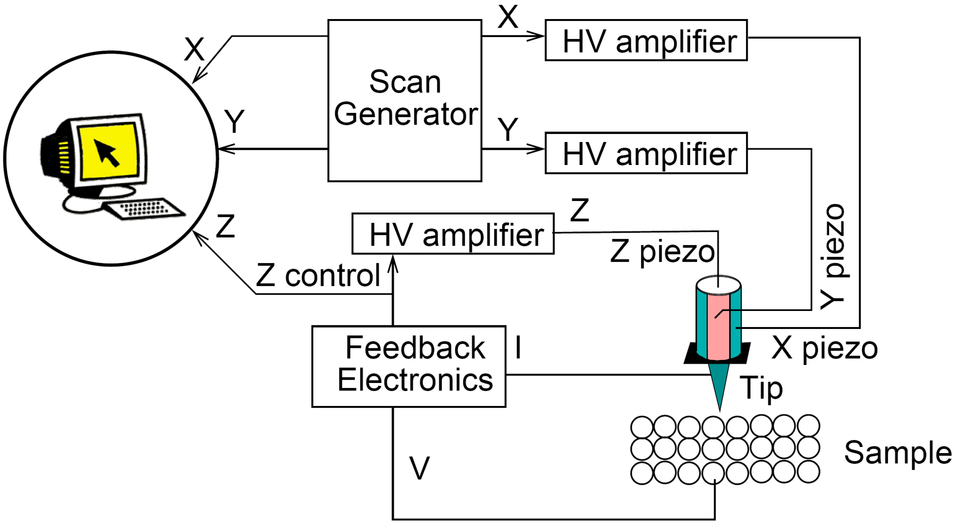

Figure 2.7: Schematic illustration of an STM set-up

1. Surface structures, either given by nature or artificially created, e.g. by MBE, can be monitored and controlled on the atomic scale.
2. Based on the atomic resolution capability, the tip can be positioned with atomic accuracy above a pre-selected atomic site and a local experiment can be performed. In this regard, electronic local density of states (LDOS) can be determined through I-V measurements using scanning tunneling spectroscopy (STS).
3. The capability of monitoring surface structures with atomic resolution combined with the ability to position the tip with atomic accuracy leads to the ability to perform direct and controlled manipulation at the atomic level, offering the opportunity to create atomic-scale devices.

The main components of a scanning tunneling microscope (STM) are discussed below. A block diagram of STM operation is shown in Fig.2.7.

- *Atomically sharp tip*: The STM tips are typically fabricated from metal (e.g. W, Pt-Ir, Au) wires. The preparation procedure of the atomically sharp tip includes preliminary *ex-situ* treatments, like mechanical grinding, cleavage, or electrochemical etching and subsequent *in-situ* treatments, like annealing, field emission/evaporation and even a "soft crash" of the tip by touching a sample surface.
- *Scanner*: To raster the tip over the area of the sample to be studied, a scanner is attached with the tip. Piezoelectric ceramics are used in scanners as electromechanical transducers, as they can convert electric signals of 1 mV to 1 kV into mechanical motion in the range from fractions of an $\mathring{A}$ to a few μm.
- *Feedback electronics*: This circuit controls the tip-sample gap.
- *Computer system*: This is necessary to control the tip position, to acquire data and to convert the data into an image.

Apart from these, a coarse positioning system is attached with the scanner to bring the tip to within the tunneling distance of the sample and to retract it back to a sufficient distance (a few mm). For stable operation of the STM, a vibration isolation system is essential. The changes of the tip-sample separation caused by vibrations should be kept to less than $\sim 0.01\mathring{A}$. The required vibration damping is achieved by suspending the inner STM stage with the tip and sample on very soft springs and by using the interaction between the eddy current induced in cooper plates attached to the inner stage and the magnetic field of the permanent magnets mounted on the outer stage.

During imaging the STM tip is placed very close to the surface. In this condition the wave functions of the closest tip atoms and the surface atoms overlap. The typical tip sample gap is about $\sim$ 5 - $10\mathring{A}$. If one applies a bias voltage V between the tip and the sample, a tunneling current will flow through the gap. In simplified form, the tunneling current density j is given by:

$$j = \frac{D(V)V}{d} exp(-A\phi_B^{1/2}d) \tag{2.6}$$

where, d is the effective tunneling gap, D(V) reflects the electron density of states, A is a constant and ϕ_B is the effective barrier height of the junction [17]. A schematic of energy diagram of the tunneling is shown in Fig.2.8.

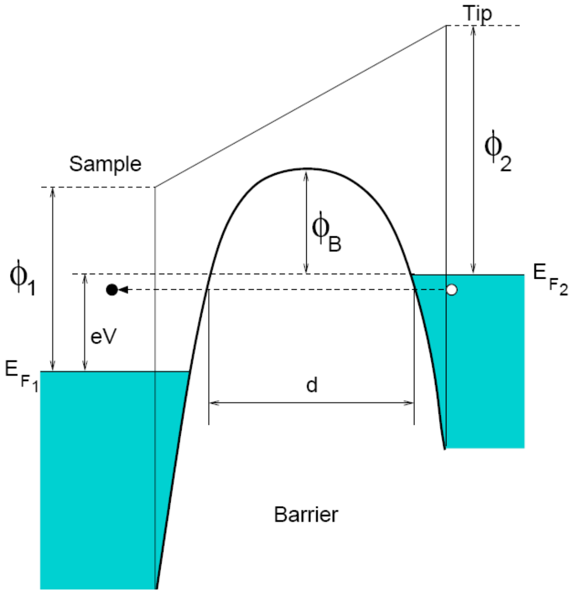

Figure 2.8: Energy diagram of the tunneling contact of the STM tip and the metallic sample. E_{F_1} and E_{F_2} are the Fermi levels of the surface and the tip, ϕ_1 and ϕ_2 are the work functions of the surface and the tip, ϕ_B is the effective barrier height, d is the effective tunneling gap and V is the bias voltage. The diagram illustrates the situation when STM probes the empty states of the surface [50].

The sharp dependence of the tunneling current on the gap width determines the extremely high vertical resolution of STM. Typically, a change of the gap by $\Delta d = 1\mathring{A}$ results in a change in the tunneling current by an order of magnitude or if the current is kept constant to within 2%, the gap width remains constant to within $0.01\mathring{A}$. As for the lateral resolution of STM, this is determined by the fact that up to 90% of the tunneling current flows through the gap between the "last" atom of the tip and the atom of the surface, which is the closest to it. Surface atoms with an atomic separation down to $\sim 2\ \mathring{A}$ can be resolved.

Tunneling through the barrier is due to the overlapping of the wave functions of tip and surface atoms. So STM topography is sensitive to LDOS. When the tip bias voltage is positive with respect to the sample, the STM image corresponds to the surface map of the filled electronic states. With a negative tip bias voltage, the empty-state STM image of the surface is obtained. The basic parameters for STM operation are the lateral coordinates, x and y, height h, the bias voltage V and tunneling current I. There are different modes of operation of STM depending on the manner in which these parameters are varied. Three main modes of STM operation are defined, depending upon the manner in which these parameters are varied:

- *Constant-current mode*: In this mode, I and V are kept constant, x and y are varied by rastering the tip and z is measured.

- *Constant-height mode*: It is also called current imaging. In this mode, z and V are kept constant, x and y are varied by rastering the tip, and I is measured.
- *Scanning tunneling spectroscopy (STS)* : This is rather a series of various modes, in which V is varied.

2.5.2 Reflection High Energy Electron Diffraction

Reflection high-energy electron diffraction (RHEED) is a technique for surface structural analysis that is remarkably simple to implement, requiring at the minimum only an electron gun, a phosphor screen, and a clean surface. Its interpretation, however, is complicated by an unusually asymmetric scattering geometry and by the necessity of accounting for multiple scattering processes. First performed by Nishikawa and Kikuchi (1928) at nearly the same time as the discovery of electron diffraction by Davison and Germer (1927), RHEED has assumed modern importance because of its compatibility with the methods of vapor deposition used for the epitaxial growth of thin films. We take RHEED to encompass the energy range from about 8 to 20 keV, though it can be employed at electron energies as high as 50 to 100 keV.

Because of its small penetration depth, owing to the interaction between incident electrons and atoms, RHEED is primarily sensitive to the atomic structure of the first few surface laayers. In the RHEED geometry, an incident beam directed at a low angle to the surface has a very strong effect on both the diffraction and its interpretation. For example, atomic steps can produce large changes in both the measured intensity and the shape of the diffracted beams when the important atomic separations are parallel to the incident beam direction; in contrast, the role of atomic structure in the diffracted intensity is primarily determined by the atomic separations perpendicular to the beam direction. Both of these phenomena result from the low glancing angle of incidence. The extent of these sensitivities, the importance of multiple scattering, the shape of the diffraction pattern, and the salient features of calculation are all determined by the combination of a small glancing incident angle and the conservation of parallel momentum.

Diffraction techniques utilizing electrons or X-ray photons are widely used to characterize the structure of surfaces. The structural information is gained conventionally from the analysis of the particles/waves scattered elastically by the crystal. The intensities of the diffracted beams contain information on the atomic arrangement within a unit cell. The spatial distribution of the diffracted beams tells us about the crystal lattice. The evaluation of the crystal lattice is straightforward, as the diffraction pattern is directly related to the crystal reciprocal lattice by the condition:

$$k - k_0 = G_{hkl} \tag{2.7}$$

where k_0 is the incident wave vector, k is the scattered wave vector, and G_{hkl} is the reciprocal lattice vector. As scattering is elastic,

$$|k| = |k_0| \tag{2.8}$$

from the laws of conservation of momentum and energy. This condition may be satisfied by an infinite number of k vectors pointing in many directions. Diffraction is often discussed with the help of an Ewald sphere. An Ewald sphere is a sphere with its centre as the origin and its radius as $|k_0|$. Hence, the Laue condition may be re-formalized as diffraction occurs for all $|k_0|$ connecting the origin of the sphere and a reciprocal-lattice point [59,60]. The magnitude of $|k_0|$ from the relativistic expression is:

$$k_0 = \frac{2\pi}{\lambda} = \frac{1}{\hbar}\sqrt{2m_0qV + \left(\frac{qV}{c}\right)^2} \tag{2.9}$$

where m_0 is the electron rest mass, q is its charge and V is the accelerating potential. Reflection high energy electron diffraction (RHEED) is a widely used technique to study the growth and the structure analysis. Although high-energy electrons are used for RHEED, it is very surface sensitive as the incidence and detection angles are grazing ($\sim$ 1-3°). As a result, on its relatively long mean free path through the sample, high-energy electrons still keep in the near-surface region of only a few atomic layers deep. The geometry of RHEED is such that the electron gun and the screen are placed far apart from the sample. Thus, the front of the sample is open for the deposition process. Therefore, RHEED can be used as an in-situ technique to study the structure of a growing surface directly during growth.

The Ewald sphere construction in RHEED conditions and the schematic of the experimental arrangement are illustrated in Fig.2.9. A flux of high energy electrons from the electron gun is incident under grazing angles and diffracted beams produce a RHEED pattern on a fluorescent screen.

The reciprocal lattice for a two dimensional layer is a set of one dimensional rods perpendicular to the surface. Since the reciprocal rods are continuous rods, every rod produces a reflection in the diffraction pattern as shown in Fig.2.9. The

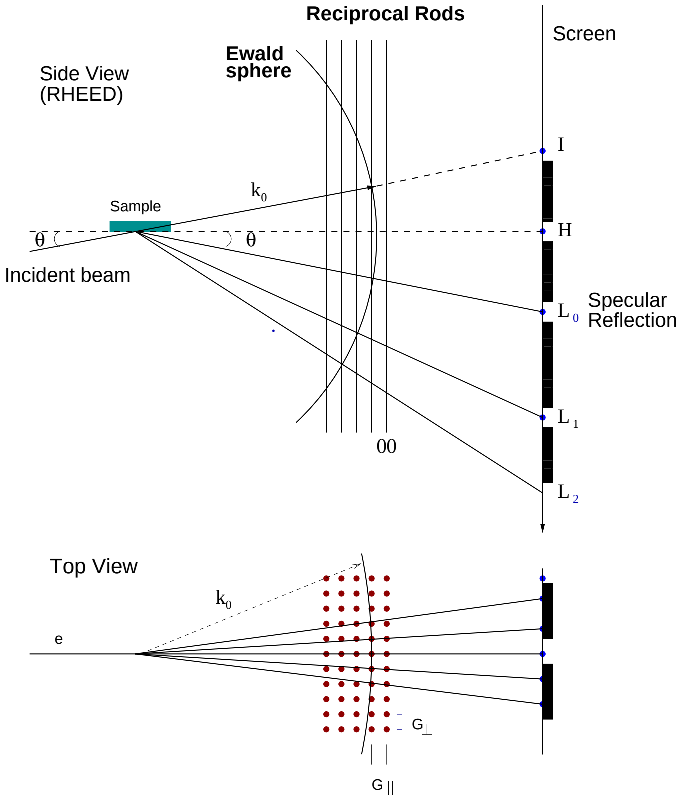

Figure 2.9: Ewald sphere construction and diffraction geometry of RHEED. Intensity maxima on the screen correspond to projected intersection of Ewald sphere with the reciprocal lattice.

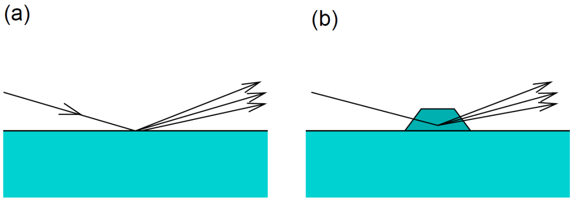

Figure 2.10: Two possible situations for high energy electron diffraction: (a) surface scattering on a flat surface and (b) transmission diffraction from 3D crystalline islands located on the surface.

reflections occur on Laue circles of radius L_n with n=0,1,.. centered at *H*. The origin of the reciprocal lattice is projected onto I. The reciprocal rod separations $G_{\parallel}$ and $G_{\perp}$ are parallel and perpendicular to the beam direction, respectively.

Apart from the structural information, RHEED provides additional information which appear to be specifically useful for studying thin film growth and monitoring the formation of multilayer epitaxial structures. By monitoring the intensity of the diffracted spot(s), one observes the intensity oscillation during the layer-by-layer growth. If 3D crystalline islands form on the surface, they can be readily identified by the appearance of new spots in the RHEED pattern. These spots are produced by transmission electron diffraction in the islands as shown in Fig.2.10.

2.5.3 Transmission electron microscopy

Transmission electron microscope (TEM) has turned out to be one of the crucial characterization techniques with increasingly high spatial resolution coupled with various other accessories such as energy dispersive x-ray spectroscope, STEM, energy filtered TEM (EFTEM) etc. It has been fast developing and spreading its wings in all possible areas of science. TEM is the major tool for complete characterization of nanoscale materials and devices [61–63].

Inability of optical microscopes to resolve sub-micron features not withstanding, Knoll and Ruska proposed the idea of using an energetic electron beam (instead of light) for building a microscope [64]. In this paper, they developed the idea of electron lenses into a practical reality.

Interaction of electrons with matter

Electrons being charged particles interact elastically and inelastically with the electrons as well as nuclei of a material. In the process, it produces a lot of secondary signals (figure 2.11) which can be used for *analytical electron microscopy* (AEM). When a beam of electrons impinges on a material, they interact with the target atoms and the forward scattered electrons form most of the signals used in TEM. If they interact with thinner/low Z region of the sample, image gives a brighter contrast and with thicker/high Z region of the sample, internal scattering will be more and the image appears to be of darker contrast. This is called *mass-thickness contrast.* On the other hand, crystallinity of the specimen also gives a contrast called *diffraction*

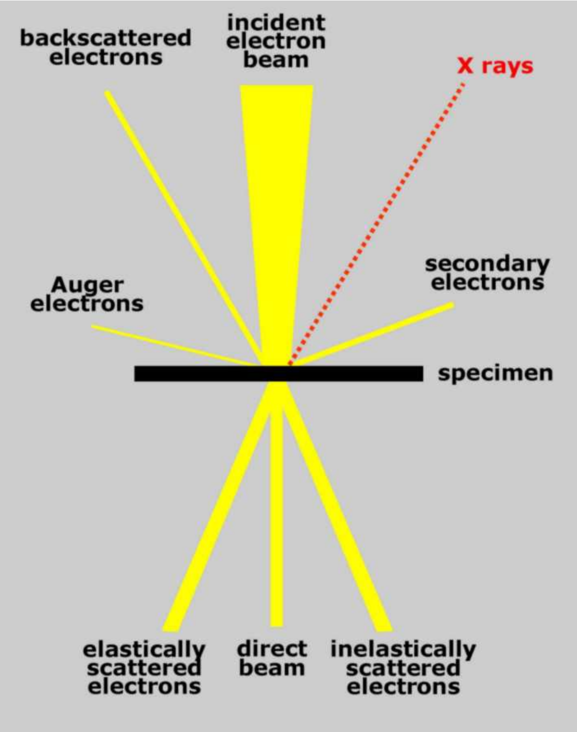

Figure 2.11: A schematic diagram of different processes taking place during electron−solid interaction.

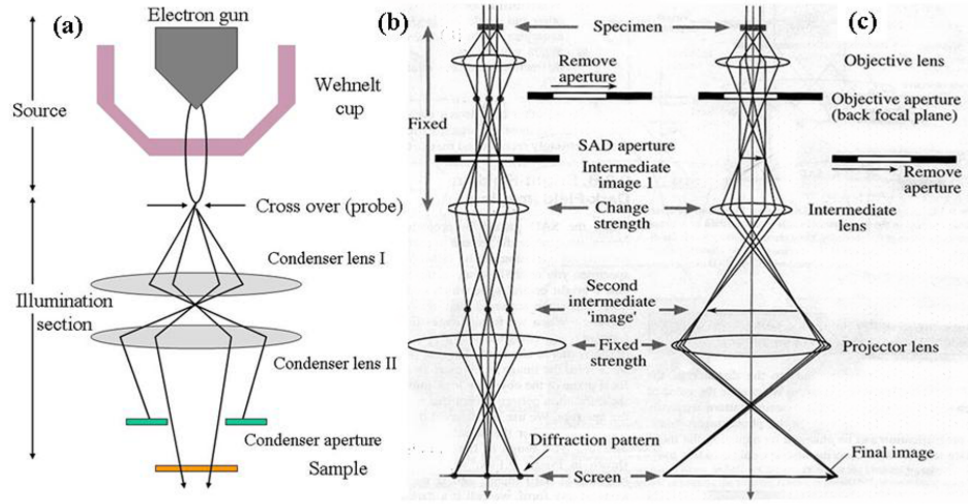

Figure 2.12: A schematic diagram of (a) Filament and illumination part, (b) Diffraction pattern formation and (c) Image formation [61].

contrast. However, for thin specimens at high resolution, the wave nature of the electrons become predominant. If the specimen is thin enough and crystalline, then elastic scattering is usually coherent and these electrons contribute to the image formation. Elastically transmitted coherent electron beam coming out of the specimen form the diffraction spots and image at back-focal plane and image plane of the objective lens (OL), respectively. The formation of diffraction pattern (DP) is schematically shown in figure 2.12(b). The diffraction pattern is the fast Fourier transformation (FFT) of the wave function of electron at the back focal plane of OL. The formation of image is also schematically shown in figure 2.12(c). Another FFT of this wave function at back focal plane of OL gives the high resolution (HR) lattice image. The HR image will form due to interference between the direct and diffracted beams.

Instrumentation:

A typical TEM can be divided into three major components: the illumination system, the objective lens/stage and the imaging system. The illumination system takes care of transferring the electron beam emitted from the gun towards the sample stage. Electron guns can be of two types: thermionic gun (W, LaB_6) and field emission gun (FEG). Work function, operating temperature, current density, life time and cost together decide as to which kind of material to be used for the manufacture of guns.The only electrostatic lens in the form of Wehnelt is placed just below the gun which helps to converge maximum number of electrons emitted from the gun (Figure 2.12(a)). The objective lens/stage is the most crucial part of TEM. Usually, it covers about a centimeter along the length of the column, but this is the region where the electron beam interacts with the specimen and because of which we create bright field, dark field images and selected area diffraction (SAD) patterns. Here, the quality of the image is taken care by the objective lens which eventually decides the resolution of the microscope. The imaging system consists of several magnifying lenses (termed as intermediate lenses), which magnify the image or SAD formed by the objective lens. Projector lens system projects the image onto electron detector (CCD/TV Camera), which is coupled to a computer to grab such images. Electrons being charged particles, TEM column is always kept at high vacuum ($\approx 10^{-7}$ mbar) in order to get a collimated beam of electrons.

In this thesis, all the TEM measuements have been carried out using JEOL 2010 TEM operating at 200 keV (Fig. 2.13). The OL pole piece is an ultra high resolution pole piece (UHR-URP22) with a spherical aberration coefficient (C_s) of 0.5 mm, which helps to achieve a point-to-point resolution of 0.19 nm. For imaging as well as real-time studies, a charge-coupled-device (CCD) based detector with 40 ms time resolution and with 4008 × 2672 pixels (Model 832, Gatan Inc.) has been used. Scanning TEM (STEM) measurements were also carried as a part of the thesis work. The details of the STEM would be given at section following the TEM section.

Sample preparation:

The first and foremost requirement of a TEM specimen is that, it has to be electron transparent (less than 100 nm). Now, the type of TEM specimen to be prepared depends on what kind of information the user expects from the specimen. If the sample is in chemical powder form which can be dissolved/dispersed in some organic/inorganic solution without losing the identity of the sample, a drop of such solution can be put on a carbon coated copper grid and let it dry. The sample is ready to be loaded in a TEM. This is the easiest way of preparing a sample. If the specimen is self supporting and it can tolerate mechanical thinning without changing its chemical identity, the electron transparency could be achieved by mechanical thinning followed by ion milling. There are again two ways of preparing TEM sample depending on whether one wants to investigate the surface morphology or the interface of the specimen.

Figure 2.14 and 2.15 show the schematic diagrams to prepare both planar and cross sectional TEM sample preparation, respectively. Normal TEM sample would be a 3.0 mm disc. So, the first step for preparing a planar sample would be cut a 3.0 mm disc out of actual sample. A GATAN made ultra sonic disc cutter was used for this purpose. A cylindrical tool with tube diameter of 3.0 mm vibrates with ultrasonic frequency and the underlying fine SiC slurry would cut the specimen into a 3.0 mm disc because of this vibration. Then such a disc is lapped (SBT, LPS model 900) using different sizes of emery papers to get a final thickness of about 100 μm. This much thickness at the periphery will be maintained till the end to give mechanical stability to the specimen. Now, a dimple is created at the center of the sample using a dimple grinder (DG, GATAN, model 656), still maintaining 100 μm thickness at the periphery for the handling purpose. Then, electron transparency is achieved through

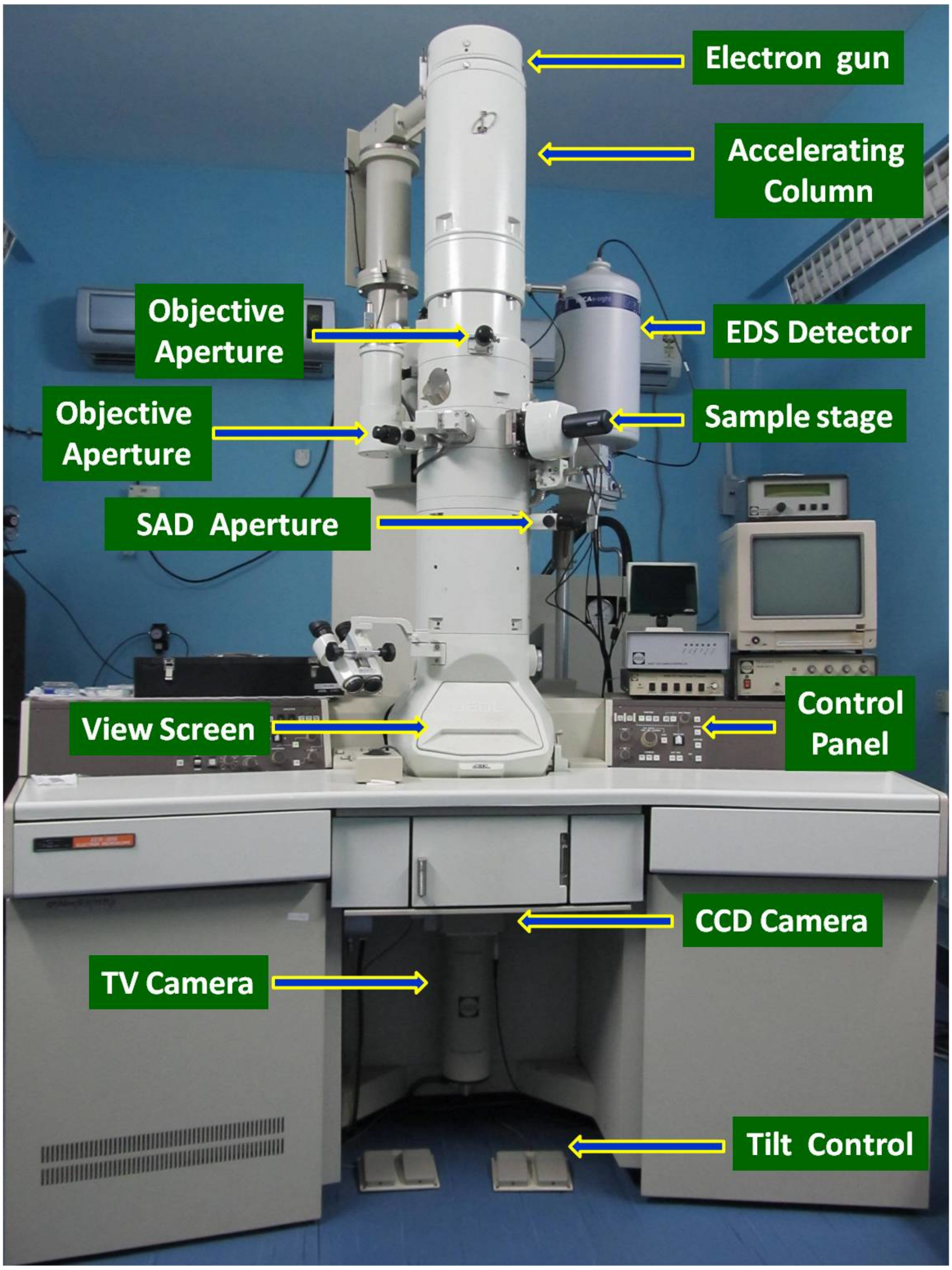

Figure 2.13: 200 keV JEOL HRTEM installed at Institute of Physics, Bhubaneswar.

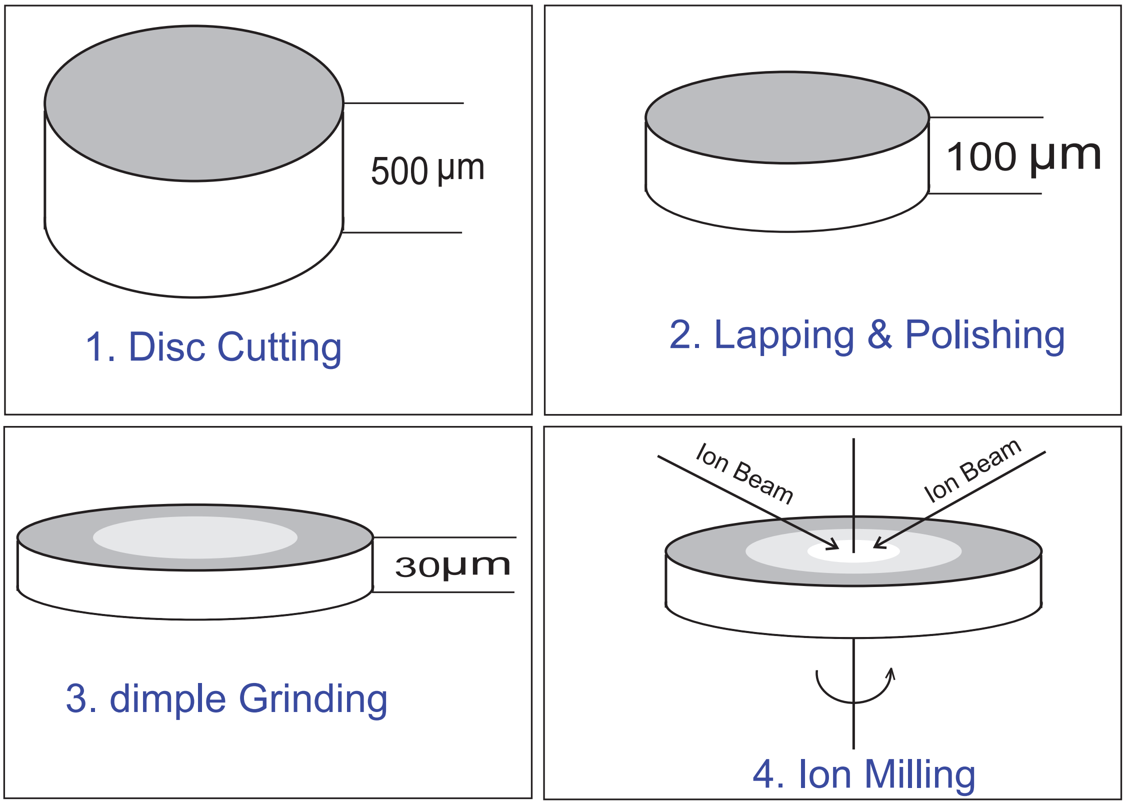

Figure 2.14: A schematic diagram of procedure to prepare a typical planar TEM specimen.

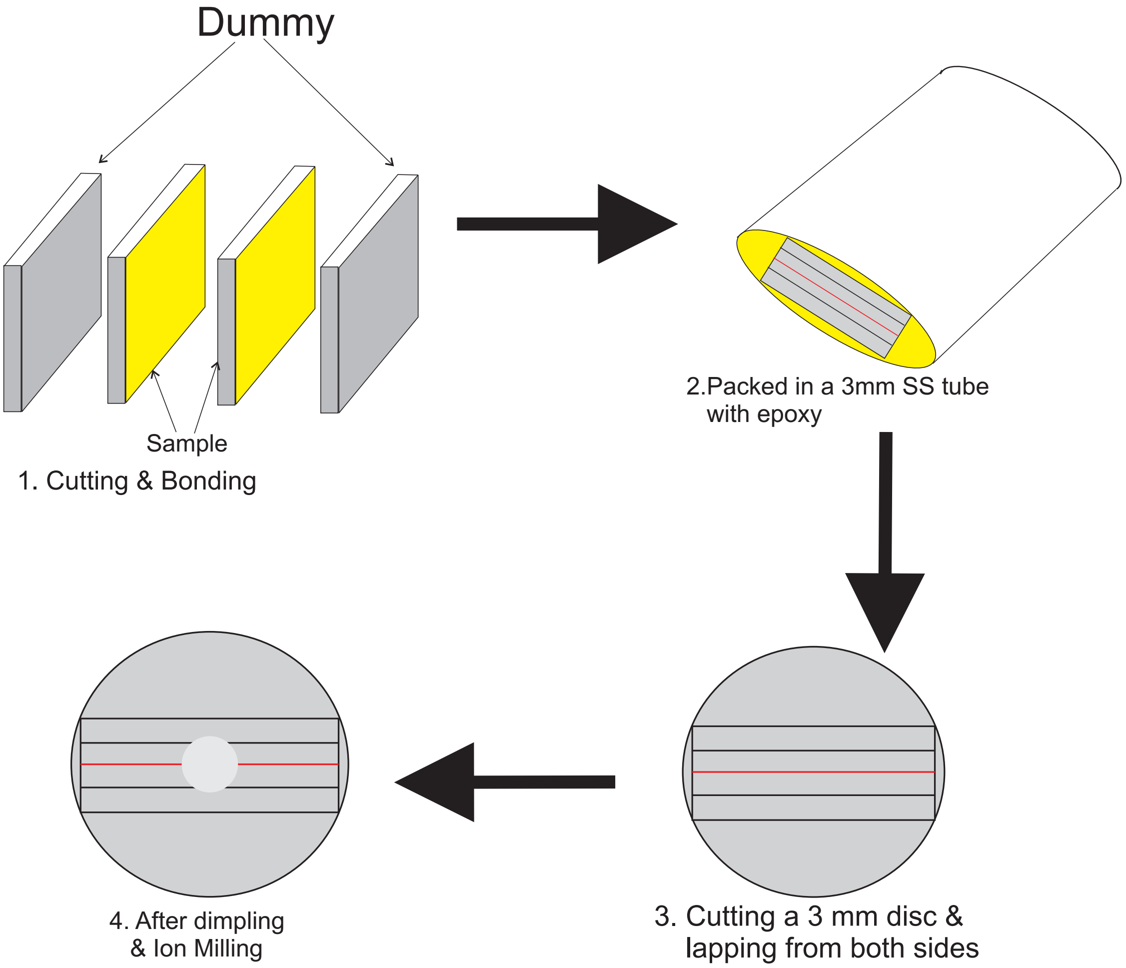

Figure 2.15: A schematic diagram of procedure to prepare a typical cross-sectional TEM specimen.

3.0 kV Ar ion milling (PIPS, model 691) (Fig. 2.14). All these above processes like cutting, lapping, dimpling and milling were done on the rear side of the specimen without affecting the features to be observed in TEM. Preparing a XTEM specimen is a much more laborious process. The specimen is cut into two 2.5 mm slides and are glued *face-to-face* using GATAN G1-epoxy glue (Fig. 2.15). Two dummy pieces of silicon are glued on each of these specimens, on the rear side. This was inserted into a 3.0 mm SS tube and glued together. A thin slice of this can be cut using a diamond wheel saw (SBT, model 650). Now the sample is ready in the form of a 3 mm disc, as required. Electron transparency can be achieved in the same way as it was done for planar sample.

Image analysis

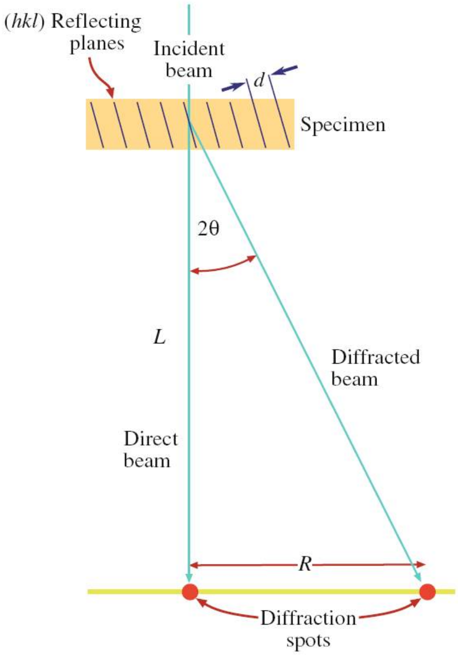

Figure 2.16: A schematic diagram showing the geometry of diffraction pattern formation [61].

The basic information that can be obtained from a selected area diffraction pattern (SAD) or a high resolution image of a specimen is its crystallinity. For example, given a SAD pattern of a single crystalline specimen, the first step is to calculate d-spacings (distance between two consecutive atomic planes) of all the visible reflections around the central spot. A schematic diagram showing geometry of a diffraction pattern is shown in figure 2.16. When a beam of electrons is incident on a specimen, most of electrons pass through the specimen forming the direct beam. Some of them gets scattered (diffracted) at an angle 2θ and forms diffraction spot at a distance R from the central spot. Camera length, L, is the effective distance between the specimen and viewing screen. With increase in magnification, L also increases, which results in an increase in R as well. Thus, if electrons are scattered through an angle 2θ at the specimen, then the separation of the direct and diffracted beams as measured on the screen is determined by L since,

$$\frac{R}{L} = \tan 2\theta \sim 2\theta \tag{2.10}$$

From the Bragg equation, we know that $\lambda/d = 2\sin\theta \sim 2\theta$, so we get,

$$Rd = \lambda L \tag{2.11}$$

The quantity $L\lambda$ is called *camera constant.* If we know the camera constant, then we can determine d simply by measuring R on the pattern. To measure this distance R accurately, a software called ImageJ [65]could be used. In ImageJ, given a single crystalline SAD pattern, a line profile should be obtained. Thus, distance between two symmetric spots on either side of the central spot can be measured. Half of this distance will give R. As camera constant is already known, inter-planar spacing d can be calculated easily using equation 2.11. If the SAD image is in DM3 format (as obtained from Digital Micrograph), distance between central spot and diffracted spot directly gives inverse of d. This is applicable only when a DM3 plugin is included in the ImageJ software. Similarly, given a high resolution image, d-spacing can again be calculated by taking a line profile perpendicular to a set of lattice spacings and then taking an average.

2.5.4 Scanning Transmission Electron Microscopy

In a normal TEM, condenser lenses would be tuned in such a way that a parallel beam hits the specimen to create a diffraction contrast image or SAD. However, there are times when we need a convergent beam. Sure, it doesn't give immediate images, as the beam is not parallel any more and we lose the image contrast, but there are other advantages with reduced probe size. To see an image, one has to scan the beam and this mode of operation is often referred to as *Scanning Transmission*

Electron Microscopy (STEM). Since the resolution of scanning technique is limited by probing beam, sub angstrom level resolution can be achieved by using a very fine electron probe with a beam diameter of the order of a few nm. With this technique, it is possible to image single atoms even in non-crystalline specimens and hence this mode of TEM is being increasingly used in the recent past for the microanalysis of thin sections of material [70]. Moreover, small size of the probe helps in getting compositional information via energy dispersive x-ray analysis (EDX), electron energy loss spectroscopy (EELS) and high angle annular dark field imaging (HAADF) (figure 2.17).

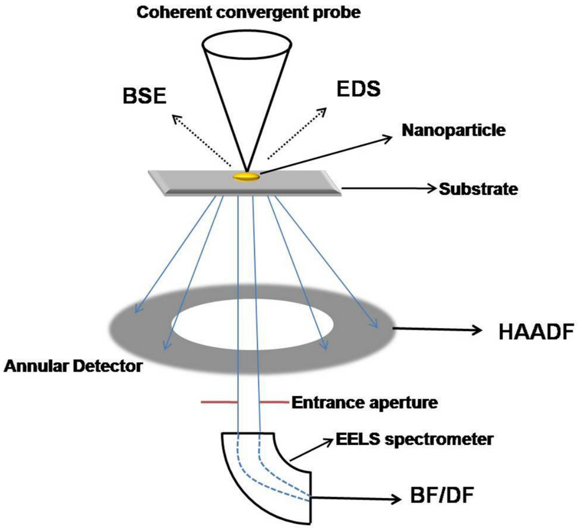

Figure 2.17: Schematic diagram of various kinds of detectors used in a STEM.

High Angle Annular Dark Field Imaging (HAADF)

The fundamental difference between TEM-DF mode and a STEM-DF mode is that, in TEM-DF mode, only a fraction of scattered electrons are allowed to enter the objective aperture, where as in STEM, the images are formed by collecting most of the electrons on the ADF detector. So, ADF images are less noisy than TEM-DF images. Contrast depends Z^2 of the material under observation. Electrons scattered from high Z elements will be collected at high angles in an ADF and hence better contrast is obtained as compared to TEM-DF images.

Energy dispersive x-ray spectroscopy (EDS)

When an electron beam interacts with a specimen, it gives out x-rays as well, which is a characteristic of the specimen under observation. If these x-rays of different energies are dispersed, it gives a spectrum which helps to know the elemental composition of the specimen. Normally, Li drifted Si (Si-Li) detectors are used for this purpose. In a STEM, probe size being very small, chemical composition of nanosized structures are also possible to findout using EDS.

2.5.5 Rutherford Backscattering Spectrometry

Rutherford backscattering spectrometry (RBS) is an analytical technique used in materials science. Sometimes referred to as high-energy ion scattering (HEIS) spectrometry, RBS is used to determine the structure and composition of materials by measuring the backscattering of a beam of high energy ions impinging on a sample. In 1911, Ernst Rutherford demonstrated that an atom comprises of heavy positive mass called nucleus [66]. This, he found out, when a beam of energetic α particles was incident on a thin gold foil and fraction of them were backscattered. Then he concluded that there is a heavy mass at the center of each atom (contrary to the earlier plum pudding model), which is positive in charge. This principle was developed into a popular spectroscopic technique, where measuring the number and energy of ions in a beam which backscatter after colliding with atoms in the near-surface region of a target would be analyzed to get atomic mass and elemental concentration of a material. More about various aspects of RBS technique can be found in ref. [67].

Kinematic factor:

The ratio of the projectile energy after a collision to the projectile energy before a collision is defined as the kinematic factor (K_{M_2}). When a projectile with mass and energy M_1 and E_0 collides elastically with a stationary particle (target atoms) of mass M_2 ($M_2 > M_1$), energy will be transferred from the projectile to the target atoms. If the projectile energy (E_0) is much larger than the binding energy of the target atoms, but less than the energy required for nuclear reactions and resonances, then the kinematic factor for this system shown in figure 2.18 can be expressed as:

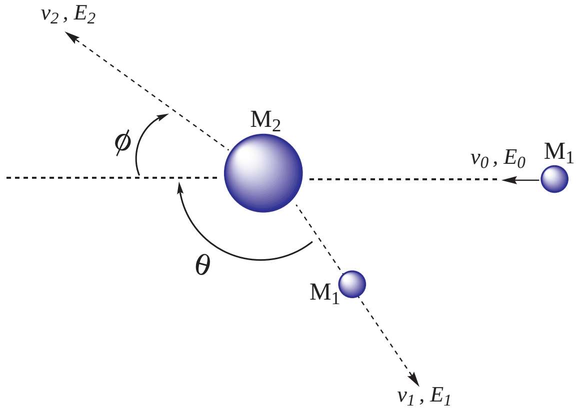

Figure 2.18: A schematic diagram of the interaction of two particles.

$$K_{M_2} = \frac{E_1}{E_0} = \left[\frac{M_1 cos\theta + (M_2^2 - M_1^2 sin^2\theta)^{1/2}}{M_1 + M_2}\right]^2 \tag{2.12}$$

Thickness analysis:

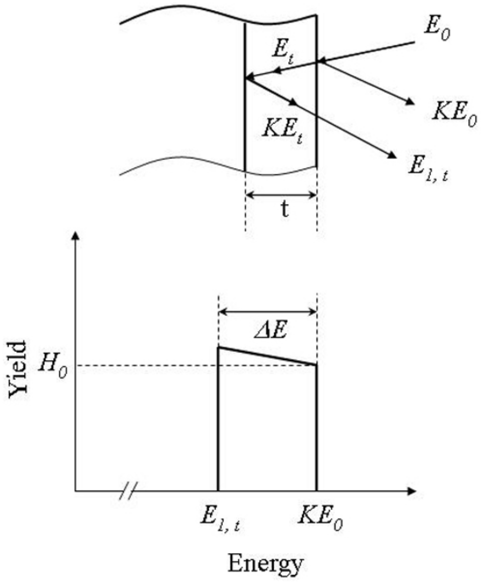

Figure 2.19: A schematic diagram of the RBS spectrum for a thin film [67].

In a real experiment, instead of particle-particle collision, a beam of light positive ions (He ions or protons) are incident upon a target material. Relative number of backscattered ions from a target atom that are directed towards a certain solid angle $d\Omega$ is termed as differential scattering cross section.

$$\frac{d\sigma}{d\Omega} = \frac{1}{Nt}\frac{dQ/d\sigma}{Q} \tag{2.13}$$

where N is the atomic density of the target atoms and t is its thickness. σ is called average differential scattering cross section and can be defined as,

$$\sigma = \frac{1}{\Omega}\int_{\Omega}\frac{d\sigma}{d\Omega}d\Omega \tag{2.14}$$

and the differential scattering cross-section for an elastic collision between two atoms is given by Rutherford's formula,

$$\frac{d\sigma}{d\Omega} = \left[\frac{Z_1 Z_2 e^2}{4E_0}\right]^2 \frac{4}{sin^4\theta}\frac{\left[[1-(\frac{M_1}{M_2}sin\theta)^2]^{1/2}+cos\theta\right]^2}{\left[1-(\frac{M_1}{M_2}sin\theta)^2\right]^{1/2}} \tag{2.15}$$

where Z_1 and Z_2 are the atomic numbers of the projectile and target atom respectively. From the above equations, simple way to get the thickness is dividing the term Nt by the atomic density N. In other words, the total number of detected particles can be written in terms of the height of the spectrum as $H_i = \sigma(E_i)QN.dt$, when the beam is falling normally onto the sample. Here, i denotes the number of equally smallest slabs for which backscattered energy can resolute, that means $t = i.dt$ and $\sigma(E_i)$ must be calculated at each backscattered energy E_i. Now, the total number of counts (area under the curve) is $A = \sum_i H_i$. In figure 2.19, H_0 denotes the total number of counts at energy KE_0. So total no of counts is given by,

$$A = H_0 = \sum_i H_i = \sum_i \sigma(E_i)\Omega QN.dt = \sigma\Omega QNt \tag{2.16}$$

The value of A can be obtained by taking the area under the spectrum.

Instrumentation:

RBS instrumentation can be broadly divided into three parts: accelerator, target chamber and energy analyzer. In the first part, H or He ions are generated through ionization process. Then these ions are accelerated using the accelerator upto an energy of 1−3 MeV. Selection of the required isotope is done by passing the beam through a mass analyzer. Finally, the collimated beam falls on the sample (target chamber). In the target chamber, a surface barrier detector (SBD) is used to detect backscattered projectiles kept at a very high angle ($\geq 150^0$) . The sample is connected with the current integrator to get the total number of incident ions (total charge accumulated on the target). The energy related output from SBD goes through the energy analyzer. It consists of preamplifier, amplifier, analog to digital converter and multi channel analyzer (MCA). Finally, the output of MCA can be fed to the computer, where the resulting RBS spectrum can be stored. For the present thesis work, we have used 45^0 degree beam line of the 3 MV tandem Pelletron accelerator (9SDH2, NEC, USA) facility at IOPB [68]. Surface barrier detector was placed at 160^0 at a distance of about 11 cm from the sample holder. For the RBS measurements, 1.35 MeV He^+ ions were used and RBS simulation was carried by SIMNRA software package [69].

2.5.6 High Resolution X-ray Diffraction

High Resolution XRD (HR-XRD) is a well known method for measuring the composition and thickness of compound semiconductor materials such as SiGe, AlGaAs and InGaAs. In the case of a Si lattice, the presence of Ge atoms in the lattice results in compressive strain. This strain changes the spacing of the Si lattice, and the difference can be detected by HR-XRD.We have used the P08 beamline at Petra - III for carrying out HRXRD measurements for compositional analysis. Using the Bragg angles, we determined the corresonding lattice planes of Si-Ge alloy structures.

2.5.7 Scanning Electron Microscopy

In a scanning electron microscope , an electron beam with primary energy typically of $\sim$ 1 - 30 keV is focused by a lens system in to a spot of 1- 10 nm in diameter on the sample surface. The focused beam is scanned in a raster across the sample by a reflection coil system in synchronism with an electron beam of a video tube, which is used as an optical display. Both beams are controlled by the same generator and the magnification is just the size ratio of the display and scanned area on the sample surface. A variety of signals can be detected including secondary electrons, back scattered electrons, x-rays, cathodoluminescence and sample current. The main applications of the SEM concern visualization of the surface topography and elemental mapping.

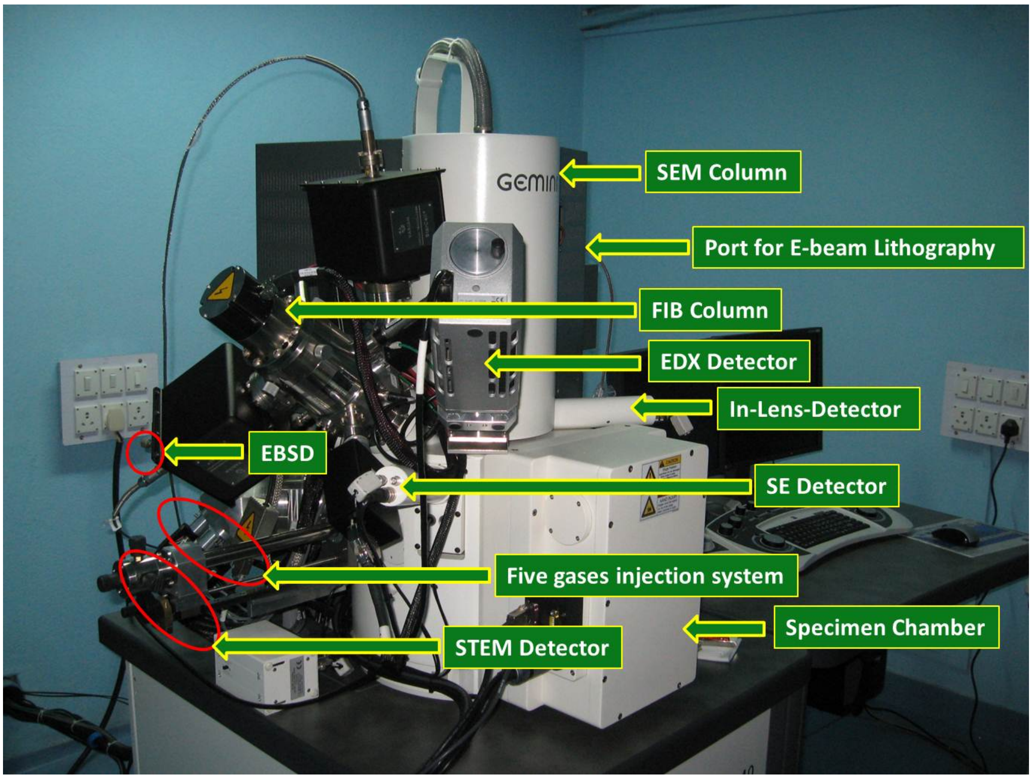

Figure 2.20: SEM(Carl Zeiss , Neon 40) installed at Institute of Physics, Bhubaneswar, with Resolution : 1.1nm @ 20 kv , 2.5nm @1kv , Probe current : 4pA - 20nA and Accelerating Voltage : 0.1 - 30kV.

2.6 Conclusions

Different techniques used to grow epitaxial thin films have been highlighted. Molecular beam epitaxy is one of the most important techniques for growing epitaxial nanostructures with precise control over growth. The role of lattice misfit in the heteroepitaxial growth and the various growth modes have been discussed. Self-organized growth of epitaxial nanostructures via selective growth modes, e.g., Stranski-Krastanov and Volmer-Weber modes, has been emphasized.Depending on the nature of investigations, several characterization techniques are needed to study various aspects of the MBE-grown self-organized nanostructures. Principles of operation of different microscopic (e.g., STM,TEM,STEM,SEM) and diffraction (e.g., RHEED, HR-XRD) techniques used for structural characterizations and Rutherford backscattering spectrometry(RBS) have been discussed briefly in this chapter.

Chapter 3

Ge growth on ultraclean high index Si(5 5 12) surfaces and DC heating induced shape transformation

3.1 Introduction

High index Si surfaces have been a main focus of surface science research due to their anisotropic atomic structure, high vicinal angles and symmetric surface reconstructions [71–73]. Ultraclean high index silicon surfaces consist of alternating terraces and atomic steps. Several authors have exploited this anisotropy to form aligned one-dimensional (1D) nanostructures of different adsorbates [74–79]. Atomic steps on the semiconductor surfaces play an important role in many surface dynamic processes such as surface migration and crystal growth. The highly anisotropic behavior of metal films due to surface diffusion and surface electromigration on the vicinal Si(111) has been reported [80, 81]. Among the high index silicon surfaces oriented between (001) and (111), Si(5 5 12) exhibits relatively stable reconstruction having 1D symmetry with a $(1\bar{1}0)$ mirror plane [71, 83]. Si(5 5 12) is oriented 30.5° away from (001) towards (111) and offers a stable 2×1 surface reconstruction with one-dimensional periodicity over a large unit cell [71].

Self-assembled nanostructures on Si substrates have attracted much attention due to their interesting physical properties and possible application in optoelectronic devices [84, 85]. In particular, the growth of Ge nanostructures on clean silicon surfaces

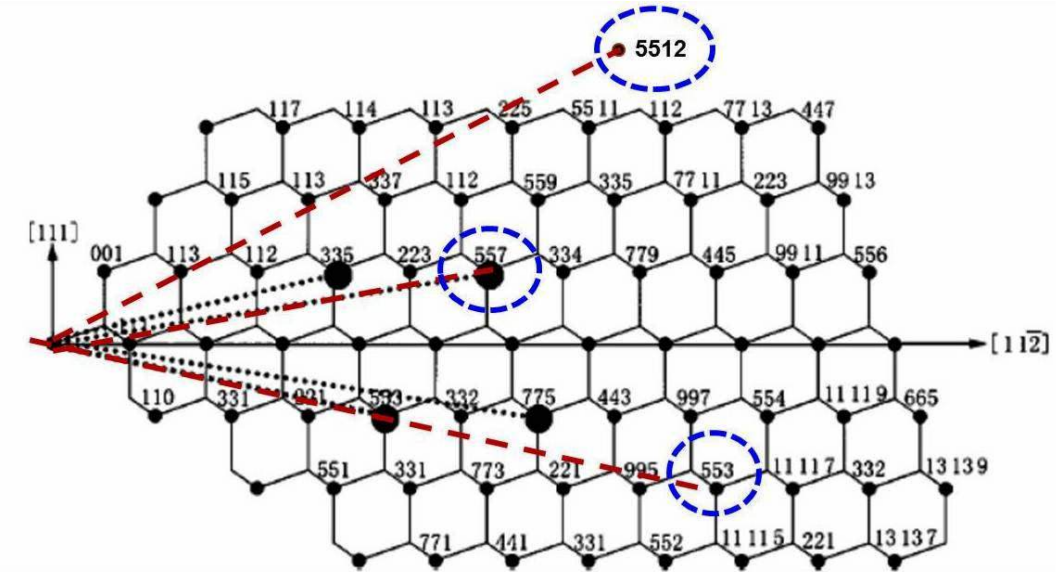

Figure 3.1: Crystallography of high index silicon surfaces [71].

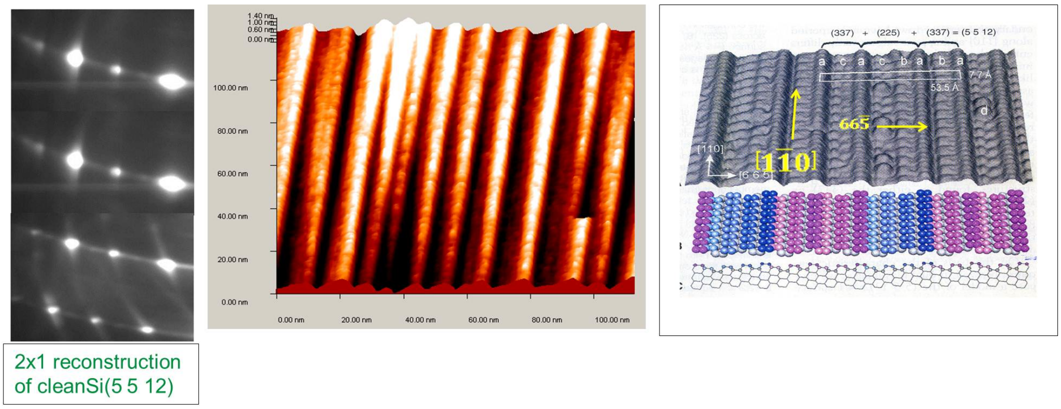

Figure 3.2: RHEED and STM image of ultra-clean reconstructed Si(5 5 12) Surfaces taken at Institute of Physics, Bhubaneswar,India. Schematic of the reconstruction is taken from the ref. [71].

(with various substrate orientations and vicinal angles) has been extensively studied due to its use as a model system to understand complex issues related to hetero-epitaxy and technological applications [86–95]. An important aspect of the Ge/Si system is its compatibility with the standard CMOS technology that is used for the production of most semiconductor devices. Applications of Ge/Si may be found in silicon-based optoelectronics. Due to the indirect band gap, Si devices are not well suited for optoelectronic applications. New devices employing Ge/Si epitaxial layers are expected to overcome this restriction [94, 95]. Due to a 4.2% lattice mismatch between Ge and Si crystals, a pseudomorphic Ge film grows with strain up to a certain thickness as a wetting layer and then after a certain critical thickness, islands are formed (often known as the Stranski-Krastanov (SK) growth mode). Since strain depends on the surface symmetry of the substrate, the morphology of self-assembled Ge nanostructures will be influenced by the symmetry of the reconstructed Si surface. Therefore, in the Ge/Si system, following the SK growth mode, stress relaxation and diffusion are crucial for the controlled fabrication of Ge nanostructures on Si substrates [86–91]. Strain relief in hetero-epitaxial system like Ge or $Si_{1-x}Ge_x$ on a single crystalline silicon surface is a major factor for determining the various shapes formed during the growth process. It is known that strained epitaxial layers tend initially to grow as dislocation-free islands and as they increase in size, may undergo a shape transition [92, 93]. Below a critical size, islands can have a compact symmetric shape. But at larger sizes, they adopt a long thin shape, which allows better elastic relaxation of the islands stress [92, 93]. Sekar et al reported the shape transition as one of the strain relief mechanism in the formation of aligned gold silicide structures (triangular to trapezoidal shape transformation) [93]. Berbezier et al [90, 91] showed that self-organized growth instabilities can be used to create full scale wafer periodic nanopatterns which can serve efficiently as a template for selfassembling Ge dots. They have also shown that Ge dots preferentially nucleate on specific sites of the self-organized template layers, depending on the driving forces involve. The preferential nucleation of Ge dots in the valley between step bunches is explained by a reduced surface diffusion, while their position on the top of strained undulations is explained by elastic energy relaxation [91]. Also, on a nanofaceted surface, the effect of surface energy anisotropy is found to be the dominant driving force [91].

The study of Ge growth on high index surfaces, such as Si(5 5 12), Si(5 5 7), is an area where very limited research work has been carried out [96–98]. A previous study by Kim et al [27] reported on relatively thinner Ge growth on Si(5 5 12) and did not observe any shape transformation of the Si-Ge structures. Zakurdaev et al reported formation of ordered Ge nano-islands (10 - 20 nm dimensions) during the growth on Si(1 1 1) under electromigration conditions [99]. We report that the DC current acted as an additional factor in stimulating the motion of germanium adatoms towards the edges of nanosteps (that are formed due to surface reconstruction) [99]. The work presented in this work would be among the first few of this kind, in particular on the growth of SiGe structures on Si(5 5 12) under DC heating conditions. We show a shape transformation from rectangular to trapezoidal structures as a function of Ge overlayer thickness. We also discuss the possible growth mechanism of the aligned microstructures.

3.2 Experimental methods

The depositions of Ge on Si(5 5 12) were carried out in a custom built molecular beam epitaxy (MBE) system (from OMICRON Nanotechnology, Germany) [58]. The Si(5 5 12) substrate of size 8 × 3 mm^2 was prepared through cutting from a p-type boron doped wafer (of resistivity of 10 - 15 Ω cm) and degreasing with acetone. The samples were loaded into the MBE chamber where a base pressure of $\approx 2.5 \times 10^{-10}$ mbar was maintained. Substrates were degassed at 600°C for about 12 h followed by repeated flashing for 30 s at a temperature of ≈ 1250°C to remove the native oxide layer. Prior to the Ge thin film deposition, a 2×1 reconstruction was confirmed using reflection high energy electron diffraction (RHEED). During the deposition, the pressure in the MBE chamber was $\approx 6.9 \times 10^{-10}$ mbar. Ge was deposited to various thicknesses of 3.0 to 12.0 monolayer (ML) at a typical deposition rate of 0.6 ML.min^{-1} where one ML corresponds to 7.8 $\times 10^{14}$ atoms.cm^{-2} for a Si(1 1 1) surface. The Si(5 5 12) surface was kept under three substrate heating conditions: (i) at room temperature (RT), (ii) at 600°C where heating is achieved through a filament underneath (radiative heating: RH), and (iii) at 600°C but with heating achieved by passing a direct current (DC). In the second case, the sample was annealed at a temperature of 600°C for 15 minutes after deposition using RH, and for case (iii) the annealing was performed by passing the direct current through the sample with a power of 7.95 W (1.5 A and 5.3 V). The direction of the ($\langle 1\bar{1}0\rangle$) planes of the Si(5 5 12) sample was determined prior to the MBE growth. Based on this, the DC current direction was varied along three directions with respect to the $\langle 1\bar{1}0\rangle$: (a) along $\langle 1\bar{1}0\rangle$, (b) perpendicular to $\langle 1\bar{1}0\rangle$, and (c) at 45° to $\langle 1\bar{1}0\rangle$, the directions being shown in the insets of the SEM images in figure 7. To compare with growth on a high index surface, we also carried out 10 ML thick Ge growth on a Si(1 1 1) substrate with a resistivity of 0.5 - 30Ω cm. The base pressure inside the MBE chamber was $\approx 3.5\times 10^{-10}$ mbar and during the growth the chamber pressure was $\approx 6.8\ \times 10^{-10}$ mbar. A direct current of 1.5 A (5.7 V) was applied along the $\langle 1\bar{1}0\rangle$ direction. The post-growth characterization of the samples was carried out ex situ by field emission gun based scanning electron microscopy (FEGSEM), scanning transmission electron microscope (STEM) and MeV ion scattering (Rutherford backscattering spectrometry (RBS)). The FEGSEM measurements were carried out with 20 kV electrons using a recently installed Neon 40 cross-beam system (M/S Carl Zeiss GmbH) at the Institute of Physics (IOP), Bhubaneswar, India. STEM and TEM measurements were carried out with 300 keV electrons using a Cs-corrected FEI Titan 80/300 system at the University of Bremen, Germany. The TEM specimen was prepared by mechanical thinning followed by low-energy Ar-ion milling procedures (using PIPS, Gatan Inc.). The RBS measurements were carried out using 2.0 MeV He^+ ions generated from 3.0 MV Pelletron accelerator (NEC, USA) at IOP. Compositional depth profiling was obtained using the RUMP simulation of the RBS spectra [100].

3.3 Results and discussions

The main focus in this work is on the shape transformations of Ge structures under various substrate heating conditions. The DC heating induced shape transformation occurred for the Ge overlayer thickness of ≥ 8.0 ML. We first present results for the 10 ML Ge film thickness. Fig.3.3 shows representative FEGSEM micrographs for various substrate heating conditions. Fig.3.3(a) depicts the FEGSEM image for 10 ML thick Ge film deposited while keeping the substrate at RT during the germanium deposition. The average island size to be 504 ± 38 nm in diameter has been determined by averaging many particles from several frames. No aligned structures were observed in this case. Fig.3.3(b) shows the morphology for a 10 ML Ge film deposited at a substrate temperature of 600°C followed by a post-anneal of 15 minutes at the same temperature with RH heating. In this case, a distribution of bigger spherical Ge islands surrounded by a large number of smaller islands was observed, showing a kind of Oswald ripening process. But surprisingly, the sizes of the islands are much smaller than in case (i). A typical particle size histogram is shown in figure 2(a). We have fitted a lognormal distribution to obtain an average value for the size of the smaller islands, which was found to be 15.8 ± 1.5 nm with the distribution having a half width at half maximum (HWHM) of 5.5 nm. The bigger islands are found to have an average size of 54.0 ± 7.0 nm. Fig.3.4(a)is distribution of smaller islands.

Figure 3.3(c) depicts the formation of an ordered trapezoidal structure for a system in which DC heating was used with current along $\langle 1\bar{1}0 \rangle$. In the following figures, we show the effect of the DC current direction and the substrate orientation on the shape transformation. We have found circular to irregular shapes of Ge structures for the RT and RH conditions as shown in figures 3.3(a) and (b), but for the case of DC heating applied along $\langle 1\bar{1}0 \rangle$, there was also a shape evolution of the islands in contrast to the RH growth condition. Figures 3.4(b) and (c) show histogram distributions of the length of the base of the trapezium structures and aspect ratio (length to height ratio), respectively. These are obtained from several frames of SEM images for samples with 10 ML of Ge on DC heated Si(5 5 12) substrates.

It is to be noted that the SEM based energy dispersive system (EDS) would not help much to determine the composition of these trapezoidal structures as it is difficult to remove the contribution from the substrate silicon if there is intermixing or alloy formation. Hence, we have used the Rutherford backscattering spectrometry (RBS) to obtain an average depth profile (which will be presented at later stage in this paper) and cross-sectional TEM studies to determine the composition from single trapezoidal structures (published elsewhere). From these studies, we found that the Ge structures are actually mixed layer with $\mathrm{Si}_{1-x}\mathrm{Ge}_x$ composition with a composition gradient. Figure 3.6 depicts the shape evaluation of the $\mathrm{Si}_{1-x}\mathrm{Ge}_x$ structures as a function of various overlayer thickness of Ge on the DC heated Si(5 5 12) surface followed by 15 minutes annealing. The corresponding Ge thickness values are: (a) 3.0 ML, (b) 5.0 ML, (c) 8.0 ML and (d) 12.0ML. Figures 3.6(a) and (b) show that the structures are of rectangular shape (with length and aspect ratio corresponding to 3.0 and 5.0 ML Ge are: $2.6 \mu m$ and 2.1 and 3.5 μm and 2.2 respectively). This is clear from the inset of figure 3.6(a) which depicts higher magnification of these rectangular structures. For the 8.0, 10.0, and 12.0 ML cases, corresponding length and aspect ratios are founded to be 5.8 μm and 2.8, 6.2 μm and 3.0, and 8.9 μm and 3.17, respectively. Histogram distribution of the aspect ratios corresponding to 10 ML Ge deposition on Si(5 5 12) under the DC heating conditions can be seen in figure 3.4(c). The inset of figure 3.6(d) shows a higher resolution SEM micrograph where several coreshell like structures were seen on the large trapezoidal structure. These results exhibit a shape transition from rectangular type of structures (i.e. with aspect ratio of 2.2) to trapezoidal structures (aspect ratio of 3.1).

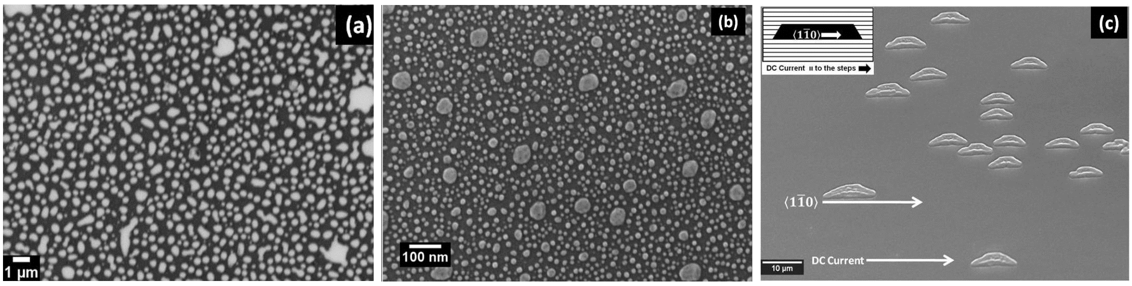

Figure 3.3: (a) SEM image of 10 ML Ge/Si(5 5 12) at RT, (b) at 600°C using the RH and (c) at 600°C using the DC heating. The inset of figure (c) shows the DC heating direction. [116].

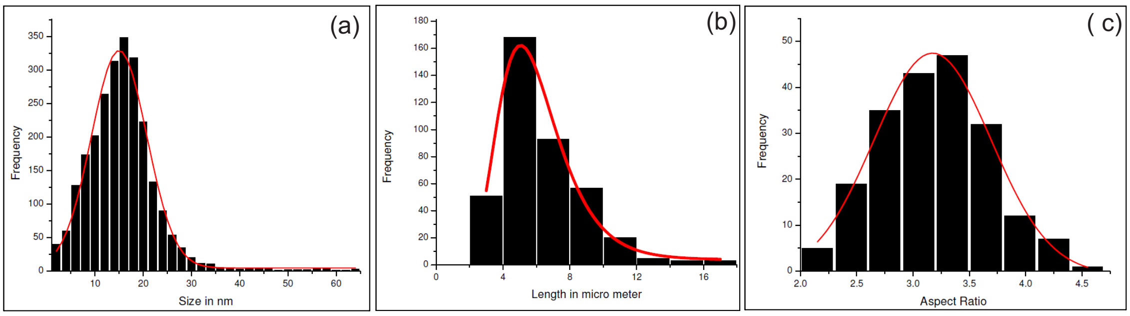

Figure 3.4: Histogram of (a) particle sizes in the case of RH, 10 ML Ge on Si(5 5 12), (b) length and (c) the aspect ratio of trapezoidal structures for the DC heated, 10 ML Ge on Si(5 5 12). [116].

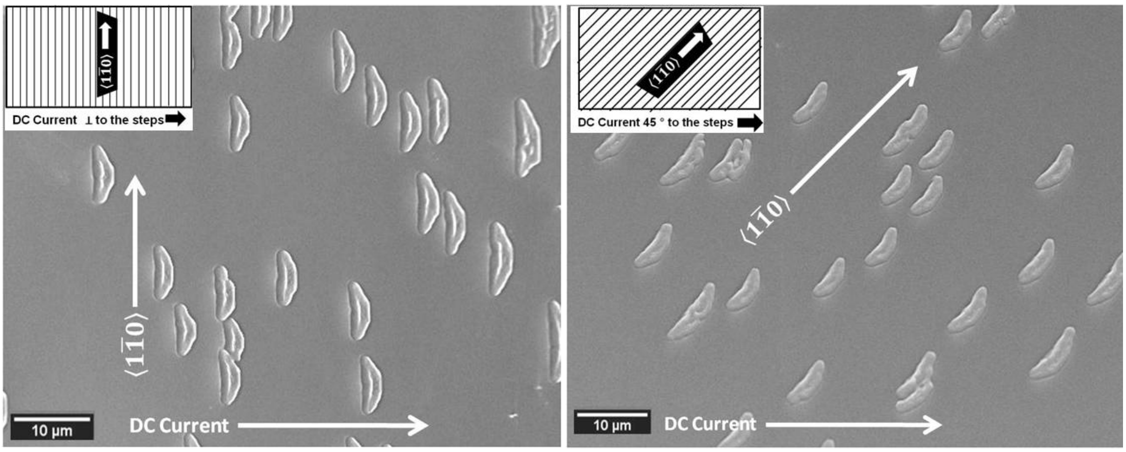

Figure 3.5: SEM micrographs of aligned trapezoidal structures of SiGe for different DC heating directions (a) perpendicular to ⟨1$\bar{1}$0⟩ and (b) at 45° to ⟨1$\bar{1}$0⟩. The inset shows the DC directions with respect to a set of planes. [116].

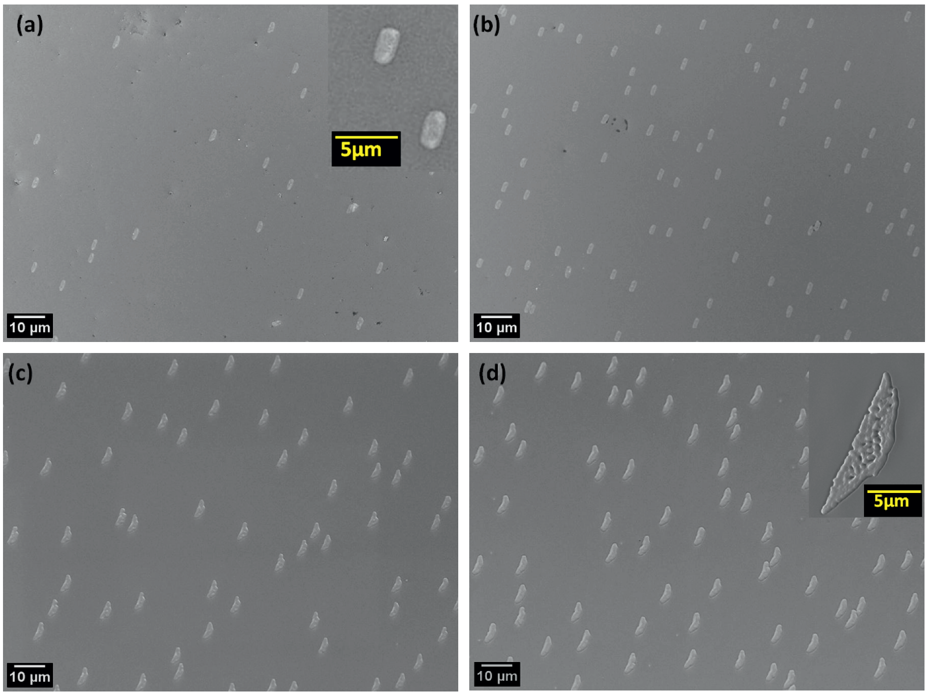

Figure 3.6: SEM image obtained from the DC heated sample (a) 3 ML Ge/Si(5512), (b) 5 ML Ge/Si(5512), (c) 8 ML Ge/Si(5512) and (d) 12 ML Ge/Si(5 5 12). The insets of (a) and (d) show magnified images of single microstructures [116].

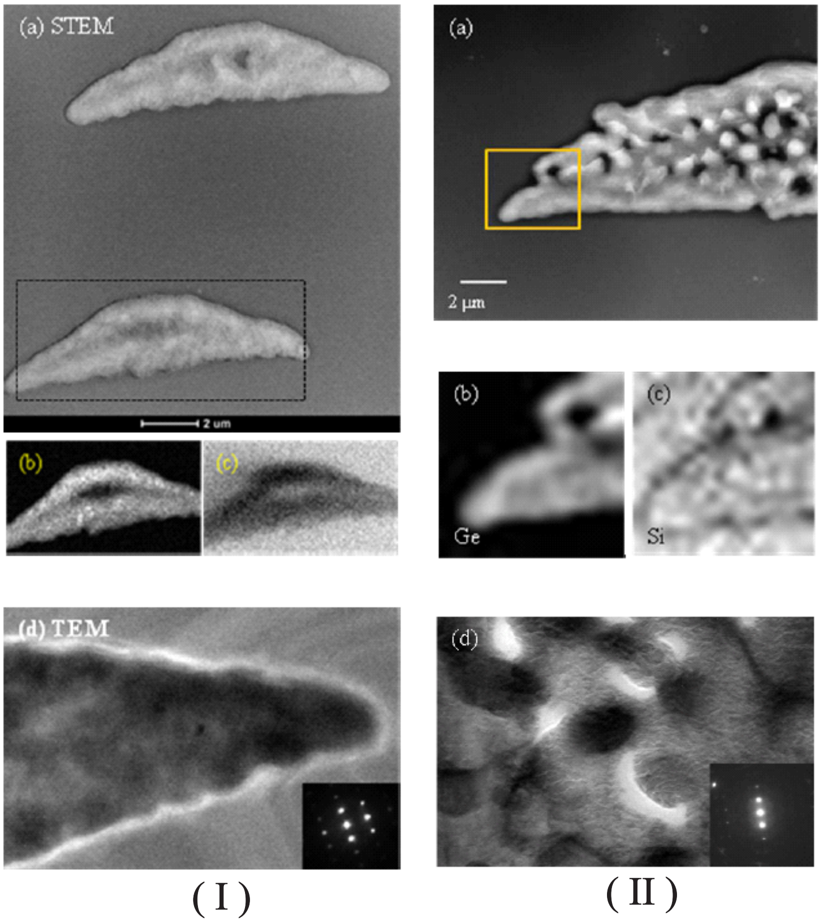

Figure 3.7: **I.**(a) STEM-HAADF image of a smaller SiGe structure: the contrast shows the depletion of Ge at the center of the island structure. (b) The image formed with Ge x-ray fluorescence signals (K_α) in the STEM-energy dispersive mode, where as in (c) the image is formed with Si x-ray fluorescence signals (K_α). (d) Shows a bright field TEM micrograph of a part of a larger SiGe island structures. The inset shows the diffraction pattern from these structures confirming the crystallinity of the structures. **II.**(a) STEM-HAADF image of a larger SiGe structure showing many coreshell like structures. (b) The image formed with Ge x-ray fluorescence signals (K_α) in the STEM-energy dispersive mode, where as in (c) the image is formed with Si x-ray fluorescence signals (K_α). (d) Shows a bright field TEM micrograph of a part of a larger SiGe island structure and circular coreshell structures can be seen. The inset shows the diffraction pattern from these structures confirming the crystallinity of the structures. [116].

Figures 3.7.I and 3.7.II show STEM and TEM micrographs for 10 ML Ge deposition under the DC heating conditions (along the $\langle 1\bar{1}0\rangle$) respectively. Typical shapes of these structures are shown by the FEGSEM image in figure 3.3(c). The STEM images were used to determine the nature of these trapezoidal structures. We present the STEM data from two types of trapezoidal structures: (i) one smaller structure with one core shell like structure and (ii) a second one with a larger area with many coreshell like structures. The STEM-high angle annular dark field (HAADF) image in figure 3.7.I.(a), that corresponds to a small SiGe structure, shows the expected Z-contrast so that the Ge-island appears brighter than the Si. Furthermore, the contrast decreases towards the island center, suggesting the Ge depletion there. To analyze the local distribution of the Ge in these structures, an STEM x-ray fluorescence mapping (energy dispersive spectrometry, EDS) was carried out for the whole island shown in figure 3.7.I.(a). Figure 3.7.II.(b) shows the Ge elemental distribution and figure 3.7.II.(c) depicts the Si elemental distribution. These maps not only confirm that the island consists of Ge, but also the Ge-enrichment was found at the island edges. The apparent Si-depletion in figure 3.7.II.(c) may be attributed to the formation of coreshell like structures in the islands. It should be noted that this could also be the case for $\mathrm{Si}_{1-x}\mathrm{Ge}_x$ structures with varying x values. Preliminary results based on EDS from a focused ion beam (FIB) prepared TEM specimen from single structure show a presence of Si and Ge mixing [117]. Figure 3.7.I.(d) depicts a low magnification TEM bright field image of a part of a smaller island. The selected area diffraction confirms (shown in the inset of figure 3.7.I.(d)) the crystallinity of these structures as no amorphous or polycrystalline ring like structures were seen. Figure 3.7.II shows a STEM-HAADF image from much larger trapezoidal structure. Several Si-Ge coreshell like structures were observed to grow inside these trapezoidal structures. A detailed high resolution TEM analysis could help us in determining the strain distribution around these structures and lead us to understand the governing mechanisms. As shown in figure 3.7.I, the elemental maps shown in figure 3.7.II.(b) (for the Ge) and figure 3.7.II.(c) (for the Si), confirm that the island consists of Ge, and also that Ge-enrichment can be found at the island edges. The circular holes like structures have much less Ge and more Si signals and confirms the presence of core-shell like structures. To confirm a possible intermixing of Si and Ge in these microstructures, RBS measurements were carried out. Figure 3.8 shows the RBS spectrum from the DC heated (along the $\langle 1\bar{1}0\rangle$) 10 ML of Ge/Si(5512) sample. The figure depicts raw data and the simulation with two sets of model depth distributions taken into account. The simulations were carried out using the RUMP code [100]. For the simulations, the specimen is treated as a multilayer with variation of Si and Ge concentrations in each layer. We have considered 12 layers for a model with SiO_x (figure 3.8(a)) and 7 layers without SiO_x (figure 3.8(b)). The scheme of layers used in the simulation is shown as the bottom-right inset in their respective figures. The outcome of the simulation (shown in figures 3.8(a) and (b)) is comprehensively tabulated in table-I. On careful examination of the RBS simulation, the fit is more reasonable for the Si (bottom-left insets) and the Ge (top-right insets) backscattered signals only in the case when a thin layer of the SiO_x is introduced (figure 3.8(a)). The SiO_x layer would have possibly formed due to the oxidation of the free Si surface (unoccupied area by the $Si_{1-x}Ge_x$ clusters) as the RBS measurements were carried out after several days of preparation of MBE specimen. Before loading into the RBS chamber, the samples were exposed to the atmosphere, so a possibility of formation of SiO_x cannot be ruled out on the surface. It should be noted that the FEGSEM images were taken soon after the specimen were taken out of the UHV chamber after the deposition and annealing in the MBE system. Also, the rectangular and trapezoidal structures were observed only under the DC heating conditions and not for the RT and the RH heating conditions. This confirms that the interfacial oxide layer does not play any role in the formation of such structures. The absence of any interfacial oxide layer was also evident from cross-sectional TEM data (described in the later chapters). Additionally, the inward diffusion of Ge (channels 12501350, top-right inset) into bulk Si and the outward diffusion of Si (channels 900940, bottom-left inset) can be clearly seen from figure3.8. The change in the composition of $Si_{1-x}Ge_x$ (as in table-I) as a function of depth may have a bearing on the kind of inter-diffusion process involved in the mixing of Si and Ge. We would like to emphasize that the RBS results correspond to a depth profile of Ge and Si and confirms the intermixing of Ge and Si. The RBS simulations show a presence of oxygen (around channel no. 600) which is absent in the experimental spectrum. One reason is the lower Rutherford cross-sections found experimentally compared to theory for the oxygen atoms. To determine an accurate oxygen depth profile, one needs to carry out nuclear reaction (NR- RBS) based experiments. As the role of the oxide layer is not a major factor, we do not propose to do these complicated NR-RBS experiments as of now. We also need to take note on a simple multilayer model that was used in the present RBS simulations. Realistically, one is required to take the surface roughness into consideration as well and this could help to get a proper understanding of the surface edges in RBS spectrum. As the emphasis of the present paper is on the formation of the various structures of Si-Ge system, we plan to carry out detailed RBS simulations at a later date.

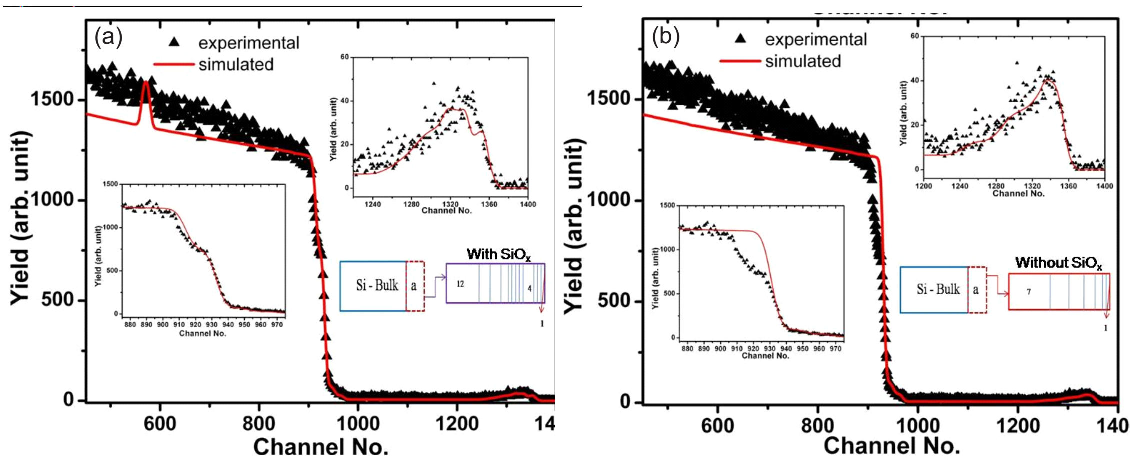

Figure 3.8: Experimental RBS spectrum from the DC heated (along $\langle 1\bar{1}0\rangle$) 10 ML Ge/Si(5 5 12) shown along with simulated data (a) with SiO$_x$ layer and (b) without SiO$_x$ layer. The insets show the enlarged portion of Si (bottom-left) and Ge (top-right) backscattered signals [116].

It is evident from the aforementioned results that a shape transformation has been achieved for the DC heating along $\langle 1\bar{1}0\rangle$. One of the immediate points that arise is that of the role of electromigration in the formation of aligned trapezoidal like structures. The drifting of defects and impurities in a crystal when it is subjected to an electric current is known as electromigration [81]. The drift may be due to charging of atoms and/or from the transfer of momentum from the charge carriers to the mobile atoms in the crystal [81]. Sakamoto et al found a temperature dependence of surface mass transport of In film over Si(100) vicinal surfaces [82]. Interestingly, in this case, surface electromigration was found to be dominant above a critical temperature while below it, only surface diffusion was observed in these studies [82]. Recently, Ware and Nemanich have reported on the surface morphology of strained and relaxed SiGe layers grown on the Si substrates with surface normals rotated off of the [001] axis towards [111] by 0°, 13°, and 25° [98]. Atomic force microscopy has revealed surface corrugations in thin layers prior to plastic relaxation on each of the surfaces due to the initial deposition of the strained films [98]. Wu et al [101] investigated the influence of surface step on the mass transport and observed a great anisotropy of the surface migration with an extraordinary enhancement in the direction parallel to the edge of the step for the Ag on the vicinal Si(111). To understand the dependence of the DC direction on the orientation of the trapezoidal structures, we have carried out a 10 ML thick deposition of Ge on the Si(5 5 12), by changing the substrate orientation with respect to the DC direction. Figures 3.5(a) and (b) depict the SEM micrographs for the case where the DC current was applied perpendicular and at 45° to $\langle 1\bar{1}0 \rangle$, respectively. The inset of figure 3.5 depicts the planar directions with respect to the DC current direction. Interestingly, the orientation of the trapezoidal structures did not change as per the DC current directions. In typical conventional electromigration experiments, the current densities would be $\approx 10^4$ A cm^{-2}. In our case, the typical current densities are ≈ 6.25 A cm^{-2}. Interestingly, the longer side of the trapezoidal structures is always aligned along $\langle 1\bar{1}0 \rangle$, irrespective of the DC passage direction. This clearly shows

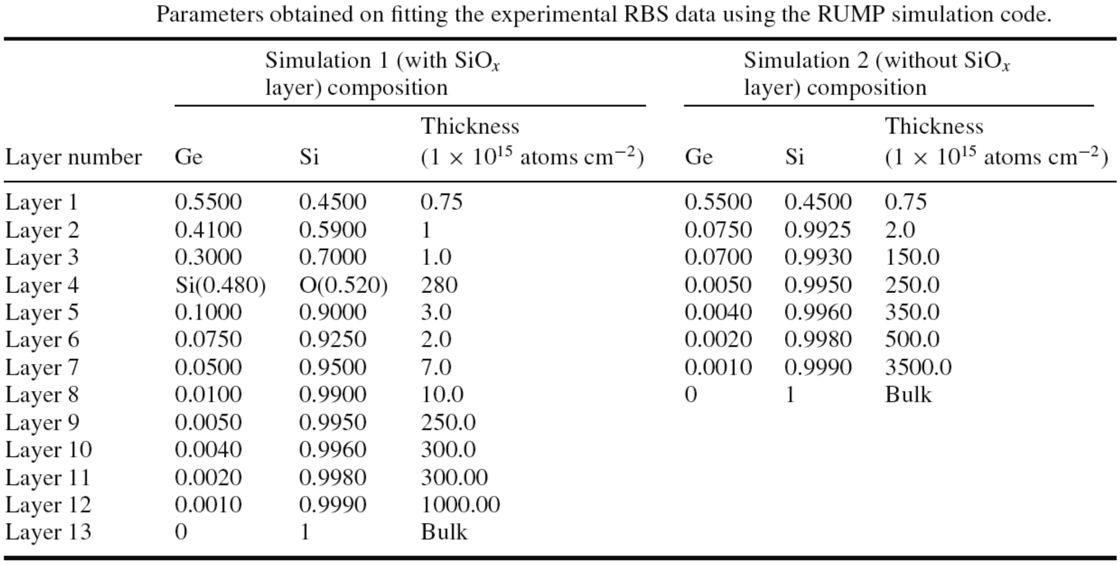

Parameters obtained on fitting the experimental RBS data using the RUMP simulation code.

	Simulation 1 (with SiO$_x$ layer) composition			Simulation 2 (without SiO$_x$ layer) composition		
Layer number	Ge	Si	Thickness (1×10^{15} atoms cm^{-2})	Ge	Si	Thickness (1×10^{15} atoms cm^{-2})
Layer 1	0.5500	0.4500	0.75	0.5500	0.4500	0.75
Layer 2	0.4100	0.5900	1	0.0750	0.9925	2.0
Layer 3	0.3000	0.7000	1.0	0.0700	0.9930	150.0
Layer 4	Si(0.480)	O(0.520)	280	0.0050	0.9950	250.0
Layer 5	0.1000	0.9000	3.0	0.0040	0.9960	350.0
Layer 6	0.0750	0.9250	2.0	0.0020	0.9980	500.0
Layer 7	0.0500	0.9500	7.0	0.0010	0.9990	3500.0
Layer 8	0.0100	0.9900	10.0	0	1	Bulk
Layer 9	0.0050	0.9950	250.0			
Layer 10	0.0040	0.9960	300.0			
Layer 11	0.0020	0.9980	300.00			
Layer 12	0.0010	0.9990	1000.00			
Layer 13	0	1	Bulk			

Figure 3.9: Table-I Si-Ge composition profile from RUMP simulation

that a major role is taken by the enhanced diffusion along the steps. It should be

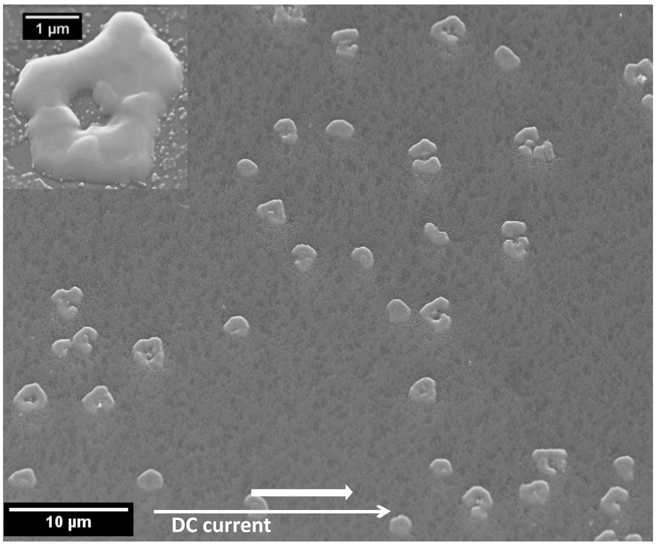

Figure 3.10: SEM micrographs of germanium islands formed during the 10 ML Ge deposition on Si(111) for the DC heating applied along $\langle 11\bar{2} \rangle$. No alignment to a particular direction is observed. [116].

noted that the steps are aligned along $\langle 1\bar{1}0 \rangle$ for the reconstructed Si(5 5 12) surface. In the clean Si(5 5 12)- 2 × 1 surfaces, the distance between the steps is 5.35 nm. So, the micrometer size trapezoidal islands needs to sprawl across many steps. In this situation, one may wonder whether the steps have any role to play in this alignment for the elongated GeSi structures. It has been reported that, islands can sprawl over many steps [102]. The role of the DC appeared to enhance the atomic mass transport quite appreciably along the steps. It is interesting to note the observations obtained from the 10 ML thick deposition of Ge on the Si(111) surface (low index substrates) under the DC heating conditions, similar to the values used for the Si(5 5 12) substrates. In this case, the DC direction was applied along $\langle 11\bar{2} \rangle$. Figure 3.10 depicts growth of microstructures that have no definite alignment along $\langle 11\bar{2} \rangle$. We plan to carry out further in-depth studies to gain a proper understanding of these experimental results that include the dependence of Ge overlayer thickness and coreshell like structure formation.

3.4 Conclusions

In this chapter, we reported the formation of aligned $\mathrm{Si}_{1-x}\mathrm{Ge}_x$ microstructures with an aspect ratio of 3.0 by passing the direct current along the $\langle 1\bar{1}0\rangle$ direction at the higher Ge overlayer thickness values more than 8.0 ML. For the rectangular Si-Ge structures, no coreshell like structures were found unlike on the trapezoidal structures. Under similar conditions, when the substrate heating was obtained by the radiative heating process, no aligned rectangular or trapezoidal structures were formed. The trapezoidal structures were found to have varying composition along their depth and be uniquely aligned along the $\langle 1\bar{1}0\rangle$ direction, irrespective of DC direction. Under similar conditions, when the DC heating was applied along $\langle 11\bar{2}\rangle$ of the Si(111) substrate, no aligned structures were found. We also argue that a possible oxide layer formed on the substrate after the deposition and annealing in a UHV system do not play a role on the various structures that are presented in this work.

Chapter 4

Growth dynamics and shape evolution of $\mathbf{Si}_{1-x}\mathbf{Ge}_x$ structures on ultra-clean high index silicon surfaces

4.1 Introduction

The use of high index silicon surfaces as substrates can enhance the formation of aligned nanostructures with self-assembled growth [71, 96–98, 104], which is not so easily achievable with lithography tools. Due to its natural process- and damage-free features, structural self-organization on high index surfaces has received much attention in the formation of coherent 1D and 2D semiconductor / metal nanostructures. High index and vicinal surfaces are found to have reconstructions into regular hill (step) and valley (terrace) structures with periods ranging from several nanometers to about one hundred nanometers. The periodicity of such structures depends mainly on the substrate orientation and miscut or vicinal angles. These self assembled nano-structures can be used as templates for the growth of low dimensional semiconductor and metallic nanostructures with controlled size and periodicity. In the past, the growth of Ge nanostructures on low index silicon substrates (such as Si(100), Si(111)) has been studied extensively. However, less attention has been paid to Ge growth on high-index Si substrates. Hence, the study of self-assembly of Ge on high-index silicon surfaces would be an important field of research in obtaining various types of nanostructures that may be useful in optoelectronic devices. The lattice mismatch between Ge and Si ($\sim$4.2%) is an important property of such quantum devices, as it determines the maximum thickness of smooth films (quantum wells) and controls band structures, mobility of carriers, and quantum confinement potential.

The implementation of Ge and $\mathrm{Si}_{1-x}\mathrm{Ge}_x$ nanostructures into Si-based devices is of great potential for future high-speed devices, due to advantages like enhanced carrier mobility and smaller bandgap [19–21]. Growth of Ge islands on clean Si substrates (particularly on low-index-oriented) has been extensively studied as a model system to understand hetero-epitaxy and Stranski-Krastanov (SK) growth mechanism [86, 87]. But, the study of Ge growth on high index surfaces, such as Si (5 5 12), Si(5 5 7) and Si(5 5 3) is an area where very limited research work has been carried out [73, 97]. Previous study by Kim *et al* [97] reported on relatively thinner Ge growth on Si (5 5 12) and did not observe any shape transformation of the Si-Ge structures. For the Ge on Si system strain relief and diffusion play a role in determining the morphology and composition of Ge or Si-Ge structures [86,87,91]. $\mathrm{Si}_{1-x}\mathrm{Ge}_x$, alloys show smaller fundamental bandgap compared to Si, because of a larger lattice constant and altered lattice constituents [105]. Strained Si-Ge technology has been recognized as a promising solution for high-performance devices,because of its cost-effectiveness and high carrier mobility.The integration of light sources, photodetectors and optical modulators into the silicon technology by using Si-Ge structures, such as multiple quantum wells has been actively dealt recently [106]. Composition grading is one of the well-established techniques to prevent dislocations from reaching the surface [107–109]. In the present work, we have observed the variation in the size of the $\mathrm{Si}_{1-x}\mathrm{Ge}_x$ structures depending on the substrate orientation while having the similar aspect ratio values for all three substrate orientations. The variation in the size of the islands has been explained by considering the experimentally observed composition of the structures and strain associated in them. The universal nature of shape evaluation is simulated with 2D kMC simulations.

Reconstructed high index silicon surfaces consisting of alternating terraces and atomic steps can be used as templates to form aligned one dimensional (1D) nanostructures [71, 74, 76]. Atomic steps on the high index silicon surfaces are responsible for many surface dynamic processes like surface migration and step diffusion. It is possible to use the high index substrates for the growth of self-organized nanostructures [73]. Like Si(5 5 12), Si(5 5 7) is also a vicinal silicon surface having a vicinal angle of 9.45° from (111) towards $(11\bar{2})$ [110].The highly corrugated triple step structure of the Si(5 5 7) surface is easier to detect than other long-range surface reconstructions [fig.4.1]. Si(5 5 3) , tilted at -12.27° from the (111) plane towards the (001) plane [111], are important high index Si surfaces[fig.4.2]. In all the above vicinal surfaces, the step edges are along $\langle 1\bar{1}0 \rangle$ direction.

It is known that strained epitaxial layers tend initially to grow as dislocation-free islands and as they increase in size, may undergo a shape transition [91, 92]. Below a critical size, islands can have a compact symmetric shape. But at larger sizes, they adopt a long shape, which allows better elastic relaxation of the island's stress [91,92,112]. Tersoff and Tromp proposed a model to explain the growth kinetics involving a shape transition at a critical size by finding an expression for energy of dislocation-free strained islands [92]. Also, Heyn reported the kinetic Monte Carlo (kMC) methods to study the influence of the anisotropy of surface diffusion and of the binding energies [113]. Kinetic Monte Carlo methods have been used to study the formation of nanoisland structures in a number of works [114, 115], however, shape transition phenomena has hardly been studied.

In this chapter, the shape evolution of MBE grown $\mathrm{Si}_{1-x}\mathrm{Ge}_x$ islands on ultraclean reconstructed high index Si(5 5 12), Si(5 5 7) and Si(5 5 3) surfaces has been studied experimentally and explained using a phenomenological kinetic Montecarlo (kMC) simulation. We show that a self assembled growth at optimum thickness leads to interesting shape transformations, namely spherical islands to rectangular rods up to a critical size beyond which the symmetry of the structures is broken, resulting in a shape transition to elongated trapezoidal structures. We observe a universality in the growth dynamics in terms of aspect ratio and size exponent , for all three high index surfaces, irrespective of the actual dimensions of Ge-Si structures. The shape evolution has been simulated using kMC by introducing a deviation parameter (ϵ) in the surface barrier term (E_D) to take the effect of anisotropic diffusion, as one of the plausible mechanisms.

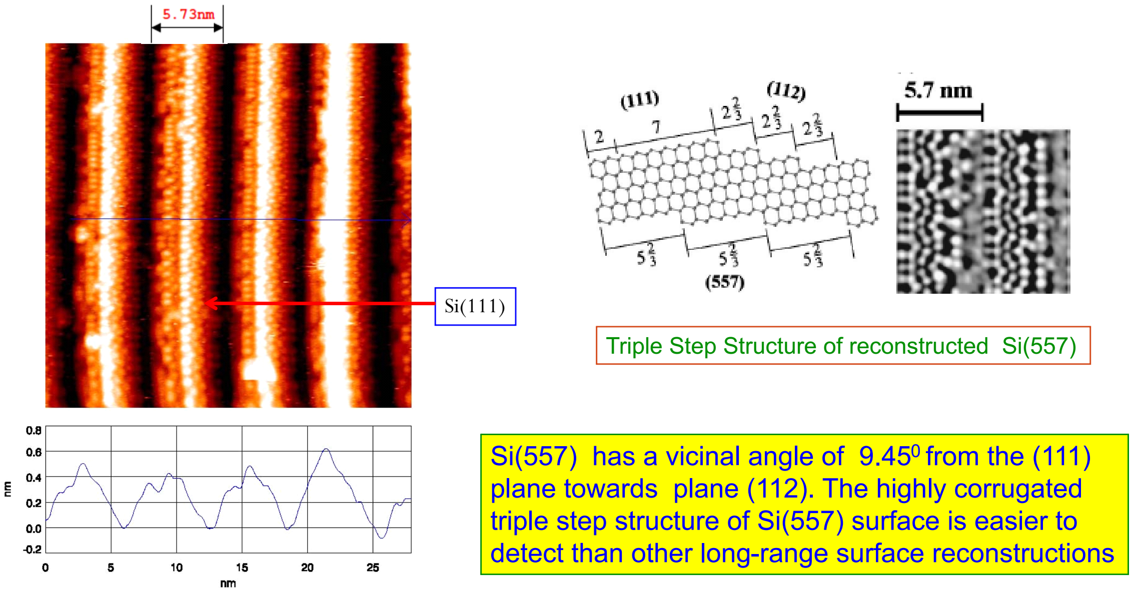

Triple Step Structure of reconstructed Si(557)

Si(557) has a vicinal angle of 9.45^0 from the (111) plane towards plane (112). The highly corrugated triple step structure of Si(557) surface is easier to detect than other long-range surface reconstructions

Figure 4.1: STM image of reconstructed Si(5 5 7)surface taken at center for atomic wires and layers, Yonsei University,South Korea. The schematic of the surface reconstruction is from ref. [110].

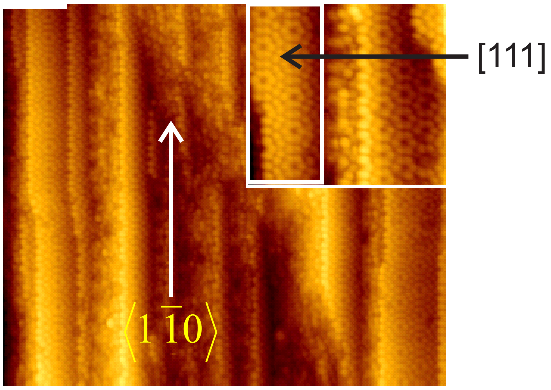

Figure 4.2: shows an STM image of clean Si(5 5 3) surface, which is a stepped Si(111) surface with a single domain. The inset is an enlarged image with a (7×7) structure. (image taken at center for atomic wires and layers, Yonsei University, South Korea).

4.2 Experimental methods

For the sake of continuity, we briefly describe the experimental conditions during the growth. The Ge depositions on Si(5 5 12), Si(5 5 7) and Si(5 5 3) were carried out under ultrahigh vacuum (UHV) condition in a custom-designed molecular beam epitaxy (MBE) system with a base pressure of $\sim 2.5 \times 10^{-10}$ mbar in the growth chamber. The substrates used were of size 8×3 mm^2 cut from p-type (boron doped) single crystal Si wafers with a resistivity of 10 to 15 Ω-cm. Atomically clean, reconstructed surfaces were prepared by following the usual thermal cleaning procedure: the samples were first degassed at about 600°C for 12-14 h followed by a repeated flashing for 30 s at $\sim$ 1250°C. The reconstructed surfaces were confirmed by in-situ reflection high energy electron diffraction (RHEED). Ge film were deposited to various thicknesses at a typical deposition rate of 0.6 ML.min^{-1} (one ML corresponds to 7.8 $\times 10^{14}$ atoms.cm^{-2} for a Si(111) surface). The substrates were kept under three substrate heating conditions: (i) at room temperature, (ii) at 600°C-RH and (iii) at 600°C-DH. In the second case, the sample was annealed at a temperature of 600°C for 15 minutes after deposition using RH, and for case (iii), the annealing was done by passing the direct current through the sample corresponding to a temperature of 600°C . The post-growth characterization of the samples was carried out ex-situ by field emission gun scanning electron microscopy (FEGSEM) and scanning transmission electron microscopy (STEM) based x-ray energy dispersive spectrometry (EDS). The FEGSEM measurements were carried out with 20 kV electrons using a Neon 40 cross-beam system (M/S Carl Zeiss GmbH) at Institute of Physics, Bhubaneswar, India.

4.3 Results and discussions

4.3.1 Comparative study on surface morphology of Ge/Si(5 5 12), Ge/Si(5 5 7) and Ge/Si(5 5 3) systems

In this section, we present a comparative study of aligned Si-Ge structures formed at the interface of ultra clean reconstructed Si(5 5 12) and Si(5 5 7) surfaces and Ge, where the substrates were heated by direct current (DC) and radiative heating (RH) during deposition of Ge. The size of the aligned Si-Ge Structures depends on the substrate orientation and over-layer thickness.

Figure 4.3(a) and (b) show the morphology for 10 ML Ge on Si(5 5 12) and Si(5 5 7) respectively, at a substrate temperature of 600°C followed by a post-anneal of 15 minutes at the same temperature with RH heating. In this case, a distribution of bigger circular Ge islands surrounded by a large number of smaller islands was observed. This type of distribution is consistent with Ostwald ripening. Figure 4.3(c) shows the typical particle size histogram for 10 ML Ge/Si(5 5 12)-RH depicting a bimodal size distribution with an average value for the size of the smaller islands of 15.8 ± 1.5 nm and for the bigger islands of 54.0 ± 7.0 nm. In figure4.3(d), a bimodal distribution of particle size is shown for the spherical Ge islands grown on Si(5 5 7) in RH condition as well. In this case, the number of bigger islands is also significant, unlike in the case of Si(5 5 12). The average values for the size of the smaller islands and bigger islands are 12.8 ± 0.5 nm and 37.2 ± 2.1 nm respectively. To have a complete understanding, Similar analysis were done for 10 ML Ge/Si(5 5 3) system. We have observed the similar growth dynamics in this case also. For the RH-case the spherical islands show a bimodal distribution [Fig.4.4] ,where the mean size of the bigger and smaller islands are 31.8 ± 1.5 nm and 11.3 ± 0.3 nm respectively.

In the next section, we'll discuss the growth dynamics in the DC condition. Also the shape evolution will be explained using kinetic Monte Carlo simulation. We'll also present a quantitative estimation of optimal area of the Ge-Si structures to have a shape transition.

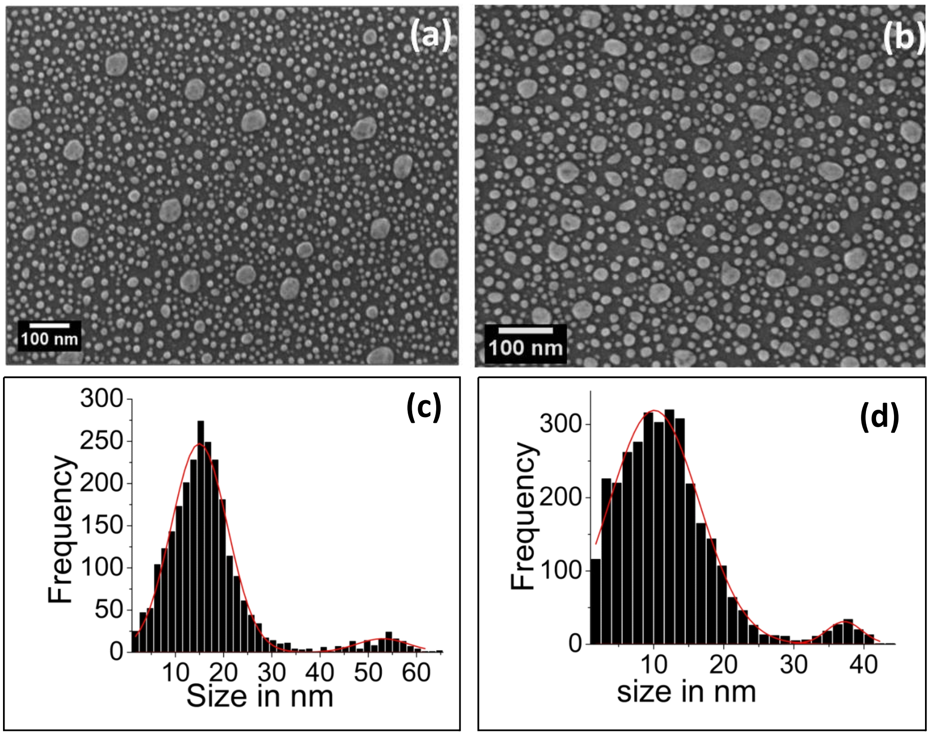

Figure 4.3: (a) and (c) SEM image and island size histogram of 10 ML Ge/Si(5 5 12) at 600°C - RH. (b) and (d) SEM image and island size histogram of Ge/Si(5 5 7) at 600°C - RH [117].

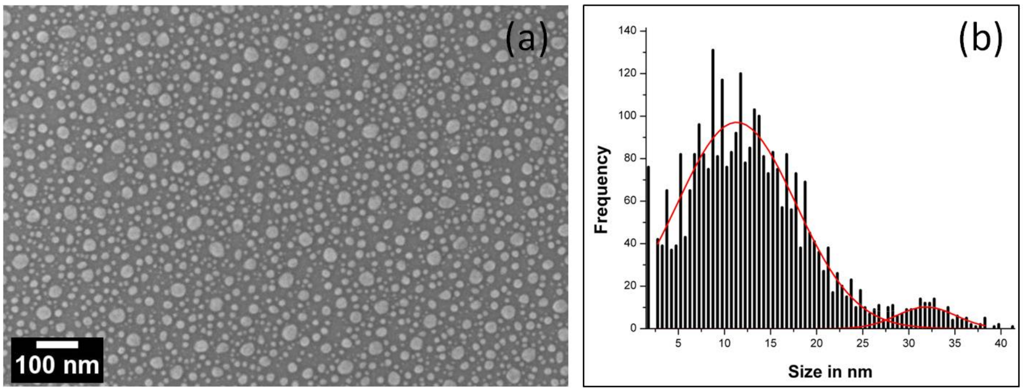

Figure 4.4: (a) SEM micrograph (b) histogram (size) of the spherical islands for 10 ML Ge/Si(5 5 3) at 600°C-RH.

4.4 Universality in growth dynamics and shape evolution of $\mathbf{Si_{1-x}Ge_x}$ structures

Figure 4.5 (a) and (b) depict the FEGSEM image for 2 ML and 5ML thick Ge film deposited on Si(5 5 12) substrate. As shown in Fig 4.5(a), the island structures are found to be spherical shape for a 2 ML Ge deposition, but for 5 ML Ge growth, rectangular island structures have been observed. For the 8ML and 10ML deposition cases, we observe trapezoidal structures [Fig.4.5(c),(d)]. It was reported earlier that DH is a necessary condition to form trapezoidal structures on Si(5 5 12) [116]. The composition of these nanostructures has been characterized by using STEM - EDS [116,117], Rutherford backscattering spectrometry (RBS) [116] and the synchrotron-based high resolution x-ray diffraction (HRXRD). The HRXRD showed presence of graded $Si_{1-x}Ge_x$ system for the Si(5 5 12)and is also confirmed by RBS measurements, while RBS measurements show no prominent graded $Si_{1-x}Ge_x$ structures for the case of Si(5 5 3)and Si(5 5 7) substrate orientations (described in chapter 6).

In fig.4.6, Ge growth of overlayer 3ML to 10ML on Si(5 5 7) has been shown where spherical nanoislands and rectangular nano rods are formed for 3ML and 5ML thicknesses [Fig.4.6(a),(b)] and nano trapezoid for the case of 8 ML and 10 ML Ge growth [Fig.4.6(c), (d)]. We have maintained the same growth condition for Si (5 5 3) substrate and seen that the growth kinetics and shape transformation follow in a similar way resulting from rectangular nano rod to nano trapezoid, as shown in fig.4.7.

We have measured the length and aspect ratio (length/width) of all the Ge-Si structures which has been shown in a tabular form in table 4.1 and table 4.2. In the case of Ge/Si (5 5 12) system, the size of the aligned structures are of micrometer size. But for the Si(5 5 7) and Si(5 5 3) systems,the size of the aligned structures are of nanometer size, though the shape evolution and also the aspect ratios are similar to that of Si(5 5 12) .

From table4.1, it is clearly seen that with increasing thickness, the size and aspect ratio of the Ge-Si structures increase accordingly. The aspect ratios of the Si-Ge

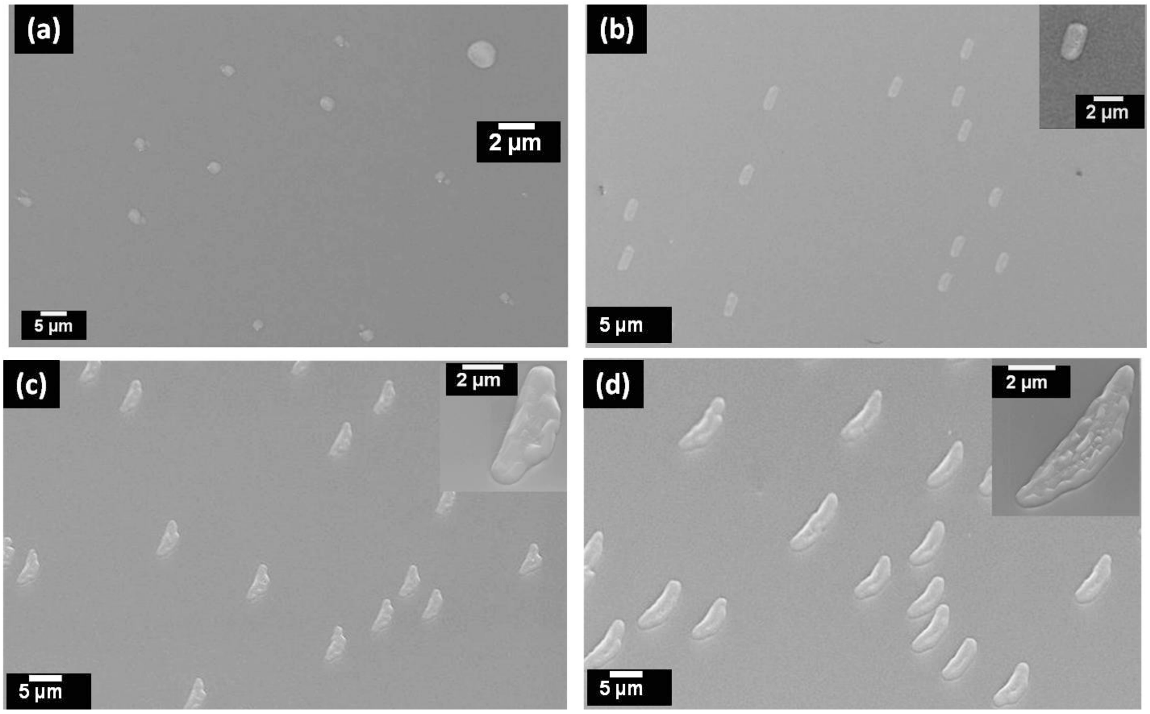

Figure 4.5: SEM micrographs of (a)2 ML(b)5 ML(c)8 ML (d)10 ML Ge/Si(5 5 12) at 600°C-DC condition. Insets show magnified image of one structure [120].

Table 4.1: Mean Length (L)

Thickness	Ge/Si(5 5 12)	Ge/Si(5 5 7)	Ge/Si(5 5 3)
(ML)	Mean L in (μm)	Mean L in(nm)	Mean L in(nm)
3	2.63 ± 0.14	115.5 ± 7.2	117.5 ± 8.2
5	3.51 ± 0.12	200.6 ± 8.7	189.8 ± 9.7
8	5.85 ± 0.22	250.6 ± 9.6	248.7 ± 11.6
10	6.25 ± 0.27	297.8 ±11.4	288.3 ± 12.4

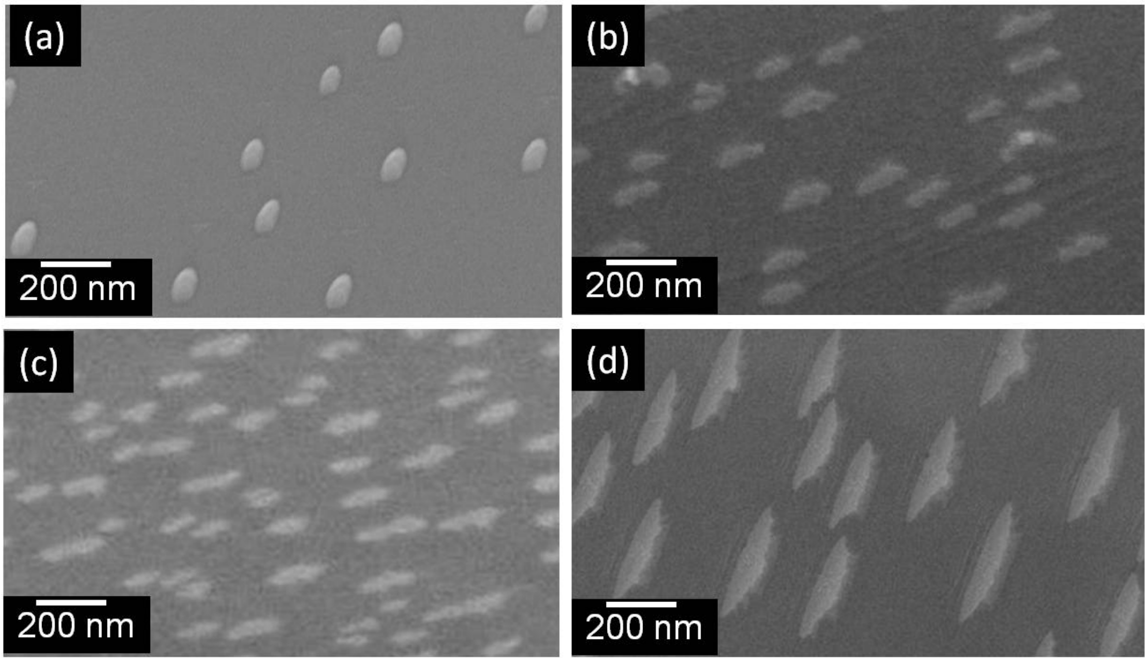

Figure 4.6: SEM micrographs of (a)3 ML(b)5 ML(c)8 ML (d)10 ML Ge/Si(5 5 7) at 600°C-DC condition. Insets show magnified image of one structure [120].

elongated structures on Si(5 5 12),Si(5 5 7) and Si(5 5 3) increase in a similar fashion as a function of increasing Ge growth coverages, which has been shown in table 4.2.

We found from our experiments that the mean length of islands $\langle L \rangle \sim t^{\alpha}$ where t is the time of deposition.The length exponent from the experimental data is found to be about 0.75 ± 0.02 for the case of direct heating and 0.5 ± 0.01 for the radiative heating condition, in all the three systems [table 4.3].

Table 4.2: Aspect Ratios (length/width)

Thickness	Ge/Si(5 5 12)	Ge/Si(5 5 7)	Ge/Si(5 5 3)
(ML)	Aspect Ratio	Aspect Ratio	Aspect Ratio
3	2.10 ± 0.1	1.79 ± 0.2	1.74 ± 0.6
5	2.20 ± 0.1	2.28 ± 0.6	2.34 ± 0.8
8	2.84 ± 0.5	2.88 ± 0.3	2.92 ± 0.9
10	3.13 ± 0.3	3.17 ± 0.4	3.15 ± 0.5

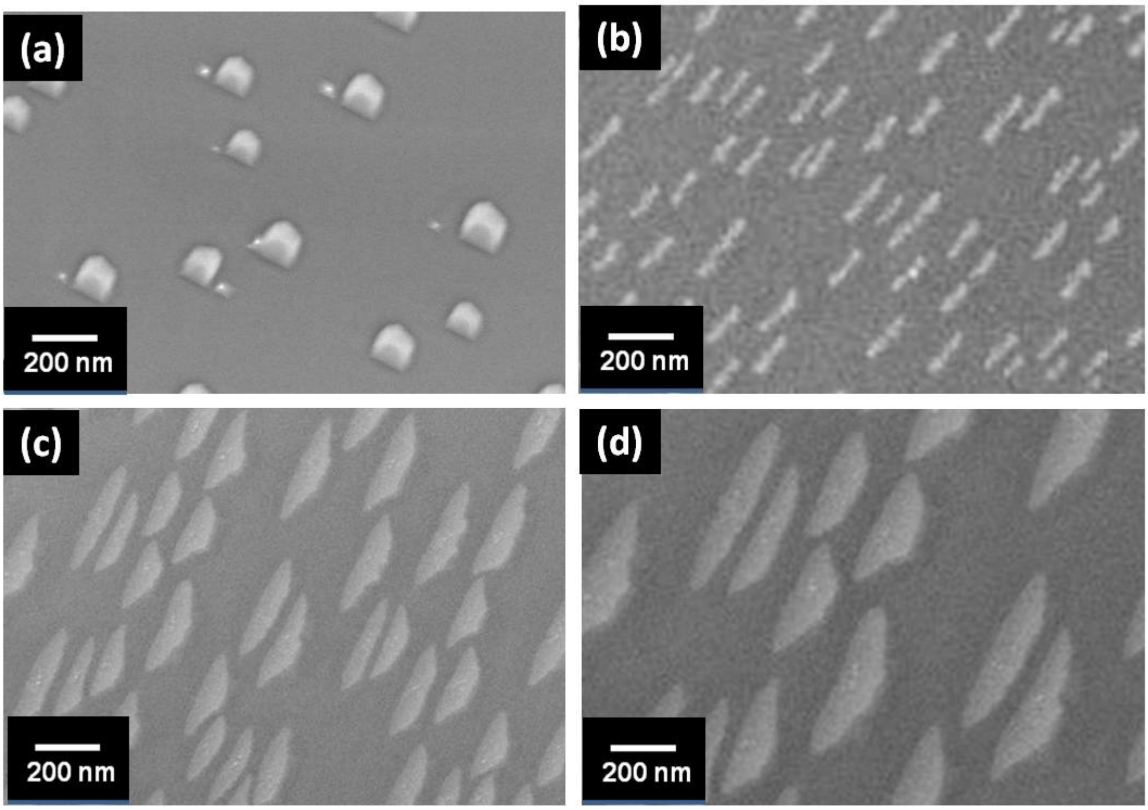

Figure 4.7: SEM micrographs of (a)3 ML(b)5 ML(c)8 ML (d)10 ML Ge/Si(5 5 3) at 600°C-DC condition. Insets show magnified image of one structure [120].

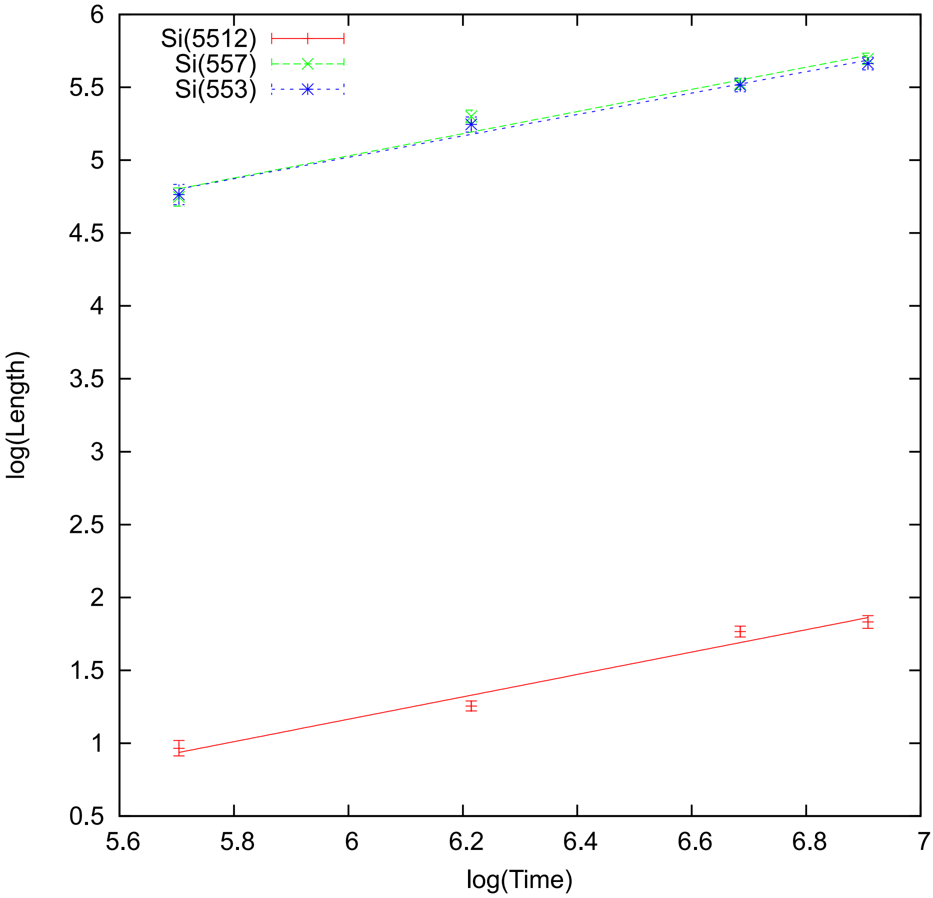

Figure 4.8: Plot showing the Length Exponents of the strucrures formed on Si(5 5 12), Si(5 5 7)and Si(5 5 3) surfaces [120].

Table 4.3: Length Exponent (α)

Exponent	Ge/Si(5 5 12)	Ge/Si(5 5 7)	Ge/Si(5 5 3)
DC	0.77±0.04	0.76±0.03	0.73±0.02
RH	0.51±0.03	0.53±0.02	0.52±0.04

In fig 4.8, the log-log plot for size(length) vs deposition time shows almost same slope(α) irrespective of the size of the Si-Ge structures on the three substrates.

4.4.1 Theoretical Modeling

The kinetic Monte Carlo simulations were performed on a $L \times L$ square lattice with $L = 100, 200, 300, 400$. We would like to emphasize that this model is a general model which describes the shape transition on a two dimensional square lattice where the dynamics is constrained by the underlying symmetries of the high index surfaces.As we have described earlier, the step edges on the Si surfaces are directed along $\langle 1\bar{1}0 \rangle$ direction.The trapezoidal structures are aligned along the same directions.In view of this,a coordinate system has been chosen such that the x-axis is directed along perpendicular to the step edges. In this coordinate system the trapezoids have a reflection symmetry about the lines parallel to the x-axis and passing through the center of the trapezoids. We define horizontal bond as a pair of nearest neighbor atoms having the same y coordinates and vertical bond having the same x coordinates respectively.The hopping rate of an adatom is given by

$$w = \nu_0 e^{-(E_D+n_1E_1+n_2E_2+n_3E_3)/k_BT} \tag{4.1}$$

where k_B is the Boltzman constant, T is the temperature and $\nu_0 = 2k_BT/h$ is the vibrational frequency in the direction of the hopping. A typical value for our case is $\nu_0 = 3.6 \times 10^{13}$ sec^{-1}. The quantities E_1, E_2 and E_3 denote the binding energies for the horizontal bond, vertical bond and the next nearest neighbor interaction respectively ; n_1,n_2 and n_3 are the number of horizontal bonds, vertical bonds and the number of next nearest neighbors respectively and E_D is a surface barrier term. For E_D and E_i, $(i = 1, 2, 3)$ constant, we obtained spherically symmetric island structures in the kMC simulation, since the binding energies are same for all bonds and surface barrier term is independent of direction. To obtain asymmetrical structures , we need to break the hopping symmetry. In our model, we introduce anisotropy through binding energies of different types of bonds and the dependence of surface barrier on the direction of hopping. For the isotropic cases, however, the hopping rate depends only on the nearest and next nearest neighbor interactions but does not depend on the specific arrangement of the neighboring atoms. In our experiment, the shape transformation has been observed when Ge is grown under DC condition [116]. To simulate the experimentally observed shape variations, the surface barrier term is modified so that it allows an asymmetric hopping of an adatom along the direction perpendicular to the step edge (i.e. ± x direction). The values of E_D along the step edges are same in both ± y directions. When $E_1 = E_2$ and E_D does not depend on the direction of hopping,spherical islands are formed. Symmetric elongated structures are formed for $E_2 > E_1$ and E_D uniform in all the directions of hopping. Trapezoidal islands can only be obtained when an asymmetric hopping term is present. The values of E_D are defined as follows : a) $E_D = E_0(1+\epsilon)$ for hopping along the positive x-direction, b) $E_D = E_0(1-\epsilon)$ for hopping along the negative x-direction, c) $E_D = E_0$ for hopping along y-axis where ϵ depends only on the magnitude of the current (but for the simulations, this is a parameter only). Also $0 < \epsilon < 1$ so that the probabilities are strictly less than unity. Note that when $\epsilon = 0$, it reduces to the RH case and $\epsilon > 0$ leads to DC heated case. When $E_2 > E_1$, anisotropic island forms as in the case of Ref. [113] and isotropic islands forms for $E_2 = E_1$ as in Ref. [118].Therefore, in our kMC simulation a nonzero value of ϵ could correspond to the MBE growth done under DC heating. The mean shape of islands for this case is found to be trapezoids.

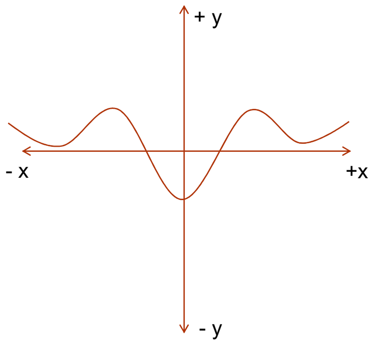

Figure 4.9: Schematic sketch of coordinate system chosen in kMC simulation

We follow the kMC algorithm in [118, 119]. We set the total coverage θ and the total number of Monte carlo steps N_{MC}. Particles are deposited at a constant flux θ/N_{MC}. Here θ may not exactly correspond to the experimental coverages, since here we are modeling the island growth by a 2D kMC simulations. However, we are successfully able to show that with an increase in coverage θ there is a shape transformation. We define a dimensionless scale parameter $\phi = E_0/K_BT$, where E_0 is the surface energy barrier of the system when $\epsilon = 0$. This sets the time step for the simulation. An atom with empty adjacent site is called 'active'. An active atom is chosen at random and a single diffusion event is allowed to occur with a probability consistent with Eq.(1). If an atom is already there on the site to which it chooses to hop, then hopping fails. Time is incremented irrespective of whether the hopping is successful or not. The following parameters were used for our kMC : $\phi = 1.0, E_1 = 1.0, E_2 = 6.0, E_3 = 0.5, E_0 = 1.0, \epsilon = 0.8$, and coverage is 2.5%. It is important to note that the relative strength of the energy values is crucial in determining the shape of the structures. The above set of energy parameters is one such example.

In fig. 4.10 (a),spherical shaped islands for $\epsilon = 0, E_1 = E_2$ are seen. For $\epsilon = 0.8$, $E_1 < E_2$ at coverage 0.2θ, rod like aligned structures formed [fig.4.10(b)]. Figure4.10 (c) is final snapshot of the trapezoidal structures formed at coverage θ for $\epsilon = 0.8$ and $E_1 < E_2$.

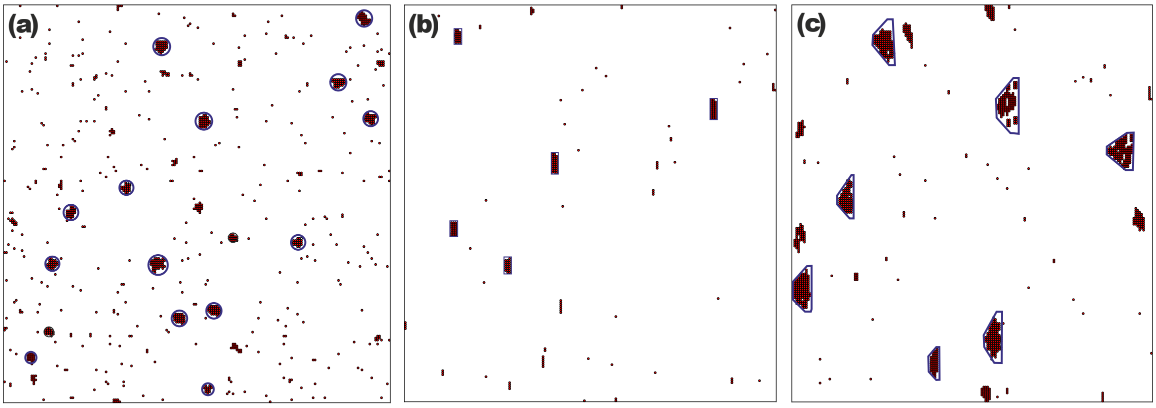

Figure 4.10: Snapshot of kMC island growth (a)spherical shaped islands at $\epsilon = 0$, $E_1 = E_2$ (b) $\epsilon = 0.8$,$E_1 < E_2$ rod like structures at coverage 0.2θ (c) $\epsilon = 0.8$, $E_1 < E_2$ showing shape transition by forming trapezoidal island structures at coverage θ [120].

4.4.2 Critical area of shape transitions

The above-mentioned high index surfaces has one-dimensional symmetry. In this case, the island growth up to to a critical size has a one-dimensional wire or quasi-one-dimensional rod shape. Beyond the critical size, the island grow in trapezoidal shape. At this point, Let us try to make a quantitative idea of shape transition. To do so, we have measured the individual length, width and area of the Ge-Si structures for for all thicknesses from 3ML to 10 ML. We calculated the area of individual structures. Here, one obvious question, one can ask is that, what is the optimal area of an island to attain rectangular rod shape? To find the answer, we have plotted L_1, L_2 vs Area of all the Ge-Si structures found. For the rod shaped island, we calculated area as $L_1 \times L_2$ and for trapezoidal structures we measured the areas as $\frac{1}{2}d(L_1+L_2)$, where d is the width of the trapezoidal structures. The nomenclature for L_1 and L_2 is shown in pictorial form[fig.4.11]. Figure4.11 (a) shows the shape transition plot for Ge/Si(5 5 12) system. Here, we notice that, the Ge-Si island grows in rectangular form ($L_1 = L_2$) up to a critical size following the one dimensional symmetry of the substrate. For the largest rectangular rod, the area is $L_1 \times L_2 = 6.48$ μm^2 (measured). Beyond this critical area the island grow in trapezoidal shape ($L_1 > L_2$).The plot clearly shows a bifurcation at the point of optimal area. When $\frac{L_1}{L_2} = 1$ the curve is linear and while $\frac{L_1}{L_2} > 1$, the curve bifurcates to show the discontinuity. The Figure4.11 (b)and (c) show the similar plots for the Ge/Si(5 5 7) and Ge/Si(5 5 3) systems , where the critical area for the shape transformations are 10845.6 nm^2 and 9456.8 nm^2 respectively. The plots are in reasonable agreement with the gross features of the Tersoff and Tromp theory [92].

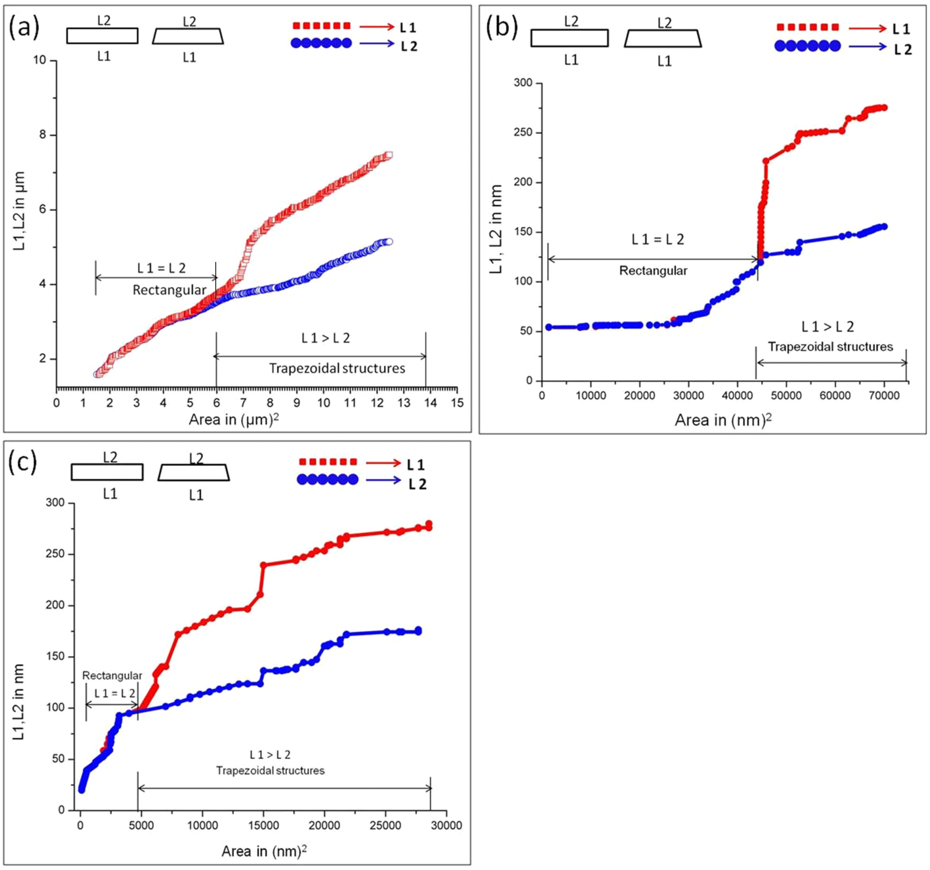

Figure 4.11: Critical area,beyond which shape transition occurs [120].

4.5 Conclusions

In conclusion,we report the shape evolution of MBE grown $\mathrm{Si}_{1-x}\mathrm{Ge}_x$ islands on reconstructed high index Si(5 5 12), Si(5 5 7) and Si(5 5 3) surfaces. We show that a self assembled growth at optimum thickness leads to interesting shape transformations, namely, spherical islands to rectangular nanostructures and then to elongated trapezoidal structures. We presented a one-step procedure to form a graded composition of $\mathrm{Si}_{1-x}\mathrm{Ge}_x$ epitaxially grown on clean high index surfaces. Trapezoidal structures of similar length/width ratio were observed. The longer side of the trapezoidal structures is $\approx$ 21 times larger in case of Si(5 5 12) compared to Si(5 5 7) and Si(5 5 3). We have experimentally observed an universality in the growth dynamics of the islands for all three high index surfaces . Our kMC simulations show that such variations can be understood by introducing a deviation parameter ϵ in surface barrier term E_D. The experimentally observed shape variations are in good agreement with kMC simulations. This suggests the role of stochastic process involved in the shape transitions of nanoscale structures.

Chapter 5

Temperature dependent shape evolution of Si-Ge structures on high index silicon surfaces

5.1 Introduction

Self-assembly of Strain-induced islands in heteroepitaxial systems is a promising route to use nanoscale particles as quantum dots in optoelectronic devices. Among the different strained material combinations investigated so far, the Ge/Si system is often considered as a prototype for understanding fundamental properties of heteroepitaxial growth. In general, Ge prefers to adsorb on the surface, since the Ge dangling-bond energy is lower than that of Si [121, 122]. However, theoretically, it is expected that the tensile stress induced due to reconstruction makes Ge atoms diffuse into the silicon subsurface and into the bulk [123]. Hence,evolution of crystallographic facets of strained Ge-Si structures and diffusion of Ge into the Si substrate depend on the kind of the substrate and nature of reconstructions [124].Faceting is a fundamental concern in crystal growth. It is observed when the system is allowed to minimize its free energy (thermodynamic equilibrium) [126–128].The growth of faceting not only depends on material properties but also on sample configurations and process conditions (pressure, growth temperature, composition, etc.). Faceting can be used in order to improve electrical performance as in folded devices or minimized and suppressed as in silicon on nothing (SON) technology [129].

The growth of Ge quantum dots on low index silicon surfaces has been studied by many groups [86–88, 125] in the last two decades. More, recently, the study of self-organization in Ge/Si system has been extended to high-index surfaces [96, 97, 116, 130]. However, the kinetic and thermodynamic factors determining the shape of the self-assembled Ge-Si structures are not yet well studied.

In this chapter, we investigate the morphological evolution of strained Ge-Si islands on high-index surfaces as a function of growth temperature and mode of heating the substrate. We show the transformation of irregular shaped Ge-Si island to faceted dome structures and well aligned trapezoidal structure after an optimum critical temperature depending upon the modes of heating the substrate.

5.2 Experimental Details

The experiments discussed in the following were performed in an MBE chamber under ultra-high vacuum(UHV), at a base pressure of $\sim 2.5 \times 10^{-10}$ mbar. Si(5 5 12), Si(5 5 7), SI(5 5 3) of size $8\times$ 3 $(\mathrm{mm})^2$ were prepared through cutting from commercially available p-type boron doped wafers (of resistivity of 10 - 15 Ω cm). Substrates were degassed at 600°C for about 12 hours followed by repeated flashing (with direct current heating) for 30 sec. at a temperature of 1250°C to remove the native oxide layer to obtain a clean and well-reconstructed surface.The reconstruction has been confirmed with in-situ reflection high energy electron diffraction (RHEED). The temperature was monitored with an infra-red pyrometer calibrated with a thermocouple attached to the sample holder. Two series of samples have been prepared.10 ML Ge deposition on Si(5 5 12) from RT to 800°C, with two modes of heating, namely, (i) heating is achieved through a filament underneath (radiative heating: RH). (ii) heating achieved by passing a direct current (DC) through the sample. The post-growth characterization of the samples was carried out ex-situ by field emission gun based scanning electron microscopy (FEGSEM), Transmission electron microscope(TEM) and MeV ion scattering (Rutherford backscattering spectrometry (RBS)).

5.3 Results and Discussions

In this report, we will emphasize on the shape transformations of Ge-Si structures on clean high index surfaces as a function of substrate temperature in two modes of heating condition.

5.3.1 Shape evolution in RH condition

Fig. 5.1 shows FEGSEM micrographs for 10ML Ge growth on Si(5 5 12) surface at various substrate temperatures in RH condition. Fig.5.1 (a) shows the FEGSEM image for Ge film deposited while keeping the substrate at RT. The average island size of the random structures is found to be 504 ± 38 nm in diameter. Fig. 5.1 (b) depicts the morphology for Ge film deposited at a substrate temperature T = 600°C. In this case, a distribution of bigger spherical Ge islands surrounded by a large number of smaller islands was observed, showing a kind of Ostwald ripening process with a bimodal distribution of islands. The mean value for the size of the smaller islands was found to be 15.8 ± 1.5 nm ,while the bigger islands are found to have an average size of 54.0 ± 7.0 nm. In the 700°C deposition case, the mean size of the island increases at the expense of decreasing the number of smaller islands. I. Daruka *et al* [131] showed the shape evolution of islands to various faceted structures in terms of surface energy minimization with increasing volume.Normally, the chemical potential of an island decreases continuously with size, due to the smaller surface to volume ratio. As a result, material diffuses from smaller to larger islands. In this coarsening or "Ostwald ripening", large islands grow while small islands shrink and disappear. Above a lower transition volume, the Ge-Si island is stable and got faceted with shallow side facets and a top facet, as seen in fig.5.1(c).The mean size of the faceted island is 150 ± 15 nm. To get a clearer view of this facet structures, cross-sectional TEM analysis has been carried out.Fig.5.2 depicts the interfacial morphology of these Ge structures grown on Si(5 5 12) under RH conditions. In fig.5.2(a) the X-TEM image of spherical islands formed at T = 700°C-RH has been displayed. Fig.5.2(b) shows a cross-sectional view of faceted island structure formed in the T = 700°C case, where the thickness of the island is 42.6 ± 2.3 nm. A set of Ge/Si(5 5 12) sample has been prepared keeping T = 800°C. Upon increasing the temperature, it causes the formation of only larger dome like structure with disappearance of smaller islands. As the

Table 5.1: Parameters obtained on fitting the experimental RBS data for Ge/Si(5 5 12) at T=800°C- RH, using the SIMNRA simulation code [134].

Layer number	Ge composition	Si composition	Thickness (1×10^{15} atoms.cm^{-2})
1	0.6000	0.4000	0.100
2	0.0600	0.9400	100.0
3	0.0075	0.9925	250.0
4	0.0070	0.9930	300.0
5	0.0050	0.9950	350.0
6	0.0020	0.9980	400.0
7	0	1	Bulk

volume increases, the top facet shrinks and the shape changes with the appearance of steep facets. Fig. 5.1(d) displays the Ge-Si dome like structures, which has shallow facets, steep facets and a top facet with average size of 630.5 ± 16.4 nm. The thickness of the faceted dome structure is found from the cross-sectional TEM view in fig. 5.2(c) , which is 122 ± 5.6 nm. Fig.5.2(d) confirms that the faceted Ge-Si structures are epitaxial.

S.A. Chaparro et al [132] showed that higher growth temperature activates additional pathways for the Ge islands to relieve their strain via Ge/Si intermixing. Si-Ge alloying causes the formation of quite large hut clusters for $T > 600$°C. Furthermore,they observe that there is an increase in the mean dome cluster size with increasing temperature. Here, we have performed RBS experiment on all the three sets of sample i.e. Ge/Si(5 5 12) at $T = 600°$ C, 700°C and 800°C to investigate the possible intermixing of Si-Ge. It is evident from. fig. 5.3 that there is Ge diffusion towards silicon for T= 700° C and T= 800°C. at channel no. 1350 to 1500 in the RBS spectrum. The simulated composition of Ge and Si are tabulated in table 5.1. Ge-Si alloying may also be attributed in the strain relief mechanism in forming the larger facets structures minimizing the surface energy.

Fig.5.4 and 5.5 depict the temperature dependent shape transition from spherical to faceted dome structures in the Ge/Si(5 5 7) and Ge/Si(5 5 3) in the radiative heating condition. In fig.5.4(a) spherical islands formed at T = 600°C -RH for the Ge/Si(5 5 7) system are shown. The average size of the smaller islands and bigger islands are

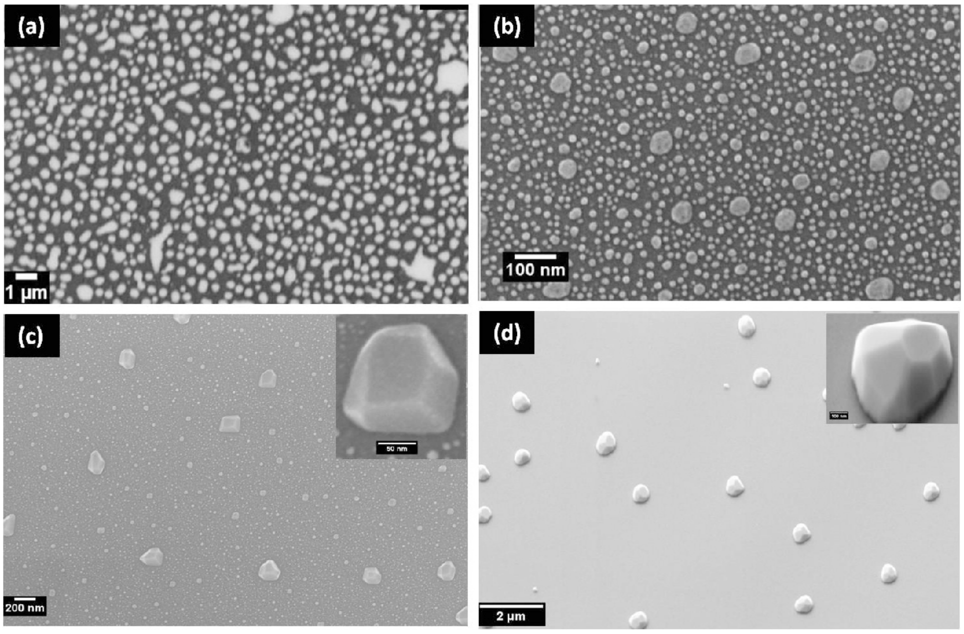

Figure 5.1: SEM micrographs of 10 ML Ge/Si(5 5 12) at (a)RT (b)600°C-RH (c)700°C-RH (d)800°C-RH [134].

12.8 ± 0.5 nm and 37.2 ± 2.1 nm, respectively. Upon increasing growth temperatures, the Ge-Si structures take the faceted structures at T= 700°C - RH and T = 800°C - RH. The mean size of the Ge-Si faceted structures at 700°C - RH is 115.8 ± 14.5 nm. The larger dome structure at T = 800°C - RH have a mean size of 215 ± 12 nm. In fig.5.5, we can see a evolution of Ge-Si structures from 600°C to 800°C of similar sizes.

5.3.2 Shape evolution in DC heated condition

We have discussed the temperature dependent shape evolution of Ge-Si islands in the radiative heating (RH) condition. In this section, we investigate the morphological change with increasing temperature in the DH condition. Fig. 5.6 is a FEGSEM micrograph of Ge-Si structures at various temperatures in the DH case. When substrate temperature T = 400°C, the Ge-Si islands starts nucleating to form random bigger islands with the reduction of smaller island density. The mean size of the bigger islands is 645.0 ± 22.0 nm. The signal of Ge diffusion in this case can be seen from the RBS spectrum in fig.4.10. The interesting shape transition occurs at T= 600°C. Well aligned $Si_{1-x}Ge_x$ trapezoidal microstrures of average length 6.25 ± 0.27 μm and

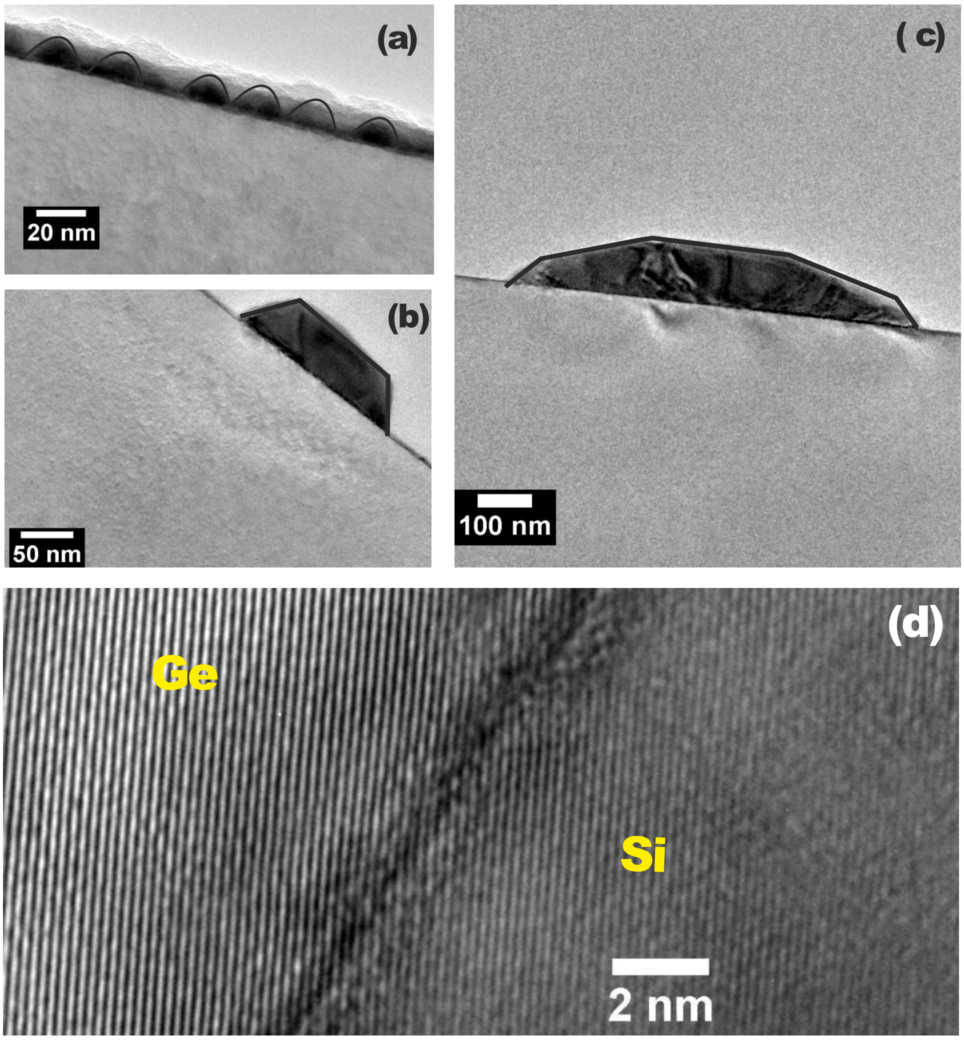

Figure 5.2: Cross-sectional TEM images of 10 ML Ge/Si(5 5 12) at (a) 600°C-RH (b) 700°C-RH (c) 800°C-RH [134].

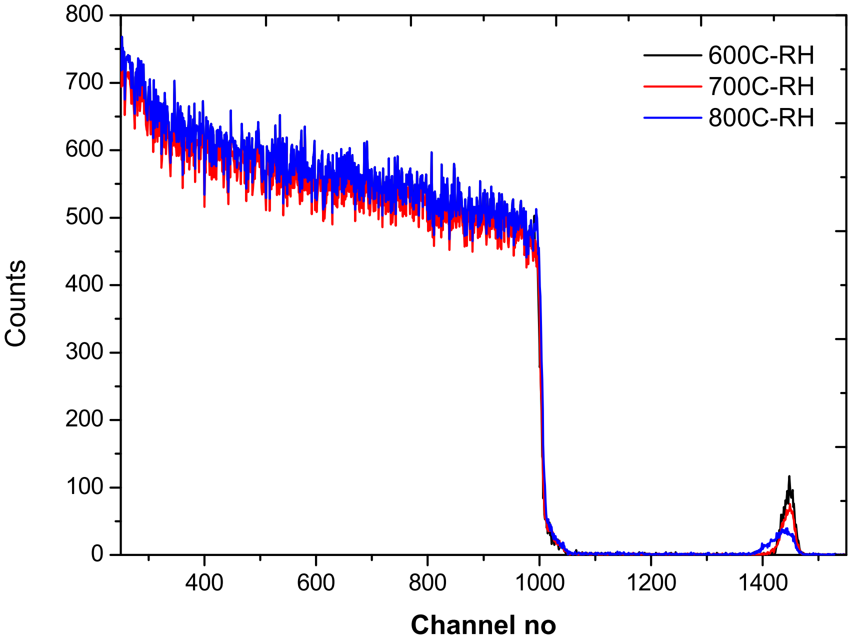

Figure 5.3: Experimental RBS spectrum from 10 ML Ge/Si (5 5 12) at T= 600°C, 700°C and 800°C in RH case [134].

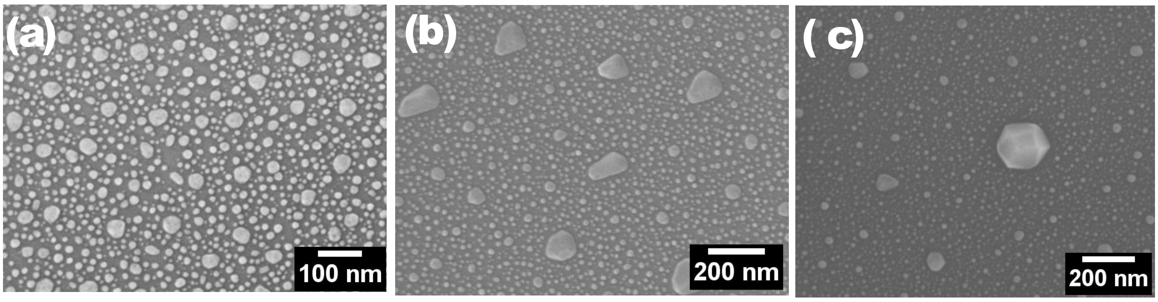

Figure 5.4: SEM micrographs of 10 ML Ge/Si (5 5 7) at T= 600°C, 700°C and 800°C in RH case.

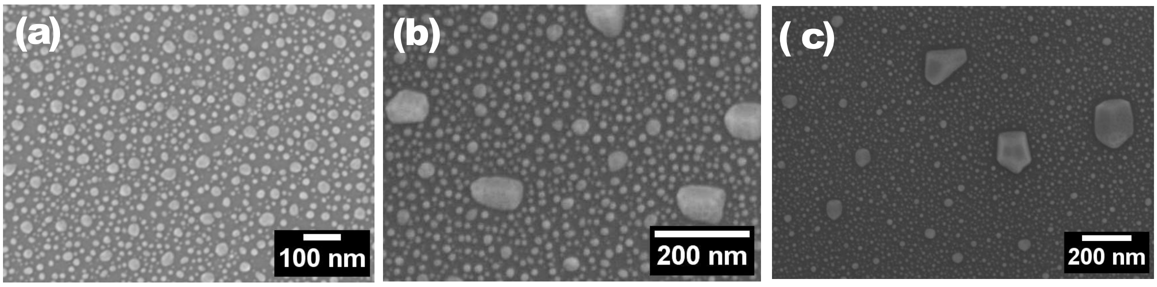

Figure 5.5: SEM micrographs of 10 ML Ge/Si (5 5 3) at T= 600°C, 700°C and 800°C in RH case.

Table 5.2: Parameters obtained on fitting the experimental RBS data for Ge/Si(5 5 12) at T=600°C- DH, using the SIMNRA simulation code.

Layer number	Ge composition	Si composition	Thickness (1×10^{15} atoms.cm^{-2})
1	0.7500	0.2500	0.75
2	0.0750	0.9250	2.0
3	0.0070	0.9930	150.0
4	0.0050	0.9950	250.0
5	0.0040	0.9960	350.0
6	0.0020	0.9980	500.0
7	0.0010	0.9990	3500.0
8	0	1	Bulk

aspect ratio 3.13 ± 0.3 form along the step edge $\langle 1\bar{1}0\rangle$ [fig. 5.6(c)]. In fig5.6,the RBS measurement has revealed the intermixing of Ge and Si. Additionally, the inward diffusion of Ge (channels 1250-1350) into bulk Si and the outward diffusion of Si (channels 900-940) can be clearly seen from figure5.7. The RBS simulation has been done treating the specimen as a multilayer with variation of Si and Ge concentrations in each layer [table5.2]. We found a graded composition of Ge-Si in these structures. The synchrotron-based high resolution x-ray diffraction (HRXRD)also showed presence of graded $Si_{1-x}Ge_x$ composition from the interface to the top of the trapezoid structures (data given in chapter 6).

Here, one may wonder about the effect of temperature in RH and DH conditions. In the DH condition, direct current acted as an additional factor in stimulating the motion of germanium adatoms towards the edges of steps. In the ref. [133], Rönspies *et al* showed that steps in a high index surface, apparently do not interrupt the conducting path, but due to local scattering at step edge increase the local resistivity by more than one order of magnitude. Hence, the local temperature along the step direction is more and stimulate the Ge-Si diffusion along the steps making the structures well elongated. On further increasing temperature to 800°C and above, the Ge-Si islands start evaporating. It can be seen from fig.5.6 (d) that thickness of the trapezoid structures starts decreasing from the edge towards the center.

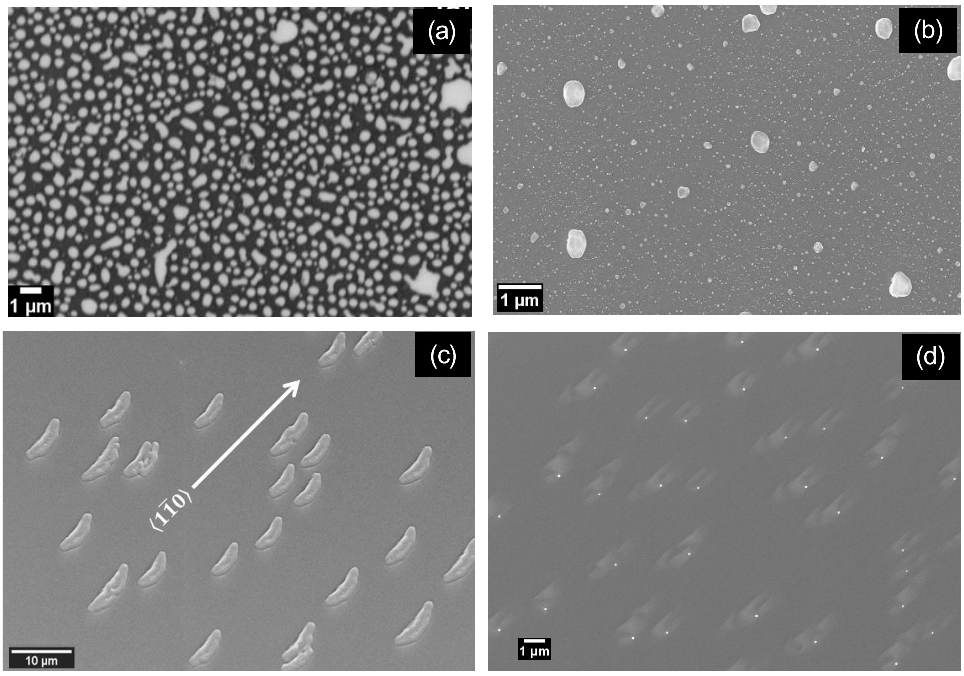

Figure 5.6: SEM micrographs of 10 ML Ge/Si(5 5 12) at (a)RT (b)400°C-DC (c)600°C-DC (d)800°C-DC [134].

The shape evolution as a function of growth temperature under DH-condition has also been investigated for Ge/Si(5 5 7) and Ge/Si(5 5 3) systems. Here, we have seen similar effects as seen in the case of Ge/SI(5 5 12). The only difference is the dimension of the Ge-Si structures(as seen in the previous chapter). From figure. 5.8 we can see the formation of irregular Ge-Si islands of mean size 170.0 ± 7.0 nm. at T = 400°C. At optimum critical temperature T = 600°C, well aligned Si$_{1-x}$Ge$_x$ trapezoidal nanostructures of average length 297.8 ±11.4 nm forms along the step edge ;while at

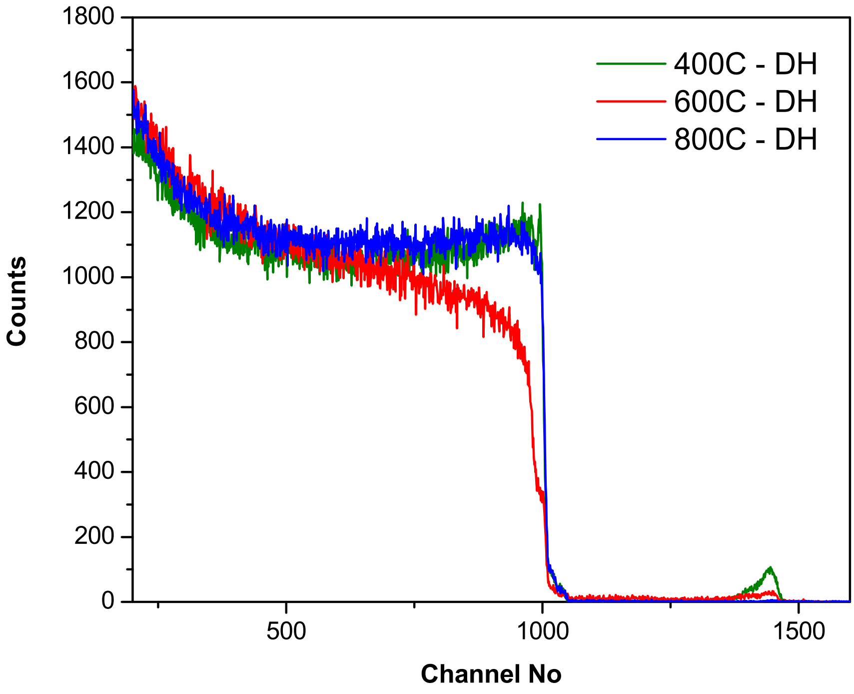

Figure 5.7: Experimental RBS spectrum from 10 ML Ge/Si (5 5 12) at T= 400°C, 600°C and 800°C in DC heated case [134].

T = 800°C or above, Ge-Si islands evaporates with depletion of materials from the edge towards the center as seen in the fig.5.8(c). The temperature dependent (DH case) shape evolution for the Ge/Si(5 5 3) system is displayed in fig.5.9.

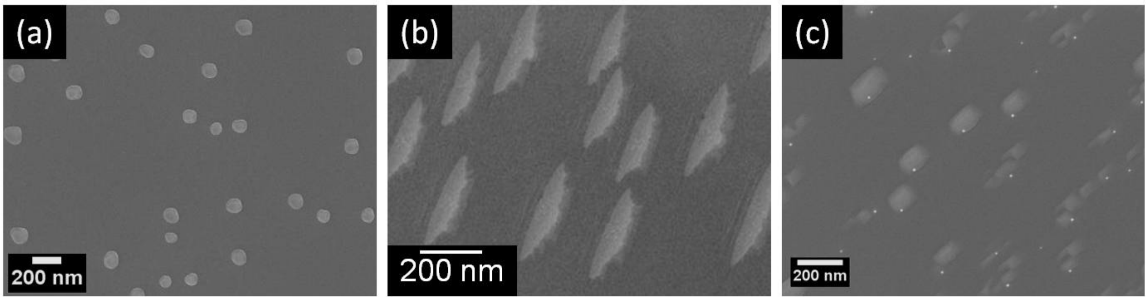

Figure 5.8: SEM micrographs of 10 ML Ge/Si(5 5 7) at (a)RT (b)400°C-DC (c)600°C-DC (d)800°C-DC

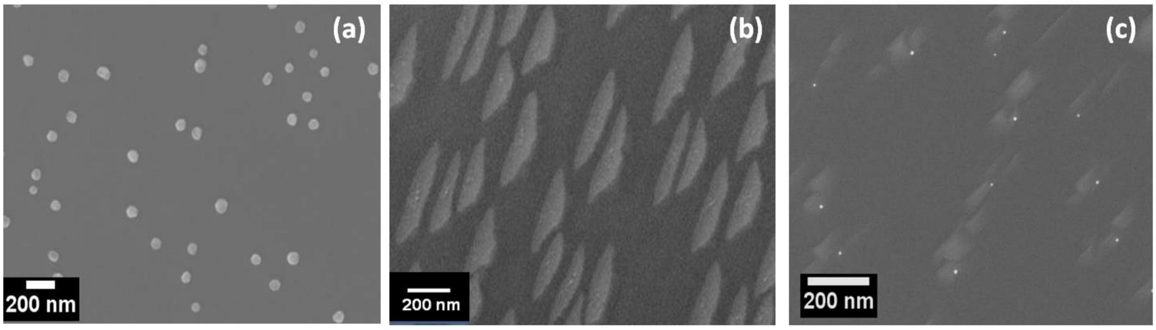

Figure 5.9: SEM micrographs of 10 ML Ge/Si(5 5 3) at (a)RT (b)400°C-DC (c)600°C-DC (d)800°C-DC

5.4 Conclusions

In summary,we report the shape evolution of MBE grown $\mathrm{Si}_{1-x}\mathrm{Ge}_x$ islands on reconstructed high index Si(5 5 12) as a function of growth temperature. Also the mode of heating (i.e. RH and DC heated) plays a vital role in the shape transformations. We show that a self assembled growth at optimum temperature leads to interesting shape transformations, namely, spherical islands to faceted dome structures in case of RH condition and to elongated trapezoidal structures for the DH case. We have also observed the intermixing of Si-Ge in the larger faceted dome structures and aligned trapezoidal structures.We look forward to carry out a spectroscopic analysis along the step edges and of the aligned $\mathrm{Si}_{1-x}\mathrm{Ge}_x$ structures as well.

Chapter 6

Compositional Analysis of $Si_{1-x}Ge_x$ structures

6.1 Introduction

The elemental semiconductors silicon and germanium form a continuous series of disordered alloys. A detailed understanding of the properties of the Si-Ge alloys is a prerequisite for successful device applications. The manipulation of semiconductor materials by the growth of superstructures leads to new and sometimes unexpected semiconductor properties. The fabrication of self-assembled Ge-Si island by means of strained layer epitaxy with Stranski-Krastanow growth mode has raised great interest in optoelectronic applications. The shape, size, and composition of quantum dots are essential in determining their optoelectronic properties.Therefore, controlling these parameters, is crucial for the growth of quantum dots with device applicable quality. In Si-Ge thin films, the influence of the composition on the morphology, electronic, and optical properties is widely exploited for technological purposes.The composition of epilayer material plays an important role in the determination of the size and shape of the islands grown under the SK mode because the island growth is strain driven and the strain is directly related to the composition of the epilayer [135, 136]. For example, although Ge/Si(5 5 12) island growth mimics Ge/Si(5 5 7) and Ge/Si(5 5 3) island growth (as described earlier), the island sizes in the Ge/Si(5 5 12) system are much larger than those in the Ge/Si(5 5 7) and Ge/Si(5 5 3) systems. Different island composition will result in different island size. In this chapter, we will present a compositional analysis of the Ge-Si structures using HRXRD, RBS and STEM-EDS.

6.2 Experimental Details

The experiments discussed in the following were performed in ultra-high vacuum(UHV) at a base pressure of $\sim 3.5 \times 10^{-10}$ mbar in a custom built molecular beam epitaxy (MBE) system . Samples of Si(5 5 12), Si(5 5 7) and Si(5 5 3) were prepared from p-type boron doped wafers (of resistivity of 10 - 15 Ω cm). Substrates were degassed at 600°C for about 12 hours followed by repeated flashing (with direct current heating) for 30 sec. at a temperature of 1250°C to remove the native oxide layer to obtain a clean and well-reconstructed surface. The reconstruction has been confirmed with in-situ reflection high energy electron diffraction. The temperature was monitored with an infra-red pyrometer calibrated with a thermocouple attached to the sample holder. Ge was deposited to various thicknesses of 3 to 10 monolayer (ML) at substrate temperature 600°C [with direct current heating(DH)]. The samples were then post annealed at a temperature of 600°C for 15 minutes by DH method. The post growth characterization of the samples was carried out *ex-situ* by field emission gun based scanning electron microscopy (FEGSEM) with 20 kV electrons. STEM and TEM measurements were carried out with 300 keV electrons using a Cs-corrected FEI Titan 80/300 system at University of Bremen, Germany. The preparation of the specimen to electron transparency was achieved by focused ion beam milling followed by low-energy-ion milling.The RBS measurements were carried at IOP, Bhubaneswar,India. We have used the P08 beamline at Petra - III for carrying out HRXRD measurements for compositional analysis. Using the Bragg angles, we determined the corresponding lattice planes of Si-Ge alloy structures.

6.3 Results and Discussion

In chapter-4, we have discussed the formation of aligned trapezoid structures on the reconstructed high index surfaces under DC heating condition irrespective of their sizes. The composition of these nanostructures has been characterized by the synchrotron-based high resolution x-ray diffraction (HRXRD). The HRXRD showed presence of graded $\mathrm{Si}_{1-x}\mathrm{Ge}_x$ system for the Si(5 5 12)and is also confirmed by RBS measurements. In fig. 6.1, the HRXRD spectrum shows corresponding compositions of $\mathrm{Si}_{0.25}\mathrm{Ge}_{0.75}$, $\mathrm{Si}_{0.5}\mathrm{Ge}_{0.5}$, $\mathrm{Si}_{0.75}\mathrm{Ge}_{0.25}$ as seen from the three peaks. It should be noted that this three-layer system has been formed in one-step growth process on high index planes. Under the similar conditions, this graded Si-Ge alloy was not formed for low-index plane systems such as Si(100) and Si(111). The formation of graded Si-Ge alloy is a necessary condition for forming large (micron size) island structures.

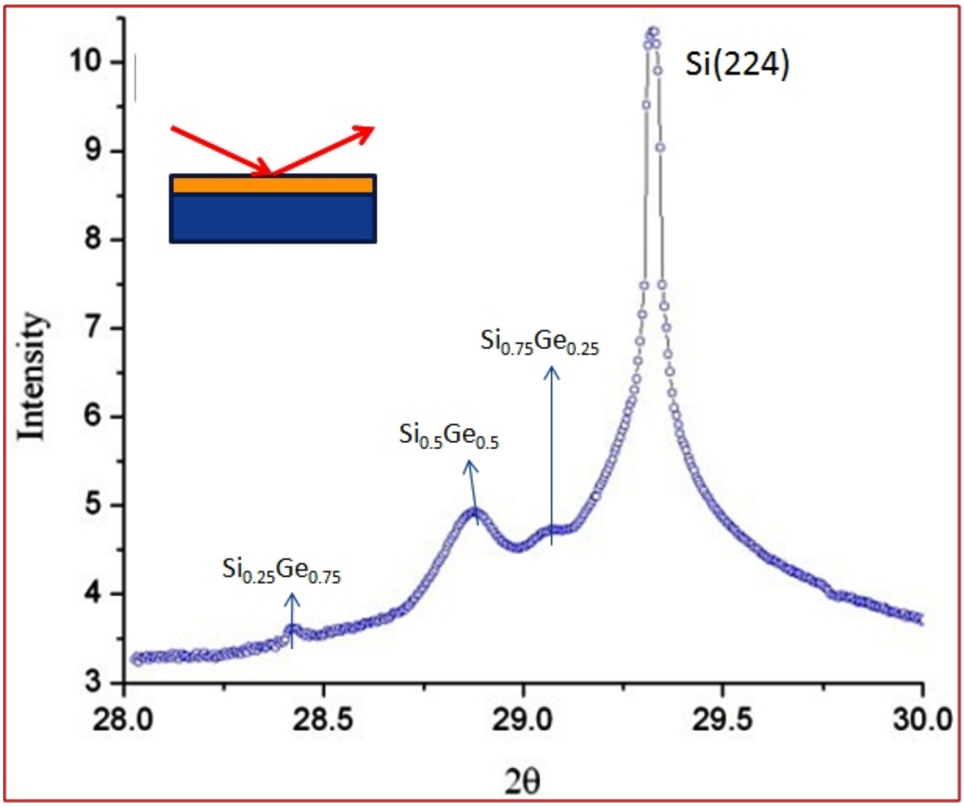

Figure 6.1: HRXRD scan on the trapezoidal Ge-Si structures formed in 10 ML Ge/Si(5 5 12) system [120].

To complement the HRXRD results, RBS experiments were carried out to analyze the composition and probable Si-Ge intermixing. The simulations were carried out using the SIMNRA code [69]. For the simulations, the samples were considered as a multilayer with variation of Si and Ge concentrations in each layer. The compositions after simulation for the 10 ML Ge/Si(5 5 12) case is tabulated in a tabular form [6.1].The RBS data is in good agreement with the HRXRD analysis.Additionally, the inward diffusion of Ge (channels 1250-1350) into bulk Si and the outward diffusion of Si (channels 900-940) can be clearly seen from figure6.2. The change in the composition of $Si_{1-x}Ge_x$ (as in table6.1) as a function of depth has a bearing on the kind of inter-diffusion process involved in the mixing of Si and Ge. Figure 6.3 and 6.4 show the experimental RBS spectra for 3 to 10 ML Ge deposition on Si(5 5 7) and Si(5

5 3) surfaces under DC heating. We did not observe prominent graded Si-Ge alloy structures in case of Si(5 5 7) and Si(5 5 3). Also the island structures are an order of magnitude smaller compared to Si(5 5 12) though they have similar shapes. This shows the importance of strain in forming large structures, as for the Si-Ge systems, the lattice mismatch is reduced by formation of an alloy structures.

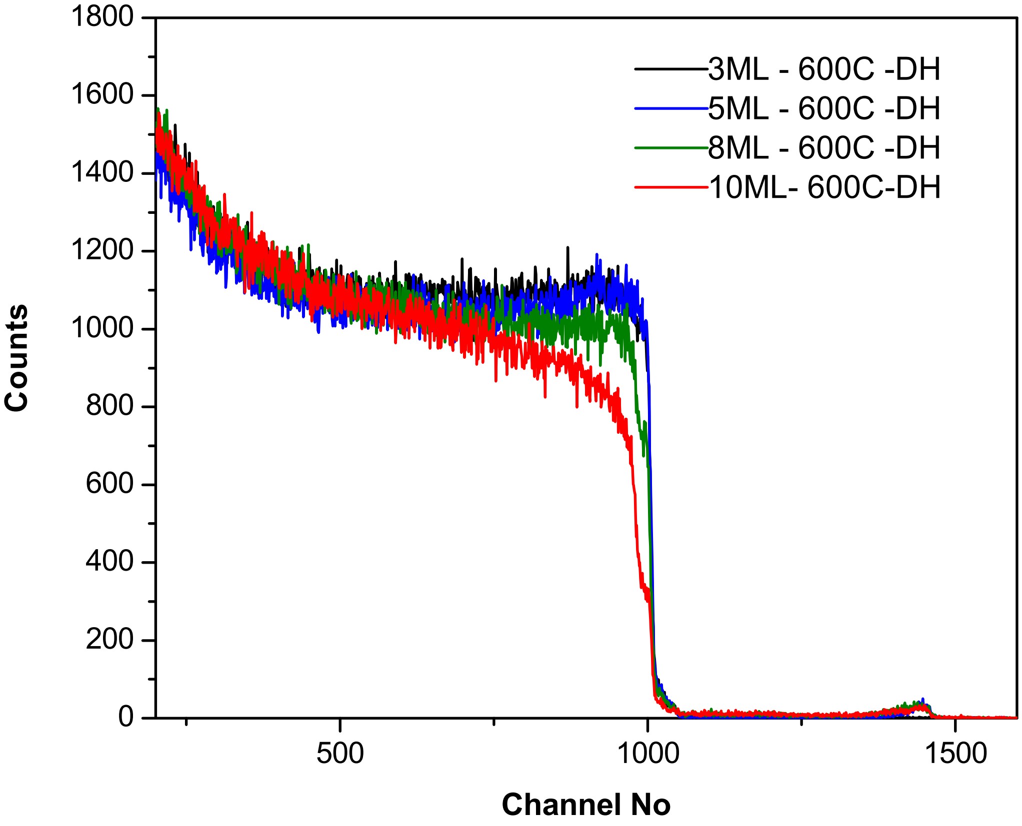

Figure 6.2: Experimental RBS spectrum from 3 ML to 10 ML Ge/Si (5 5 12)

In the following, we present the results on the composition determination of $Si_{1-x}Ge_x$ layer using STEM-EDS measurements with 300 keV electron beams. STEM measurements were carried out on Ge/Si(5 5 12) substrate under DC heating condition. Figure 6.5(a) shows a STEM image taken from this specimen. As shown in previous chapters, the Si-Ge trapezoidal structures are of an average length of 6.2 μm. Figure 6.5(a) shows a cross-section image of this island, which is a small part of the bigger

Table 6.1: Parameters obtained on fitting the experimental RBS data for Ge/Si(5 5 12) at T=600°C-DC heated, using the SIMNRA simulation code.

Layer number	Ge composition	Si composition	Thickness (1×10^{15} atoms.cm^{-2})
1	0.7500	0.2500	0.75
2	0.0750	0.9250	2.0
3	0.0070	0.9930	150.0
4	0.0050	0.9950	250.0
5	0.0040	0.9960	350.0
6	0.0020	0.9980	500.0
7	0.0010	0.9990	3500.0
8	0	1	Bulk

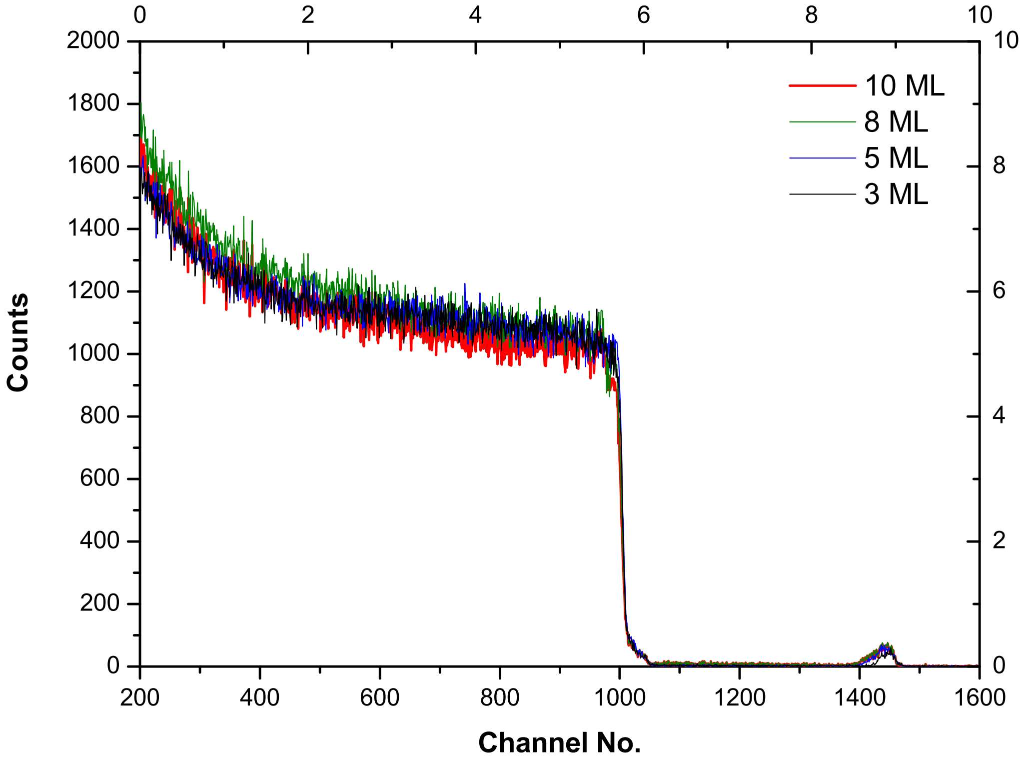

Figure 6.3: Experimental RBS spectrum from 3 ML to 10 ML Ge/Si (5 5 7)

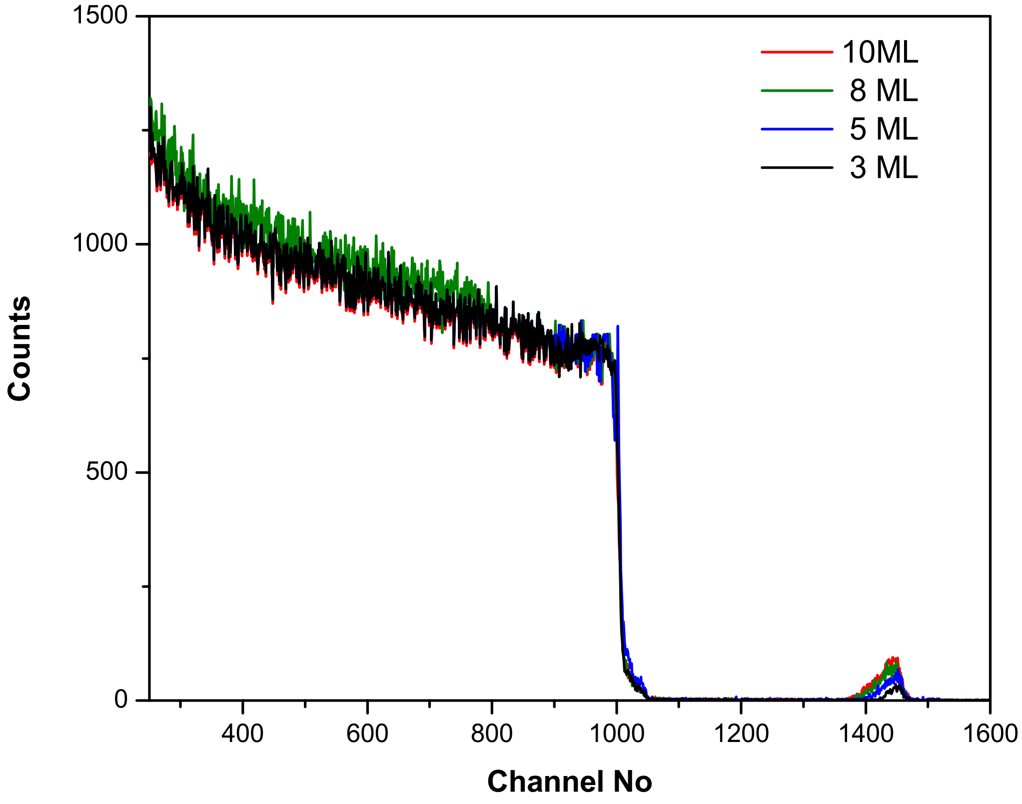

Figure 6.4: Experimental RBS spectrum from 3 ML to 10 ML Ge/Si (5 5 3)

island. For making a cross-sectional FIB specimen, two kinds of protective Pt depositions were made (one using e-beam deposition and a larger thick one with FIB based gas injection system). Pt shown in Fig. 6.5(a) is deposited by gas injection with e-beam.

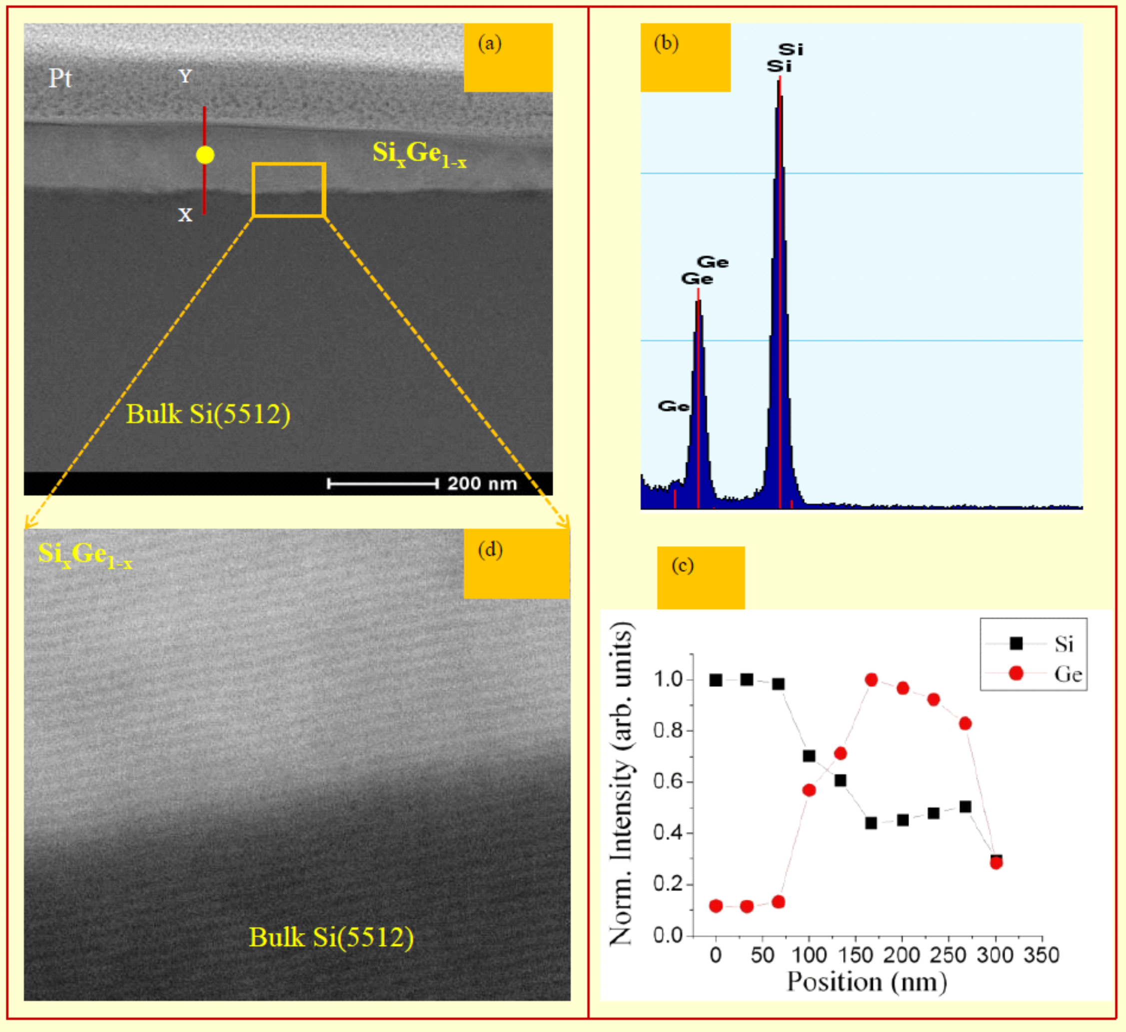

Figure 6.5: (a) and (d) STEM image (low and high magnification) of XTEM specimen corresponding to 12 ML Ge on Si(5 5 12). Figure (b) shows EDS at the middle of line XY. Figure (c) is the concentration variation of Si and Ge along XY. [117].

The energy dispersive spectrum in (b) shows Ge and Si signals from the region that is shown with a dot on the line XY in Figure 6.5(a). Figure 3(c) depicts the integrated and normalized (to maximum value of Si and Ge signals respectively) intensity of Si and Ge signals obtained at various points along the line XY (300 nm length, shown in figure 6.5 (a)). The intensity line profile confirms the variable composition of Si and Ge in the island layer in agreement with our ion scattering measurements [116]. Figure 3(d) shows a high resolution STEM image. From this figure, it is clear that the film of $\mathrm{Si}_{1-x}\mathrm{Ge}_x$ is crystalline in nature and grown epitaxially on Si (5 5 12). These results show that it is possible to make aligned structures of variable sizes and graded composition. In general, Si-Ge alloy layers are formed by either co-deposition of Si and Ge or by depositing buffer-layers of Si before the Ge deposition and followed by vacuum annealing. We presented a one-step procedure to form a graded composition of $\mathrm{Si}_{1-x}\mathrm{Ge}_x$ epitaxially grown on clean high index surfaces.

6.4 Conclusions

In this chapter, We presented a proper compositional analysis based on the HRXRD, RBS and STEM-EDS data. We showed that intermixing can have an important role in decreasing the strain energy. Si-Ge alloying reduces the strain, increasing the volume and allowing larger islands to have a micro trapezoidal shape. We observed the compositional grading in the $\mathrm{Si}_{1-x}\mathrm{Ge}_x$ structures. Strain relaxed graded Si-Ge layers can be useful as substrates for high-mobility field effect transistors(FETs).

Chapter 7

Summary

This thesis deals with the growth of Si-Ge nanostructures on ultraclean high index silicon surfaces ,such as Si(5 5 12), Si(5 5 7) and Si(5 5 3), using molecular beam epitaxy (MBE). Different techniques have been used to characterize the nanostructres. Refection high energy electron difraction (RHEED)has been used to characterize clean surfaces. Morphology of the MBE grown structures has been studied using field emission gun based scanning electron microscopy (FEGSEM) and transmission electron microscopy (TEM). To study the composition of these structures we have performed STEM-EDS, MeV ion scattering (Rutherford backscattering spectrometry (RBS) and high resolution x-ray diffraction (HRXRD). The growth dynamics has been studied by varying the deposition thickness, growth temperatures and mode of annealing the substrate. A phenomenological kMC model explains the experimental shape evolution mechanism.

The thesis work starts with the growth of self-assembled nanostructures on Si(5 5 12) surfaces. This growth is an example of classic Stranski-Krastanov (SK) mode. We made reconstructed clean high index surfaces using the thermal clean procedures inside the MBE chamber, which show periodic steps and terraces on the surface. Ge films of 2 to 12 ML were grown epitaxially on these reconstructed surfaces.The substrate temperature was maintained at 600°C during growth and post annealing.Here, two sets of sample were prepared with two modes of heating, namely radiative heating and direct currect heating . In the RH case, we observed the formation of spherical Ge nanoislands with bimodal distributions. But in the DC heating case, a sequence of shape transition occurred with increasing growth coverage. We showed the shape transformation of spherical nanoparticle to trapezoidal Ge-Si structures along the step edge. Here, it is to be noted that the alignment of the structures does not depend on the direction of the direct current in DC heating condition. This has been confirmed with direct current through the samples in three directions (perpendicular, parallel and at 45° to the step direction $\langle 1\bar{1}0 \rangle$). But in all the three cases, the Ge-Si structures were found to be aligned along the step direction $\langle 1\bar{1}0 \rangle$. Also we showed that the formation of elongated Ge-Si islands is an anisotropic effect of reconstructed high index surface unlike the case of flat low index substrates. For this, we have deposited Ge on Si(1 1 1) in the DC condition. But no alignment was found in the structures, rather forming irregular structures. So, it is confirmed the formation of trapezoidal structures is observed on anisotropic stepped surfaces with DC heating condition. Here, DC current acted as an additional factor in stimulating the motion of germanium adatoms towards the step edges.

We have reported a comparative study on Ge/Si(5 5 12),Ge/Si(5 5 7) and Si(5 5 3) systems in both RH and DC conditions. In the RH case, a distribution of bigger circular Ge islands surrounded by a large number of smaller islands was observed. This type of distribution is consistent with Ostwald ripening. In the Ge/Si(5 5 7) and Si(5 5 3) systems, the number of bigger islands is also significant, unlike in the case of Si(5 5 12). The size of the spherical islands is smaller in Ge/Si(5 5 7) and Ge/Si(5 5 3) cases. In the DC deposited case, we have observed an interesting change in the size of the trapezoid structures. In the Ge/Si(5 5 12) system, micro trapezoids of average length $\approx 6.25 \pm 0.27$ μm were formed along the step. Although, the Ge-Si structures formed in the Ge/Si(5 5 7) and Ge/Si(5 5 3) cases, maintained the same trapezoidal shape, the mean length of the structures falls down significantly to $\approx$ 300nm. Following the same growth dynamics, we were able to form micro trapezoids and nano trapezoids. Interestingly, in all the cases, the aspect ratios are almost same.

A complete study on growth dynamics of Ge-Si nanostructures on ultra-clean Si(5 5 12), Si(5 5 7) and Si(5 5 3) was presented. We observed a universality in the shape evaluation, irrespective of the substrate orientations and size of the island structures. The shape evolution mechanism seen in the experiments, was complemented by a theoretical 2D kinetic Monte Carlo simulation. We chose a suitable coordinate system such that it fits to the anisotropic reconstructed high index surfaces. The simulation was done by introducing a deviation parameter (ϵ) in the surface barrier term (E_D) to take the effect of anisotropic diffusion, as one of the plausible mechanisms.

The morphological evolution and the effect of growth temperature on size, orientation and composition of molecular beam epitaxy grown Ge-Si islands on Si(5 5 12), Si(5 57) and Si(5 5 3) surfaces have been investigated in the temperature range from room temperature (RT) to 800°C with two modes of substrate heating i.e. by radiative heating (RH) and direct current heating (DC). In the RH case, we found spherical island structures at 600°C with a bimodal distribution, which upon increasing temperature, structures got faceted at 700°C. At 800°C , thick dome like structures are formed having shallow facets, steep facets and a top facet. We showed that higher growth temperature activates additional pathways for the Ge islands to relieve their strain via Ge/Si intermixing. Si-Ge alloying causes the formation of quite large hut clusters. The mean size of the faceted structures formed in the case of Ge/Si(5 5 7) and Ge/Si(5 5 3) is less in comparison to Ge/Si(5 5 12) case. We have also analyzed the effect of DC heating as a function of temperature. In this case, after the optimum critical temperature 600°C, well aligned trapezoidal $\mathrm{Si}_{1-x}\mathrm{Ge}_x$ structures with a graded composition start forming along the step edges.Interestingly, these aligned structures have been found only around 600°C, neither at low temperature nor at higher temperatures.
The compositional analysis of the $\mathrm{Si}_{1-x}\mathrm{Ge}_x$ structures were done using HRXRD,RBS and STEM-EDS. All these measurements on the trapezoid structures show the composition grading of Ge and Si . These results showed that it is possible to make aligned structures of variable sizes and graded composition. In general, Si-Ge alloy layers are formed by either co-deposition of Si and Ge or by depositing buffer-layers of Si before the Ge deposition and followed by vacuum annealing. In this work, we presented a one-step procedure to form a graded composition of $\mathrm{Si}_{1-x}\mathrm{Ge}_x$ epitaxially grown on clean high index surfaces.

The work presented in this thesis involves self-assembled growth of Ge-Si structures and exploration of nanoscale phenomena on high index silicon surfaces. The novel growth morphology observed for aligned Ge on Si(5 5 12), Si(5 5 7) and Si(5 5 3) surfaces, may provide a way to fabricate new nanostructures , stimulating the use of stepped surfaces in device applications. Strikingly, different morphologies of Ge films grown on stepped Si surfaces of different dimensions offer a playground for the manipulation of shape, size and electronic properties of $\mathrm{Si}_{1-x}\mathrm{Ge}_x$ structures, which may increase the potential of micro/nano electronics industry with new advancement in device fabrication.

Bibliography

[1] K. Brunner, Rep. Prog. Phys. **65**, 27 (2002).

[2] I. Eisele and W. Hansch, Thin Solid films. **369**, 60 (2000).

[3] W. Eberhardt, Surf. Sci. **500**, 242 (2002).

[4] P. Moriarty, Rep. Prog. Phys. **64**, 297 (2001).

[5] J. Drucker, IEEE J. Quantum Electron. **38**, 975 (2002).

[6] J. Shen and J. Kirschenr, Surf. Sci. **500**, 300 (2002).

[7] J. R. Arthur, Surf. Sci. **500**, 189 (2002).

[8] F. C. Frank and J. H. van der Merwe, Proc. Roy. Soc. London, **A198**, 205 (1949).

[9] M. Volmer and A. Weber, J. Phys. Chem., **119**, 277 (1926).

[10] I. N. Stranski and Von L. Krastanov, Akad. Wiss. Lit. Mainz Math -Natur. Kl. IIb, **146**, 797 (1939).

[11] J. H. van der Merewe, CRC Crit. Rev. Solid State Mattr. Sci., **17**, 187 (1991).

[12] K. Brunner and G. Abstreiter, J. J. Appl. Phys. **40**, 1860 (2001).

[13] Jurgen Michel, Jifeng Liu and Lionel C. Kimerling, Nature Photonics **4**, 527 (2010).

[14] Jie Xiang, Wei Lu, Yongjie Hu, Yue Wu, Hao Yan and Charles M. Lieber, Nature(London). **441**, 489 (2006).

[15] J. C. Bean, Proc. IEEE **80**,571 (1992).

[16] C. K. Maiti, Semicond. Sci. Technol. **13**, 1225 (1998).

[17] K. L. Wang, S. G. Thomas, M. Tanner, J. Mater. Sci. **6**,311 (1995).

[18] L. Fitting, M. E. Ware, J. R. Haywood, J. J. H. Walter, R. J. Nemanich, J. Appl. Phys. **98**, 024317 (2005).

[19] Y. Wu, R. Fan, and P. Yang, Nano Lett. **2**, 83 (2002).

[20] Minjoo L Lee, Eugene A Fitzgerald, Mayank T Bulsara, Matthew T Currie, and Anthony Lochtefeld J. Appl. Phys. **97**, 011101 (2005).

[21] P. H. Wu, D. Dumcenco, Y. S. Huang, H. P. Hsu, C. H. Lai, T. Y. Lin, D. Chrastina, G. Isella, E. Gatti, and K. K. Tiong, Appl. Phys. Lett. **100**, 141905 (2012).

[22] R. N$\ddot{o}$tzel, Semicond. Sci. Technol. **11**, 1365 (1996).

[23] N. N. Ledentsov et al , Phys. Rev. B **54**, 8743 (1996).

[24] R. N$\ddot{o}$tzel, J. Temmyo, and T. Tamamura, Nature London **369**,131 (1994).

[25] M. Ja*l*ochowskia and E. Bauerb, Progress in Surface Science,**67**,79 (2001).

[26] I. K. Robinson, P. A. Bennett, and F. J. Himpsel, Phys.Rev. Lett. **88**, 096104 (2002).

[27] R. A. Zhachuk, S.A. Teys, A.E. Dolbak, B.Z. Olshanetsky Surf. Sci. **565**, 37 (2004).

[28] Hiroyuki Okino, Rei Hobara,Iwao Matsuda, Taizo Kanagawa, and Shuji Hasegawa, Phys. Rev. B **70**, 113404 (2004).

[29] S. K. Ghose, I. K. Robinson, P. A. Bennett, F. J. Himpsel, Surf. Sci. **581**, 199 (2005).

[30] A. A. Baski, K. M. Jones, K. M. Saoud, Ultramicroscopy, **86** , 23 (2001).

[31] P. Nita, M. Jalochowski, M. Krawiec, and A. Stepniak, Phys.Rev. Lett. **107**, 0261001 (2011).

[32] Praveen Kumar, Mahesh Kumar, S. M. Shivaprasad, Surf. Sci. **606**, 1045 (2012).

[33] H. C. Kang and W. H. Weinberg, J.Chemical Phys. **90**, 2824 (1989).

[34] K. E. Khor and S. Das Sarma, Phys. Rev. B **62**, 16657 (2000).

[35] K. A. Fichthorn, M. L. Merrick, M. Scheffier, Applied Phys. A. **75**, 17 (2002).

[36] S Günther, E Kopatzki, M C Bertelt, J W Evans and R J Behm,Phys.Rev. Lett. **73**, 553 (1994).

[37] Y -W Mo, B S Swartzentruber, B Kariotis, M B Webb and M G Lagally,Phys.Rev. Lett. **63**, 2393 (1989).

[38] H. Röder, E. Hahn, H. Brune, J.-P Bucher and K. Kern,Nature(London). **366**, 141 (1993).

[39] Ch. Heyn, Phys. Rev. B **63**, 033403 (2001).

[40] E. A. Fitzgerald, Y. H. Xie, M. L. Green, D. Brasen, A. R. Kortan, J. Michel, Y. J. Mii, B. E. Weir, Appl. Phys. Lett. **59**, 811 (1991).

[41] J. M. Baribeau, T. E. Jackman, D. C. Houghton, P. Maigne , M. W. Denhoff, J. Appl. Phys. **63**, 5738 (1988).

[42] F. K. LeGoues, B. S. Meyerson, J. F. Morar, P. D. Kirchner, J. Appl. Phys. **71**, 4230 (1992).

[43] S. Hasegawa, X. Tong, S. Takeda, N. Sato and T. Nagao, Prog. Surf. Sci.,**60**,89 (1999).

[44] M. Zinkeallmang, L. C. Feldman and M. H. Grabow, Surf.Sci.Rep. **16**, 377 (1992).

[45] G. Medeiros-Ribeiro, T. I. Kamins, D. A. A. Ohlberg and R. S. Williams, Phys. Rev. B **58**, 3533 (1998).

[46] F. M. Ross, J. Tersoff and R. M. Tromp, Phys.Rev. Lett. **80**, 984 (1998).

[47] I. Daruka, J. Tersoff and A. L. Barabasi, Phys.Rev. Lett. **82**, 2753 (1999).

[48] I. V. Markov, Crystal Growth for Beginners - Fundamentals of Nucleation, Crystal Growth and Epitaxy, World Scientific, Singapore, (1995).

[49] E. Bauer and J. H. van der Merwe, Phys. Rev. B **33**, 3657 (1986).

[50] K. Oura, V. G. Lifshits, A. A. Saranin, A. V. Zotov and M. Katayama, Surface Science - An Introduction, Springer-Verlag, (2003).

[51] J. G. Dash, Phys. Rev. B **15**, 3136 (1977).

[52] R. Pandit, M. Schick and M. Wortis,Phys. Rev. B **26**, 5112 (1982).

[53] C. Ebner, C. Rottman and M. Wortis,Phys. Rev. B **28**, 4186 (1983).

[54] S. J. Kennedy and J. S. Walker,Phys. Rev. B **30**, 1498 (1984).

[55] Ph.D. Thesis,Utkal University, April, 2004 by Dipak Kumar Goswami.

[56] M. H. Grabow and G. H. Gilmer, Surf. Sci. **194**, 333 (1988).

[57] K. Nakijama, The LPE Growth of InGaAsP, in Semiconductors and Semimetals vol. 22, Ed., R. K. Willardson and A. C. Beer, Academic Press,Orlando, (1985).

[58] D. K. Goswami, B. Satpati, P. V. Satyam, and B. N. Dev, Curr. Sci **84**, 902 (2003).

[59] W. Braun, Applied RHEED, Springer-Verlag, (1999).

[60] J. E. Mahan, K. M. Geib, G. Y. Robinson, and R. G. Long, J. Vac. Sci. Technol. A, **85**, 3692 (1990).

[61] D. B. Williams and C. Barry Carter, Transmission Electron Microscopy, Vol. I-IV , Plenum Press, New York, (1996).

[62] John C. H. Spence, High-resolution Electron Microscopy, Oxford University Press, 3rd Ed. (2003).

[63] Brent Fultz and James Howe, ransmission Electron Microscopy and Diffractometry of Materials, Springer, 2nd Ed., (2005).

[64] M. Knoll and E Ruska, Z. Physik. **78**, 318 (1932).

[65] http://rsbweb.nih.gov/ij/ .

[66] E. Rutherford, Phil. Mag. **21**, 669 (1911).

[67] W. K. Chu, J. W. Mayer, M. A. Nicolet, Backscattering spectrometry, Academic Press, New York, (1978).

[68] K. Sekhar, G. Kuri, P. V. Satyam, B. Sundaravel, D.P. Mahapatra and B. N. Dev, Indian J. Phys. , **684**, 1 (1994).

[69] http://home.rzg.mpg.de/ mam/ .

[70] Robert J. Keyse, Anthony J. Garrett-Reed, Peter J. Goodhew and Gordon W. Lorimer, Introduction to scanning transmission electron microscopy, Bios Scientific Publishers, (1998).

[71] A. A. Baski, S. C. Erwin, and E. J. Whiteman, Science **269**, 1556 (1995).

[72] A. A. Baski, S. C. Erwin, and E. J. Whiteman, Surf. Sci. **392**, 69 (1997).

[73] K. Ohmori, Y L Foo, S Hong, J G Wen, J E Greene, and I Petrov, Nano Lett. **5**, 369 (2005).

[74] A. A. Baski, K. M. Saoud, and K. M. Jones, Applied Surf. Sci. **182**, 216 (2001).

[75] H. H. Song, K. M. Jones, and A. A. Baski, J. Vac. Sci. Technol. A **17**, 1696 (1999).

[76] J. R. Ahn, Y. J. Kim, H. S. Lee, C. C. Hwang, B. S. Kim, and H. W. Yeom , Phys. Rev. B **66**, 153403 (2002).

[77] Mahesh Kumar, and S M Shivaprasad, J.Nanosci. Nanotechnol. **9**, 5420 (2009).

[78] Huiting Li, Y.-N. Xu, Y.-Z. Zhu, Hidong Kim, and Jae M. Seo, Phys. Rev. B **75**, 235442 (2007).

[79] H Kim, G Duvjir, O Dugerjav, Huiting Li and Jae M. Seo, Phys. Rev. B **81**, 245422 (2010).

[80] N.-J Wu, A. Natori, and H. Yasunaga, Surf. Sci. **260**, 75 (1992).

[81] H. Yasunaga and A. Natori, Surf.Sci.Rep. **15**, 205 (1992).

[82] K. Sakamoto, N.-J Wu, A. Natori, and H. Yasunaga, Applied Surf. Sci. **480**, 169-170 (2001).

[83] H. Kim, H. Li, Yong-Zhe Zhu , J. R. Hann, and Jae M. Seo,Surf. Sci. **601**, 1831 (2007).

[84] J. H. Seo and J. Y. Kim, Appl. Phys. Lett. **78**, 3124 (2001).

[85] J. Michel, J. Liu and L. C. Kimerling,Nat. Photon. **4**, 527 (2010).

[86] Y -W Mo, D E Savage, B S Swartzentruber, and M G Lagally, Phys.Rev. Lett. **65** , 1020 (1990).

[87] L. Persichetti, A. Sgarlata, M. Fanfoni, and A. Balzarotti, Phys.Rev. Lett. **104**, 036104 (2010).

[88] Bert Voigtlander, Surf.Sci.Rep. **43**, 127 (2001).

[89] J. Stangl, V. Holy, G. Bauer, 2004,Rev. Mod. Phys. **71**, 725 (2004).

[90] I. Berbezier, A. Ronda, and A. Portavoce,J.Phys. Condens. Matter **14**, 8283 (2002).

[91] I. Berbezier and A. Ronda,Phys. Rev. B **75**, 195407 (2007).

[92] J. Tersoff, and R. M. Tromp, Phys.Rev. Lett. **70**, 2782 (1993).

[93] K. Sekar, G. Kuri, P. V. Satyam, B. Sundaravel, D. P. Mahapatra, B. N. Dev, Phys. Rev. B **51**, 14330 (1995).

[94] J. D. Paul, B. Coonan, G. Redmond, B. J. O'Neill, G. M. Crean, B. Hollnder, S. Mantl, I. Zozoulenko, K.-F Berggren , J.-L Lazzari, F. Arnaud d Avitaya, J. Derrien, Thin Solid films. **336**, 130 (1999).

[95] A. I. Yakimov, A. V. Dvurechenskii, Yu Yu Proskuryakov , A. I. Nikiforov , O. P. Pchelyakov, S.A. Teys , and A. K. Gutakovskii,Appl. Phys. Lett. **75**, 1413 (1999).

[96] H. Omi and T. Ogino,Phys. Rev. B **59**, 7521 (1999).

[97] H. Kim, H. Li and Jae M. Seo,Surf. Sci. **602**, 2563 (2008).

[98] M. E. Ware and R.J. Nemanich,Thin Solid films. **518**, 1990 (2010).

[99] I. V. Zakurdaev, S. Y. Sadofyev and A. O. Pogosov, JETP Lett. **75**, 91 (2002)

[100] L. R. Doolittle, Nucl. Instrum. Methods B **9**, 344 (1985).

[101] N -J Wu, Natori A, and H Yasunaga, Surf. Sci. **242**, 191 (1991).

[102] M. Handbuecken, B. Roettger, R. Kliese, I. Vianey and H. Neddermeyer, Europhys. Lett. **23**, 573 (1993)

[103] J. K. Dash, A. Rath, R. R. Juluri, P. Santhana Raman, K. Müller, A. Rosenauer and P. V. Satyam,J.Phys. Condens. Matter **23**, 135002 (2011).

[104] R. A. Zhachuk, S. A. Teys ,A. E. Dolbak and B. Z. Olshanetsky, Surf. Sci. **565**, 37 (2004).

[105] S. S Iyer, G.L. Patton, J.M.C. Stork, B.S. Meyerson and D.L. Harame, IEEE Transactions on Electron Devices **36**, 10 (1989).

[106] Papichaya Chaisakul, Delphine Marris-Morini, Giovanni Isella, Daniel Chrastina, Xavier Le Roux, Samson Edmond, Eric Cassan, Jean-Rene Coudevylle, and Laurent Vivien,Appl. Phys. Lett. **98**, 131112 (2011).

[107] J. M. Baribeau, T. E. Jackman, D. C. Houghton, P. Maigne, M. W. Denhoff,J. Appl. Phys. **63**, 5738 (1988).

[108] E. A. Fitzgerald, Y. H. Xie, M. L. Green, D. Brasen, A. R. Kortan, J. Michel, Y. J. Mii, B. E. Weir,Appl. Phys. Lett. **59**, 811 (1991).

[109] F. K. LeGoues,Phys.Rev. Lett. **72**, 876 (1994).

[110] A. Kirakosian, R. Bennewitz, J. N. Crain, Th. Fauster, J -L Lin , D. Y. Petrovykh, and F. J. Himpsel Appl. Phys. Lett. **79**, 1608 (2001).

[111] Shinsuke Hara, Masamichi Yoshimura, and Kazuyuki Ueda, J. J. Appl. Phys. **47**, 7 (2008).

[112] D. J. Eahlesham, and M. Cerullo,Phys.Rev. Lett. **64**, 1943 (1990).

[113] Ch. Heyn, Phys. Rev. B **63**, 033403 (2001).

[114] K. E. Khor and S. Das Sarma, Phys. Rev. B **62**, 16657 (2000).

[115] K. A. Fichthorn, M. L. Merrick, M. Scheffier,Applied Phys. A. **75**, 17 (2002).

[116] J. K. Dash, A. Rath, R. R. Juluri, P. Santhana Raman, K. Müller, A. Rosenauer and P. V. Satyam,J.Phys. Condens. Matter **23**, 135002 (2011).

[117] J. K. Dash, A. Rath, R. R. Juluri, P. Santhana Raman, K. Müller, M. Schowalter, R. Imlau, A. Rosenauer, P. V. Satyam, J.Phys. Conf. Series **326**, 012021 (2011).

[118] Alan Lo and Rex T. Skodje J.Chemical Phys. **111**, 2726 (1999).

[119] Alan Lo and Rex T. Skodje J.Chemical Phys. **112**, 1966 (1999).

[120] J. K. Dash, T. Bagarti,A. Rath, R. R. Juluri and P. V. Satyam, Submitted to Eur. Phys. Lett.(2012) ; arXiv:1204.0578v1 .

[121] K. Nakajima, A. Konishi, K. Kimura, Phys.Rev. Lett. **83**, 1802 (1999).

[122] B. P. Uberuaga, M. Leskovar, A. P. Smith, H. Jnsson, M. Olmstead, Phys.Rev. Lett. **84**, 2441 (2000).

[123] J.-H. Cho, M.-H. Kang, Phys. Rev. B **61**, 1688 (2000).

[124] J. T. Robinson, A. Rasteeli, O. Schmidt, O. D. Dubon, Nanotechnology **20**, 085708 (2009).

[125] F. K. LeGoues, M. C. Reuter, J. Tersoff, M. Hammar, and R. M. Tromp , Phys.Rev. Lett. **73**, 300 (1994).

[126] J. M. Bermond, J. J. Me*é*tois, X. Egea , F. Floret, Surf. Sci. **330**, 48 (1995).

[127] C. Herring ,Phys. Rev. B **82**, 87 (1951).

[128] P. M*ü*ller, A. Sa*ù*l , Surf.Sci.Rep. **54**, 157 (2004).

[129] Cl*é*ment Pribat, Germain Servanton, Linda Depoyan, Didier Dutartre, Solid State Electron **53**, 865 (2009).

[130] Hidong Kim, Otgonbayar Dugerjav, Ganbat Duvjir, Huiting Li, Jae M. Seo, Surf. Sci. **606**, 744 (2012).

[131] I. Daruka, J. Tersoff, and A.-L. Barab*á*si, Phys.Rev. Lett. **82**, 2753 (1999).

[132] S. A. Chaparro, Y. Zhang, Jeff Drucker, D. Chandrasekhar, and David J. Smith, J. Appl. Phys. **87**, 2245 (2000).

[133] J.P. R*ö*nspies, S. Wießell, H. Pfn*ü*r, Applied Phys. A. **100**, 1007 (2010).

[134] J. K. Dash , A. Rath, R. R. Juluri and P. V. Satyam, Submitted to J. Physics D : Appl. Phys.(2012) ; arXiv:1205.6039v1.

[135] X. Z. Liao, J. Zou, D. J. H. Cockayne, Z. M. Jiang, X. Wang et al.,Appl. Phys. Lett. **77**, 1304 (2000).

[136] T. I. Kamins, G. Medeiros-Ribeiro, D. A. A. Ohlberg, and R. S. Williams, Appl. Phys. A: Mater. Sci. Process, **67**, 727 (1998).

[137] C. Lang, D. J. H. Cockayne, D. Nguyen-Manh, Phys. Rev. B **72**, 155328 (2005).

[138] F. Boscherini, G. Capellini, L. Di Gaspare, F. Rosei, N. Motta, Appl. Phys. Lett. **76**, 682 (2000).